MICROCONTROLLER - BASED CURRENT SOURCE INVERTER DRIVEN INDUCTION MOTOR DRIVE

by

William Edward Mufford
B.A.Sc., The University of British Columbia,
Vancouver, B.C., Canada, 1990

A THESIS SUBMITTED IN PARTIAL FULFILLMENT
OF
THE REQUIREMENT FOR THE DEGREE
OF
M.A.Sc.

The Faculty of Graduate Studies,
Department of Electrical Engineering

We accept this thesis as conforming to the required standard

.....

.....

The University of British Columbia
April 1992

In presenting this thesis in partial fulfilment of the requirements for an advanced degree at the University of British Columbia, I agree that the Library shall make it freely available for reference and study. I further agree that permission for extensive copying of this thesis for scholarly purposes may be granted by the head of my department or by his or her representatives. It is understood that copying or publication of this thesis for financial gain shall not be allowed without my written permission.

(S

Department of Electrical Engineering

The University of British Columbia
Vancouver, Canada

Date April 28, 1992

DE-6 (2/88)

ABSTRACT

Current Source Inverter Induction Motor Drives (CSI-IM) are well suited to large power applications when regeneration is required. This thesis deals with the design and analysis of a flexible single chip microcontroller based CSI-IM drive. In order to demonstrate the merits of the adaptable microcontroller based system, two different types of outer loop speed/torque control strategies (Flux and Vector control) are discussed and discrete control laws are developed. Furthering the theme of microcontroller agility, two different types of inner loop current control schemes are developed: simple proportional-integral feed back control, and direct model reference adaptive control (DMRAC) with feed forward back-electromotive-force (back-emf) compensation. The Vector and DMRAC is included not only to demonstrate the fact that high-performance control laws can be run on the microcontroller in real time, but also to show the benefits of these advanced control methodologies. The overall hardware and software development is discussed in detail. Experimental results, using a prototype unit, are presented to illustrate the potential of the microcontroller based CSI-IM drive.

TABLE OF CONTENTS

LIST OF FIGURES

LIST OF SYMBOLS

Flux and Vector Control

a	Referral Ratio	
E_r, E_r''	Rotor Voltage	(V)
f_m	mechanical rotor speed (electrical)	(Hz)
f_r	rotor frequency (electrical)	(Hz)
f_s	stator frequency (electrical)	(Hz)
I_m, I_r, I_s	Magnetizing, Stator and Rotor Current	(A)
$I_{ST}, I_{S\phi}$	Torque and Flux Producing Current	(A)
I_{dc}, I_r	Measured and Reference DC Link Current	(A)
L_l	Link Inductance	(mH)
L_T	Total Reflected Circuit Inductance	(mH)
L_{ls}, L_{lr}	Stator and Rotor Leakage Inductance	(mH)
L_m	Mutual Inductance	(mH)
L_s'', L_m''	Modified Stator and Mutual Inductance	(mH)
L_r, L_s	Rotor and Stator Self Inductance	(mH)
λ_r	Rotor Flux	(V•s)
λ_s	Stator Flux	(V•s)
R_r', R_r''	Standard and Modified Rotor Resistance	(Ω)
R_l	Link Resistance	(Ω)
R_T	Total Reflected Circuit Resistance	(Ω)
s	Slip Ratio	
T_{elec}	Electrical or Air Gap Torque	(Nm)
T_m	Mechanical Torque	(Nm)
T_s	Sampling Time Interval	(s)
np	Number of Pole Pairs	
P_{airgap}	Air Gap Power	(W)
ω_m	Mechanical rotor speed (electrical)	(rad/s)
ω_r	Rotor frequency (electrical)	(rad/s)
ω_s	Stator frequency (electrical)	(rad/s)
V_{ab}	Line a to Line b Voltage	(V)
V_r	Convertor Output DC Voltage	(V)

Direct-Model-Reference-Adaptive and Proportional-Integral Control

e(t)	Continuous Time Link Current Error Signal	(A)
e(k)	Discrete Link Current Error Signal	(A)
emf(k)	Estimated Discrete Back EMF	(V)
f(t)	Auxiliary DMRAC Signal	(V/A)
K	Typical Feed Back Gain	
K_d	Derivative Gain	(V/A)
K_i	Integral Gain	(V/A)
K_p	Proportional Gain	(V/A)
K_{vv}	DMRAC Discrete Control Law Derivative Gain	(V/A)
K_{ii}	DMRAC Discrete Control Law Integral Gain	(V/A)
K_{pp}	DMRAC Discrete Control Law Proportional Gain	(V/A)
q	Typical Feed Forward Gain	
q_0	DMRAC Contin. Control Law Proportional Gain	(V/A)
q_1	DMRAC Contin. Control Law Derivative Gain	(V/A)
q_2	DMRAC Contin. Control Law Derivative^2 Gain	(V/A)
q_{00}	DMRAC Discrete Control Law Proportional Gain	(V/A)
q_{11}	DMRAC Discrete Control Law Derivative Gain	(V/A)
q_{22}	DMRAC Discrete Control Law Derivative^2 Gain	(V/A)
r(t)	Weighted Contin. Link Current Error Signal	(A)
r(k)	Weighted Discrete Link Current Error Signal	(A)
W_p	Weighing Factor for proportional error	
W_v	Weighing Factor for derivative error	
δ, α, γ	Positive Integral Adaptation Gain	
ρ, β, λ	Positive proportional Adaptation Gain	

GLOSSARY OF TERMS

A.C.	Alternating Current
A/D	Analog to Digital Converter
CSI	Current Source Inverter
CSI-IM	Current Source Inverter (driven) Induction Motor
D.C.	Direct Current
DMRAC	Direct Model Reference Adaptive Control
EXTINT	External Interrupt
F/B	Feed Back
F/F	Feed Forward
FOC	Field Orientated Control
HSI	High Speed Input
HSO	High Speed Output
I80196KC	Intel's 80196KC MicroController
PD^2	Proportional, derivative and second derivative controller
PI	Proportional and integral controller
PID	Proportional,integral and derivative controller
PLL	Phase Locked Loop
RPM	Rotations Per Minute
SMC	Sliding Mode Control
XOR	Exclusive OR Gate
ZCD	Zero Crossing Detector

CHAPTER 1

INTRODUCTION

1.1 Introduction

One of the most suitable drive packages for high-power, adjustable speed applications, where regeneration is required, is the current source inverter (CSI) feeding an induction motor [1-18]. The inherent simplicity and regeneration capability of the CSI in conjunction with the desirability of the three phase squirrel cage motor (rugged, no brushes, low weight, small size) are major factors influencing this claim. Other important features of a current controlled system are the direct torque commands which give improved dynamic performance and fast short circuit protection [6,7,9,13]. The major disadvantages include: the necessity of closed loop control, low speed torque pulsations, low input power factor and high voltage stresses on the motor and CSI components [13].

1.2 Basic Current Source Inverter Fed Induction Motor Drive

The CSI induction motor (CSI-IM) drive is shown in Figure 1.1.

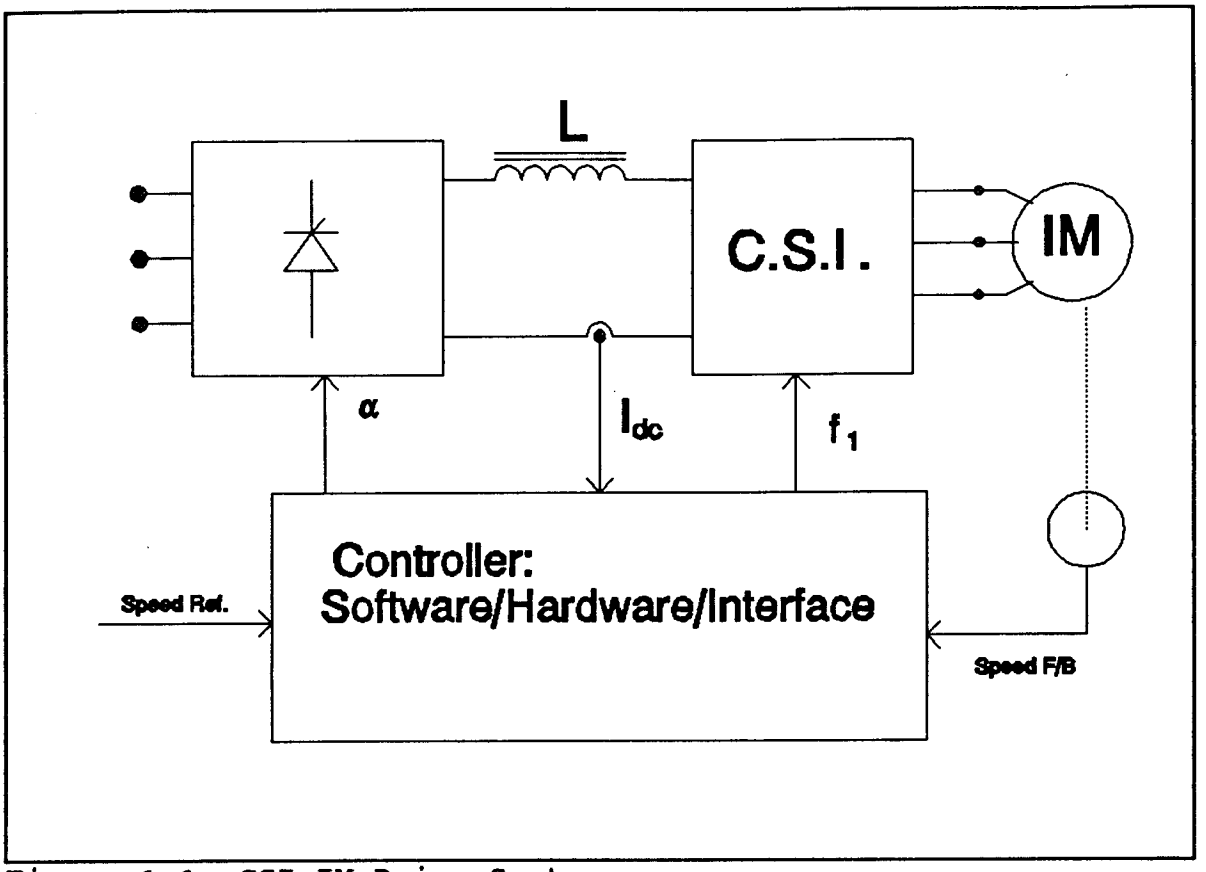

Figure 1.1: CSI-IM Drive System

A brief description of this drive systems follows and a detailed explanation can be found in [1,2,8,12,13]. The main functional blocks of this unit are: the phase controlled converter, d.c. link inductor, d.c. to a.c. inverter, three phase motor, and control loops (implemented in a microcontroller). The power circuit for the complete thyristor based CSI drive system is shown in Figure 1.2. It consists of twelve converter grade thyristors, six diodes, six commutation capacitors and a d.c. link filter.

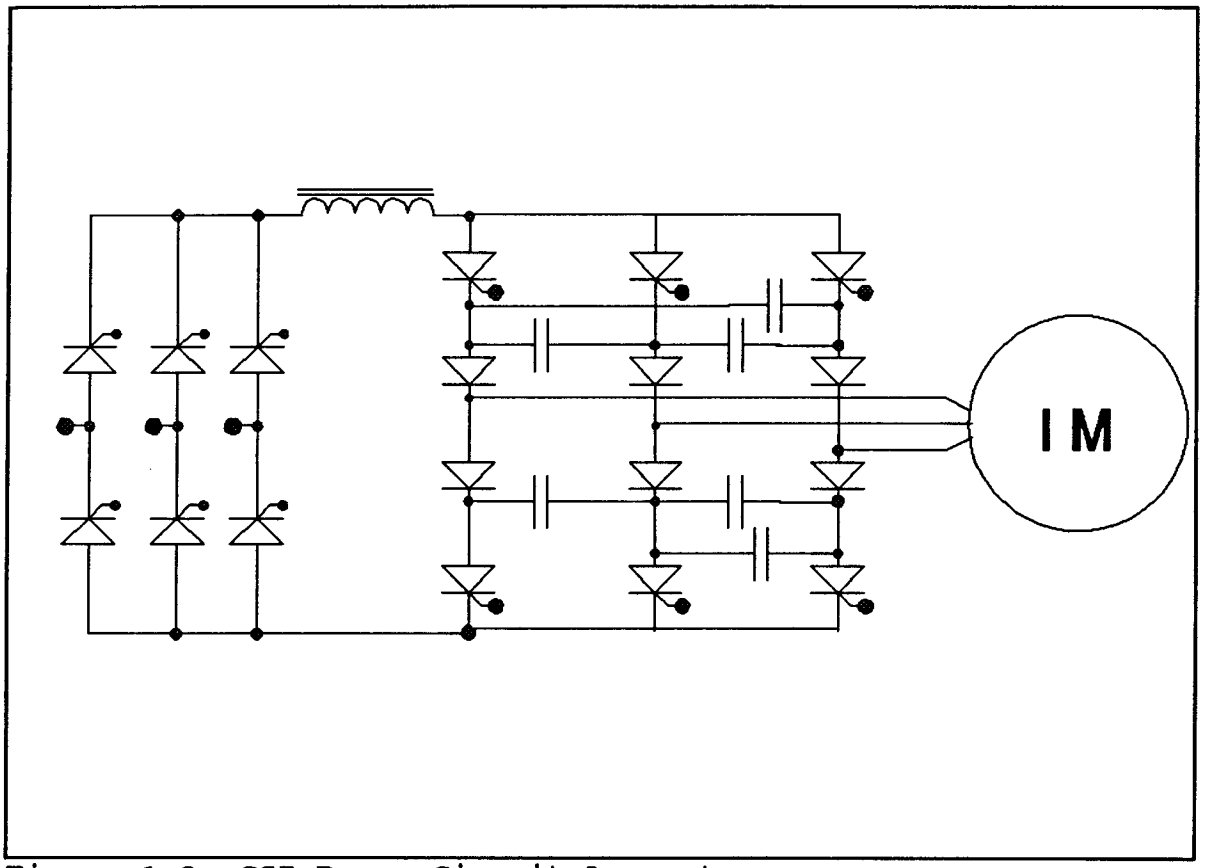

Figure 1.2: CSI Power Circuit Lay out

The controlled converter rectifies the three phase input power using six thyristors (see Figure 1.2). At any given time two thyristors will be conducting and commutation is realized through the natural reversal of the applied sinusoidal supply voltage. The average value of the output voltage is adjusted by controlling the firing delay angle, α (increasing the delay angle reduces the average output voltage). The link inductor works in conjunction with the converter and is used as a smoothing filter for the link current. The large ripple of the converter output voltage makes the

link inductor necessary [12]. Together with a microcontroller, the controlled converter and the link inductor form a unidirectional current source, which feeds regulated current into the inverter. Although the current can only flow in one direction through the thyristors, the average voltage can be positive or negative. Hence, both motoring (positive current and voltage) and regenerating (positive current and negative voltage) are possible.

The inverter, which is also controlled with the same microcontroller, inverts the direct current (d.c.) coming out of the link inductor into a variable frequency alternating current (a.c.) form. The inverter thyristors are turned on two at a time to give a variable frequency, quasi-square wave, three phase output current. The commutation capacitors are used to reverse bias the thyristors. The gate trigger of a thyristor only switches the device on, and loses control once conduction has commenced. Therefore it is necessary to have an external mechanism (the commutation capacitors) to commutate (turn off) the thyristors. A detailed analysis of the switching and commutation cycles can be found in [7,12,13]. It is possible to achieve both positive and negative phase rotation by controlling the order in which the thyristors are cycled on and off. Since the phase rotation controls the direction in which the motor rotates, and the front end current source is capable of providing both motoring and generating action, a simple four quadrant drive is achieved.

The control strategies, which are implemented in the microcontroller software, exist on several different levels. The outer most level is the speed controller. These control laws work to regulate the motor speed and can be implemented using a number of different strategies such as Proportional (P), Propórtional-Integral (PI), Proportional-Integral-Derivative (PID), Integral-Proportional (IP), Phase-Lock-Loop (PLL), Deadbeat, and Sliding Mode Control (SMC) to name a few [26].

The output signal of the speed control law determines the desired motor torque. Again many options for torque control are available. For instance a single chip microcontroller using one hardware configuration can adopt any of the following torque control strategies: constant airgap flux control [5,10,13], Volts per Hertz control [13], field oriented control (vector control) [7,13,14], torque angle control [11] or the field acceleration method (FAM) [18]. Each of these control methodologies has a particular application which suits it best. For instance a CSI-IM drive under constant airgap flux control, a relatively simple and inexpensive low performance control strategy, would be appropriate for an ore belt which has low dynamic torque response demands. Vector control, which is quite complicated (and therefore more expensive to develop), would be preferable for a winch drive on a crane, a load which requires relatively faster changes in motor torque.

The outputs of the torque control laws determine the reference values of link current and inverter frequency. Here again, different control laws can be employed to regulate these variables. For the link current, simple control strategies, such as PI control, as well as more sophisticated schemes like Direct Model Reference Adaptive Control (DMRAC) [20], with back-emf compensation [17] can be used. The inverter frequency is controlled in feed forward (F/F) manner by adjusting the switching period (the point in time when the thyristor is gated on) of the CSI thyristors.

The lowest level of control with the single chip microcontroller based system is the coordination of the gating signals to the thyristors. These consist of timed pulses which the semi-conductor switches react to by turning on and conducting current.

Thus, in the single chip system, the same microcontroller not only regulates the motor torque and speed, but also the d.c link current and inverter frequency. The control laws can be implemented using a number of different regulation strategies with absolutely no hardware changes. This gives the microcontroller based system flexibility that is simply not possible with analog circuitry. The single processor system also offers the user a more robust drive by lowering the chip count (less components means a lower probability of failure) and reducing the vulnerability to electrical noise (which is always present in power semi-conductor drives). The lower

vulnerability to electrical interference is achieved since the different levels of control systems (speed, torque, link current control etc.) communicate within the one chip and not through exposed external circuits. Thus a single chip microcontroller based drive would give an all round superior and flexible drive package.

1.3 Thesis Objectives

The previous discussion dealt with the flexiblity and advantages of a single chip microcontroller based CSI-IM drive. The primary objective in doing this thesis was to design and analyze a flexible single chip microcontroller based CSI-IM control system. To this end, some secondary objectives, which permit completion and demonstration of the primary goal, must also be defined. These are as follows:

1. Design the torque control laws. Two torque control laws will be developed: Constant Airgap Flux Control (Flux Control, a simple low performance scheme [13]) and Field Oriented Control (Vector Control, a complex high performance strategy [13,14]). This will not only demonstrate the microcontrollers flexibility in adapting different control strategies, but will also allow this microcontroller system the option of having two levels of controller performance and complexity.

2. Design the link current control laws. Again two different control methods will be developed in the interest of making the CSI-IM drive adaptable. This will further demonstrate the microcontroller's flexibility. The two methods chosen are: simple PI feedback (F/B) control and DMRAC with back-emf compensation.

3. Design and construct an experimental microcontroller based CSI-IM drive system (hardware and software).

4. Demonstrate the experimental system. Show the system going through some typical transient manoeuvres: a start up sequence, a positive step changes in speed, and a regenerative deceleration.

5. Comment on the overall system performance and suggest further areas of research that will promote the microcontroller based CSI-IM drive system.

1.4 Thesis Outline

Chapter 2 deals with the development of constant air gap flux control for induction motors. This control methodology is employed extensively with inverter driven motors now, and will be regarded as the standard by which FOC will be judged.

Chapter 3 is a development of a vector control law suitable for implementation on a microcontroller based CSI-IM drive. Vector control, as implemented here, is an attempt to maintain a constant angle (90 degrees) between the rotor flux vector and the stator magnetomotive force (mmf) vector. Both Chapters 2 and 3 begin with a discussion of the theory and lead into the development of digital control laws.

Chapter 4 describes the development of the link current controllers. Here again two different control routines are derived to show the flexibility of the microcontroller. The first method is a simple Proportional-Integral (PI) feedback control. This will be used as a baseline to evaluate the second, more complex, method. The more advanced controller uses feedforward back-emf compensation, in conjunction with a feedforward/feedback direct model reference adaptive controller (DMRAC), to regulate link current. This is done to enhance the dynamic performance of the complete motor drive system, through fast link current control. The feedforward back-emf signal generation is an attempt to remove the nonlinear term (usually treated as a disturbance and compensated in a feedback manner) in the link current control system, and was first attempted in [17] with excellent results. This now allows the linear DMRAC strategy to be applied to a simple system consisting of a voltage source feeding a resistance and inductance network (the nonlinear disturbance is compensated for separately). Since the parameters in the induction motor and link circuit R-L network

are known to vary greatly [20,21] over the expected operating range of the drive system, the adaptive control should compensate accordingly and keep the performance near optimal.

With this system, all the control laws, generation of the thyristor gating signals, and sample-and-hold analog-to-digital (A/D) conversions are executed on a single micro-processor (Intel's 80196KC microcontroller). However, the hardware simplicity obtained here is at the expense of software complexity. Since the 80196KC is a very fast (16 MHz. and 16 bit internal data bus) and flexible microcontroller, the software complication can be overcome through a modular design and extensive use of interrupts. The actual implementation of the complete software and hardware is discussed in chapter 5. The main advantages of hardware simplicity is increased robustness (a lower chip count usually means higher reliability) and lower susceptibility to electrical noise interference (all subsystem communication is within the single microcontroller chip). These key features are necessary in an a.c. drive system if it is to replace the firmly established d.c. drive in the regeneration applications such as cranes and traction.

The actual test results from the experimental drive system, which was constructed to test this design, appear in chapter 6. These test results show that the single chip microcontroller design not only provides excellent performance, but is also very flexible in its acceptance of different control strategies. The results of

the application of the advanced control methodologies, as outlined in Chapters 3 and 4, also show improved drive system performance.

Overall conclusions regarding the performance of the control system and other potential research topics are described in chapter 7.

CHAPTER 2

CONSTANT FLUX CONTROL THEORY

2.1 Introduction

The control schemes presented in this thesis are developed (and tested) with the aid of both airgap flux control and field oriented control (FOC or vector control). Thus it is useful to explain both theories in enough detail to develop the control laws. This chapter is an explanation of constant airgap flux control theory (flux control), and derivation of the control laws needed to implement it. Chapter 3 describes the single phase equivalent circuit derivation of vector control as needed for the indirect field oriented scheme. The discussion presented here is described in more detail in [4,5,13].

2.2 Flux Control Theory

The circuit model used for flux control is the familiar induction motor steady state equivalent circuit shown in Figure 2.1. In order to fully benefit from the available torque of a three phase induction machine, and thus have a reasonably fast transient response over a wide speed range, it is necessary to maintain the

airgap flux at the value of the so called name-plate level (the value of ω_r, rotor slip frequency, and i_s, stator current, with 60 Hz. supply and a full load applied) [5,13,15]. An example in [15] shows that if this methodology is not applied saturation of the airgap magnetizing flux occurs and a somewhat less than optimal torque/stator-ampere ratio results. Thus if ω_r is not controlled properly, the magnetizing current, I_m, is much higher than necessary. Through standard circuit analysis it is possible to solve for I_r (rotor circuit current) and I_m as functions of I_s (input stator current), the rotor resistance (R_r') and inductive parameter (L_{lr}' and L_m). These relationships are as follows (and the details can be found in Appendix A):

$$I_m = I_s \left[\frac{(R_r')^2 + (\omega_r * L_{lr}')^2}{(R_r')^2 + (\omega_r * (L_{lr}' + L_m))^2} \right]^{1/2} \qquad (2.1)$$

Equation 2.1 can be further manipulated to find ω_r as a function of I_m and I_s:

$$\omega_r = R_r' \left[\frac{I_m^2 - I_s^2}{(L_{lr}' I_s)^2 + I_m^2 (L_{lr}' + L_m)^2} \right]^{\frac{1}{2}} \qquad (2.1a)$$

$$I_r' = I_s \frac{\omega_r * L_m}{[(R_r')^2 + (\omega_r * (L_{lr}' + L_m))^2]^{1/2}} \qquad (2.2)$$

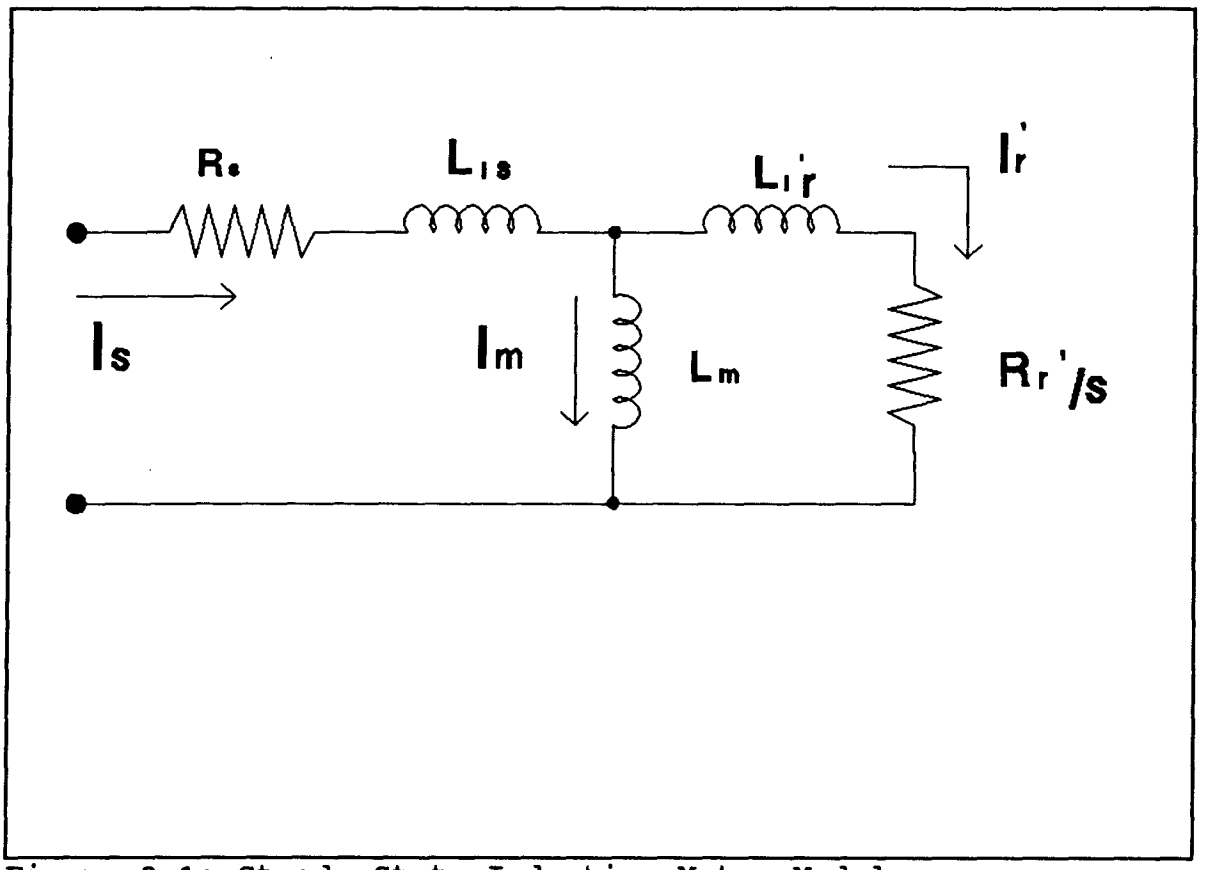

Figure 2.1: Steady State Induction Motor Model.

Since airgap flux is proportional to I_m, it turns out to be a function of stator current (I_s), and slip frequency (ω_r). The airgap flux is in fact independent of supply frequency, ω_s.

Also by referring to the analysis in Appendix A it can be seen that motor torque can be expressed as follows:

$$T=3*P*I_s^2\frac{(\omega_r*L_m)^2*R_r'/\omega_r}{(R_r')^2+(\omega_r*(L_{lr}'+L_m)^2)} \qquad (2.3)$$

As was the case with the rotor and magnetizing currents, the torque is only a function of stator current and rotor slip frequency and is independent of the supply frequency. Using equation 2.1 through 2.3, it can be seen that if it is possible to control I_s and ω_r in such a way as to avoid the magnetic saturation effects, there would be a situation of nearly optimal steady state airgap flux and hence maximum torque/stator-ampere ratio [13]. This is the goal of airgap flux control.

Since it is impractical to measure flux directly (Hall effect flux transducers are very sensitive to temperature and mechanical shocks), it must be deduced via the terminal condition of the three phase induction machine. In the case of a CSI induction motor drive, the best variables to use are stator current (fundamental of the square wave inverted d.c. link current), and slip frequency (since the mechanical speed, ω_m, is measured, and the stator frequency, ω_s, is known the slip frequency is: $\omega_r = \omega_s - \omega_m$).

2.3 Control Laws

The simple control scheme, as suggested in [13], appears in Figure 2.2. It is an attempt to regulate the airgap flux at its

full load level by maintaining the magnetizing current, I_m, at a constant value (the full load level). This is a proportional speed control scheme. A finite speed error must exist before the link current reference is increased beyond its minimum value. Thus, as load is applied to the motor the speed will decrease slightly leaving a steady state error.

With this scheme the speed error determines the link current, I_{dc}, which has a minimum value proportional to the no load level of I_s, and a maximum value related to the full load name plate current. It is possible to calculate the speed error with the microcontroller and use a function generator (lookup table) to get the reference link current, I_{dc}^* (hence I_s). The current controller in Figure 2.1 can be implemented using a number of different schemes (P, PI, PID, DMRAC etc.). This thesis uses both PI control and DMRAC (with back-emf compensation).

The other function generator which appears in Figure 2.2 is equation 2.1 solved for ω_r (equation 2.1a). Thus, this is an attempt to maintain I_m at its name plate value. This keeps airgap flux constant since it is proportional to I_m.

The inverter frequency is regulated at f_r rads/second ($\omega_r = 2*\pi*f_r$) above or below the mechanical speed. Whether the rotor frequency is added or subtracted from the mechanical speed depends on the polarity of the speed error. The speed error being positive

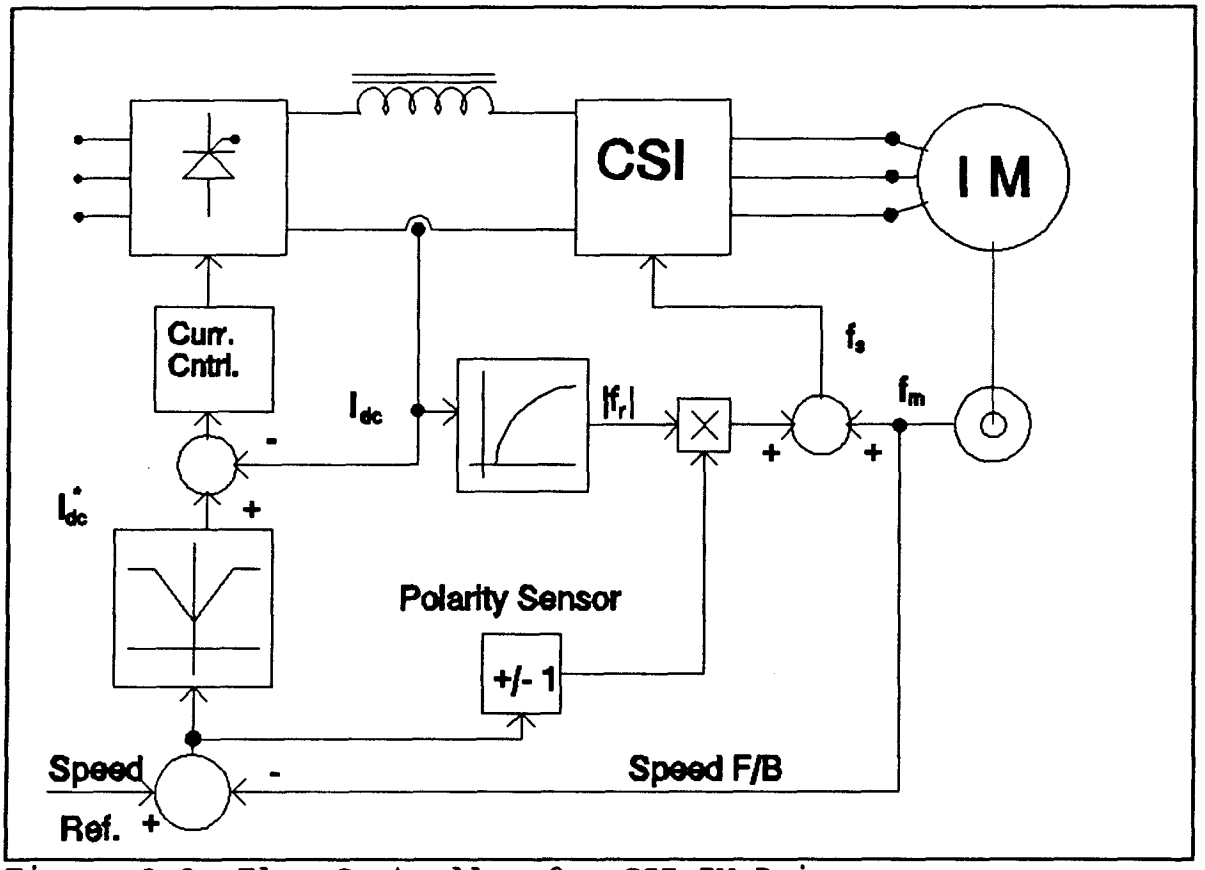

Figure 2.2: Flux Controller for CSI-IM Drive.

indicates motoring operation, whereas a negative speed error would have the drive in a regeneration mode.

Since the response time of the magnetizing branch is long, this particular method of torque control has poor transient behaviour. The simple model on which the control system is based, is only valid for the steady state case [13] and does not take into account the transient effects which impair drive system response.

To achieve better dynamic performance it is possible to use the vector control strategy, which is an attempt to have d.c. machine-like response from the induction machine. Vector control tries to regulate the instantaneous torque angle between rotor flux and stator mmf vectors [13]. This is discussed in Chapter 3.

2.4 Summary

Constant airgap flux control theory was discussed and a control scheme developed. Constant airgap flux control is an attempt to maintain the magnetizing current, I_m, (airgap flux is proportional to I_m below the saturation point) at the name-plate value, while operating at different speeds and loads. This simple control scheme will be used as a base line to judge the performance of vector control (explained in chapter 3) and to demonstrate the ability of the microcontroller to adopt different motor control strategies with no hardware changes.

CHAPTER 3

VECTOR CONTROL THEORY

3.1 Introduction

The previous chapter was an explanation of constant airgap flux control, a strategy based on a steady state model of the induction machine. Since this model is not valid for the induction machine under transient conditions [13], fast dynamic response is not possible. Since one of the greatest assets of a CSI drive is its inherent regeneration capability, it would be advantageous to have a control scheme that could handle fast deceleration transients. Vector control has this ability. This chapter is an explanation of the vector control model leading to a control scheme suitable for the CSI-IM drive.

Vector control is an endeavour to produce separately excited D.C. machine like response characteristics with an induction machine. This is achieved by decoupling the stator current into flux-producing and torque-producing components [13,14]. An effort is made to keep the phase angle between these two constituents at 90 degrees, as is mechanically done in the D.C. machine. Thus torque control becomes a matter of adjusting the torque-producing

component of the stator current, which is analogous to regulating the armature current in the D.C. machine. Field flux is controlled by manipulating the flux-producing component of the stator current, which is similar to adjusting the field current in the D.C. machine. The end result of using vector control is enhanced induction machine performance.

3.2 Induction Machine Model for Vector Control

Before proceeding with vector control it is necessary to have a transient model of the three phase induction machine. Some transient models are developed using only generalized machine theory [13,23] while others take the equivalent circuit approach [14,18]. Although ideas from both methods are used, the equivalent circuit approach is most useful when trying to develop a control strategy. To start this analysis, a few assumptions must be made to simplify the circuit model (without degrading the integrity of the motor representation):

1. Motor can be represented as a three phase wye connected circuit. Thus the per phase equivalent circuit can be used.

2. Negligible space harmonics in the airgap mmf and flux.

3. Infinitely permeable stator and rotor irons. This avoids having to deal with non-linear inductances.

4. Negligible skin effect, core losses, and slot/end effects. Therefore disallowing the resistors in our circuit model that would account for these minor losses.

These assumptions help develop a steady state model which in turn leads into the transient model needed for vector control.

By considering the standard steady state equivalent circuit, repeated here as Figure 3.1, it is possible to develop a better circuit model for induction machine torque/speed control. It is well known that the circuit of Figure 3.1 can be modified into other equivalent circuits by using the notion of a referral ratio [14,18]. Intuitively it is possible to see this by considering how this circuit was first derived. The total leakage inductance (L_{ls} + L_{lr}') is measured with the no load and locked rotor tests (or calculated during the design of the motor) and then the individual values are assumed to be equal. Since only the sum is known, an infinite number of combinations exist to satisfy the total leakage inductance relationship. Thus, an infinite number of equivalent circuits exist, all having the same behaviour at the motor terminals. Considering Figure 3.2, it can be seen that placement of circuit elements is the same, but with very different values. This circuit has the same input impedance, as seen from the motor terminals, as that in Figure 3.1. This is true for any value of referral ratio, "a", as is shown in [14,18]. Thus, by clever choice of referral ratio, it is possible to change the circuit of Figure

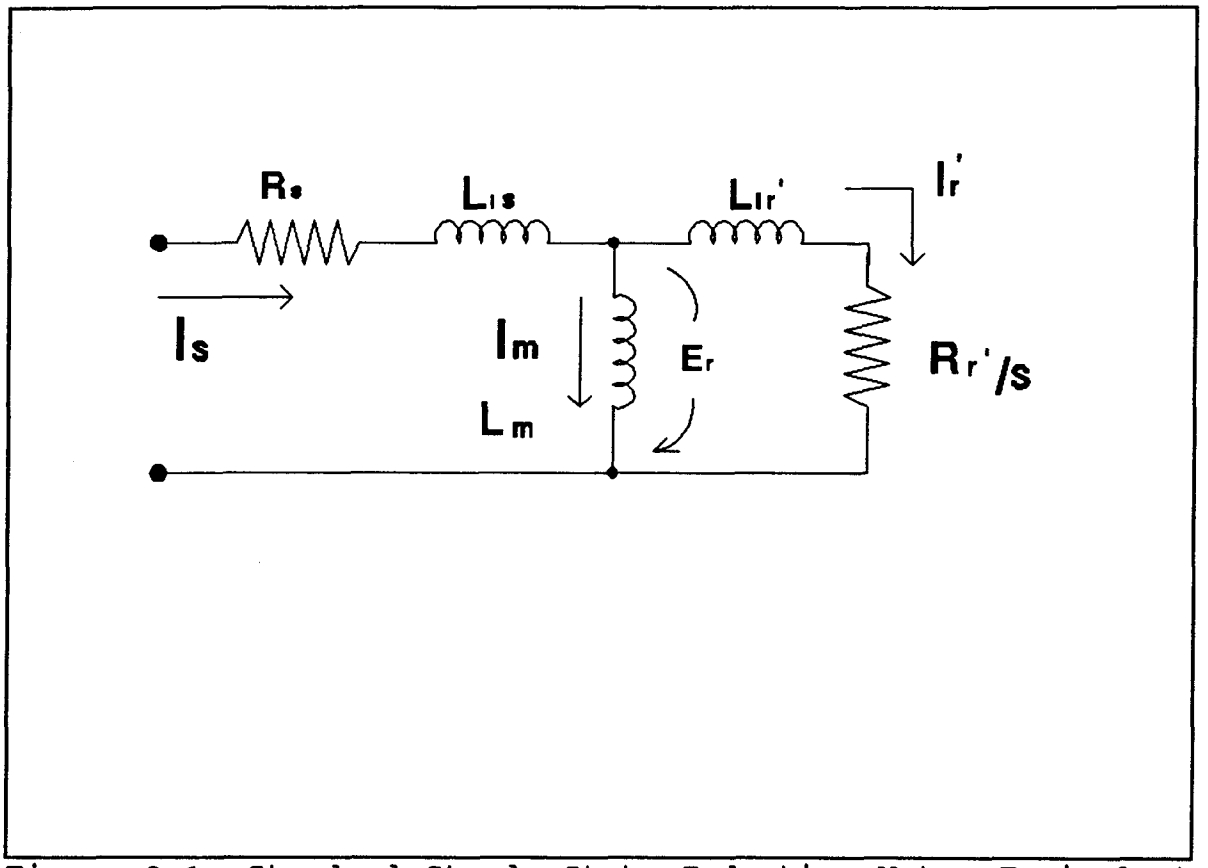

Figure 3.1: Standard Steady State Induction Motor Equivalent Circuit.

3.2 into a more suitable form, namely if "a" is chosen as follows:

$$a = \frac{L_m}{L_r} \qquad (3.1)$$

This has some advantages over the circuit displayed in Figure 3.1. The new circuit, as shown in Figure 3.3, has the new element values as shown in Equation 3.2.

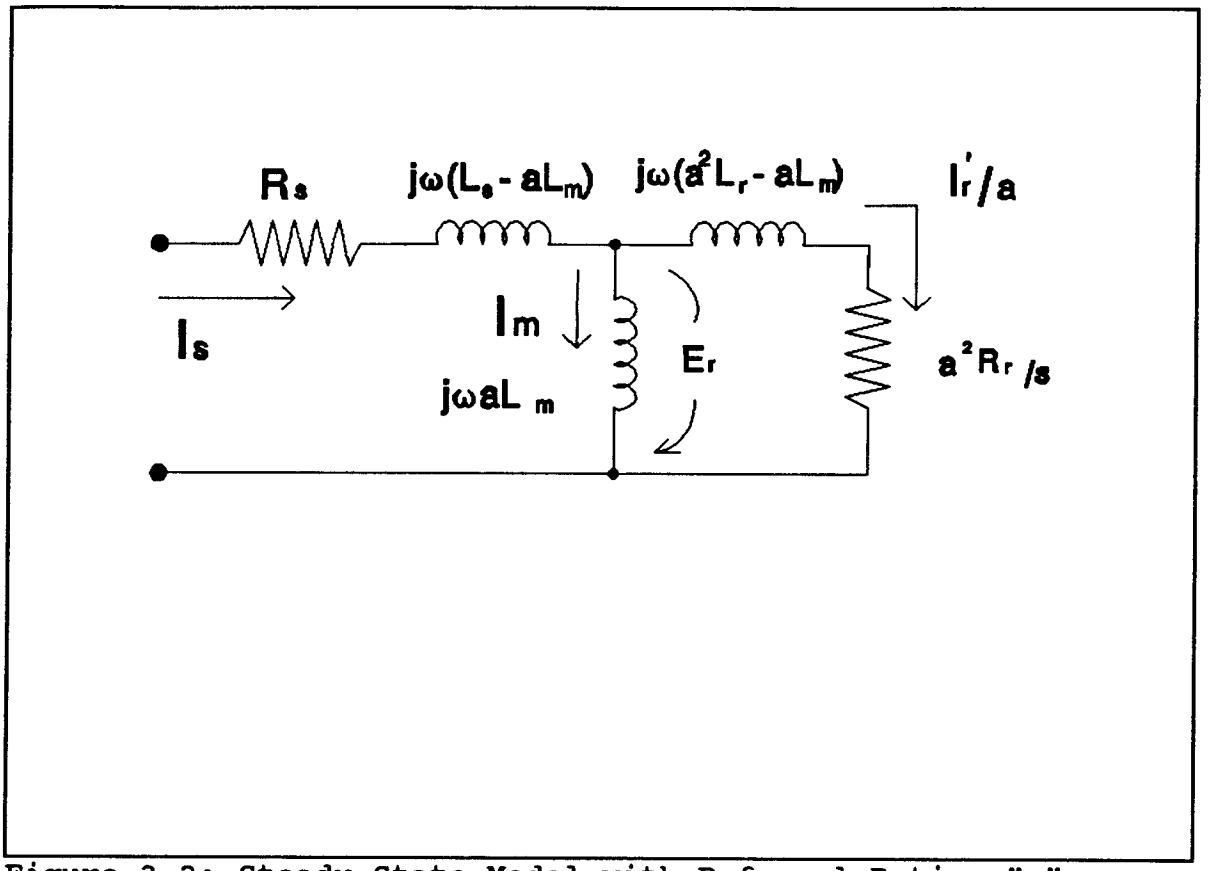

Figure 3.2: Steady State Model with Referral Ratio, "a".

$$
\begin{aligned}
L_s'' &= L_s - \frac{L_m^2}{L_r} \\
L_m'' &= \frac{L_m^2}{L_r} \\
R_r'' &= \left(\frac{L_m}{L_r}\right)^2 R_r' \\
E_r'' &= \frac{L_m}{L_r} E_r \\
L_r &= L_{lr}' + L_m \\
L_s &= L_{ls} + L_m
\end{aligned}
\qquad (3.2)
$$

The current through the reactance $j\omega L_m''$ is the rotor flux component

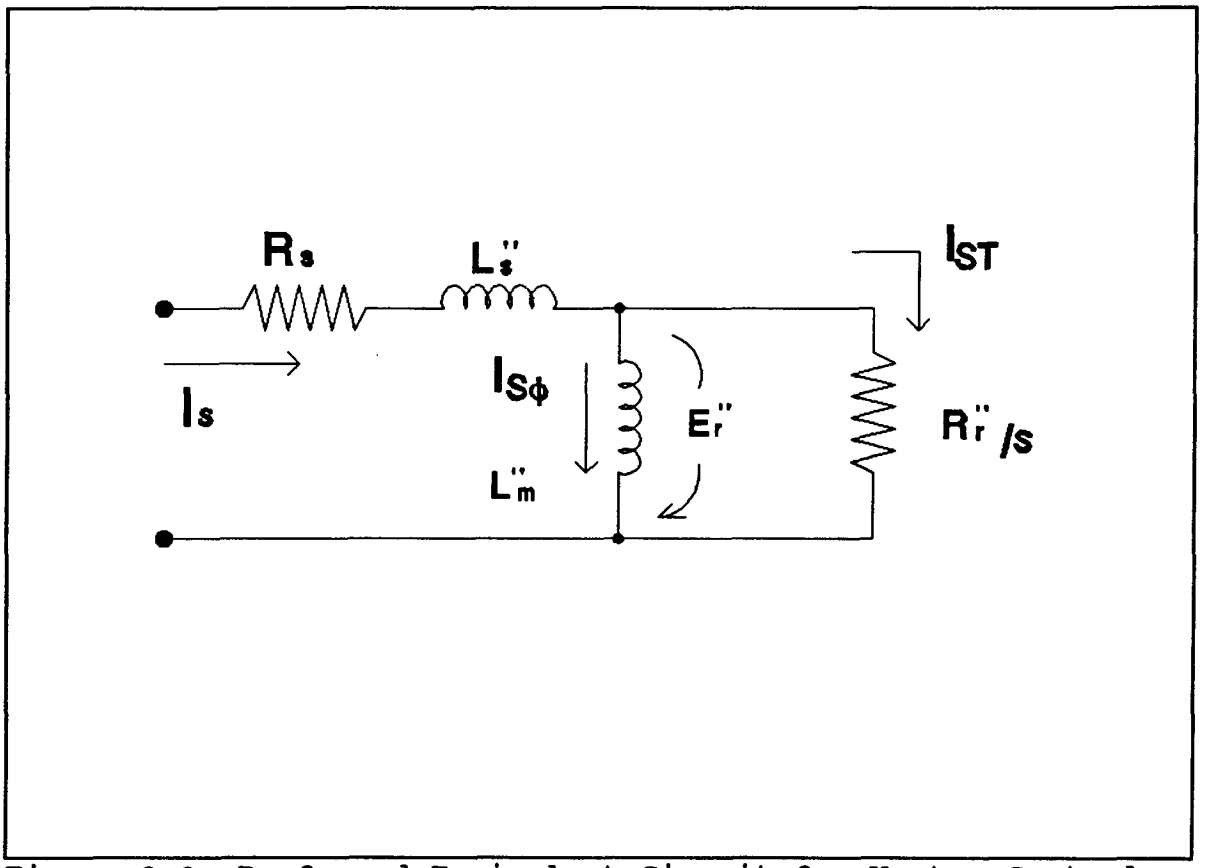

Figure 3.3: Preferred Equivalent Circuit for Vector Control.

($I_{S\phi}$), whereas I_{ST} is the current through the branch containing R_r''/s and represents the torque producing component (the only significant power absorbing term).

The induced rotor voltage (the voltage across R_r'/s) is defined as:

$$\overline{E_r} = -j\omega_s\overline{\lambda_r} \qquad (3.3)$$

This is the negative time rate of change of the rotor flux linkage. Since the flux producing portion of current, $I_{S\phi}$, can be determined through circuit analysis, Equation 3.4 is obtained.

$$\begin{aligned} I_{S\phi} &= -\frac{E_r''}{j\omega_s L_m''} \\ &= -\frac{\frac{L_m}{L_r}E_r}{j\omega_s \frac{L_m^2}{L_r}} \\ &= -\frac{E_r}{j\omega_s L_m} \end{aligned} \qquad (3.4)$$

By placing Equation 3.4 into 3.3 and solving for λ_r, Equation 3.5 is obtained.

$$\lambda_r = L_m I_{S\phi} \qquad (3.5)$$

and therefore it can be seen that $I_{S\phi}$ controls rotor flux directly.

Since R_r'/s is the only energy absorbing component (besides stator resistance), it can be deduced that I_{ST} is the torque component. This can also be seen in the following analysis, shown in [14] and repeated here:

Where:

p = the number of pole pairs.

3 = multiplication factor for a three phase machine.

$\omega_m = \omega_s/p$

$$T_{elec} = \frac{P_{airgap}}{\omega_m} = 3\frac{E_r I_r'}{\omega_s/p} = 3p\frac{E_r I_r'}{\omega_s} \qquad (3.6)$$

$E_r I_r'$ = single phase air gap power.

Also since:

$$\overline{E_r} = -j\omega_s\overline{\lambda_r} = j\omega_s L_m \overline{I_{S\phi}} \qquad (3.7)$$

and:

$$I_r' = -\frac{L_m}{L_r} I_{ST} \qquad (3.8)$$

a new expression for torque in terms of I_{ST}, and $I_{S\phi}$ is obtained:

$$T_{elec} = \frac{3p}{\omega_s}(\omega_s L_m I_{S\phi})\left(\frac{L_m}{L_r} I_{ST}\right) = 3p\frac{L_m}{L_r}(L_m I_{S\phi})\, I_{ST} \qquad (3.9)$$

The similarity between the three phase induction motor and the D.C. machine can now be seen. The torque current, I_{ST}, is similar to the armature current (the torque producing constituent), and $I_{S\phi}$

is analogous to the field current (the field flux producing component).

There is another important point to note. Since the voltages across the R_r''/s and $j\omega_s L_m''$ are equal, the following constant relationship shown in Equation 3.10 exists:

$$\frac{R_r'}{s}\left(\frac{L_m}{L_r}\right)^2 \overline{I_{ST}} = j\omega_s \frac{L_m^2}{L_r} \overline{I_{S\phi}} \qquad (3.10)$$

By substituting $\omega_r = s\omega_s$ in this relationship and solving for ω_r, the following expression is obtained:

$$\omega_r = \frac{R_r'}{L_r} \frac{I_{ST}}{I_{S\phi}} \qquad (3.11)$$

From this it can be seen that the relationship, between $I_{S\phi}$ and I_{ST} defines the slip frequency value in steady state. Thus, it can be seen that stator current and slip frequency are the direct control variables for torque control of a three phase induction motor. As a result of this analysis it is possible to employ the speed control scheme and achieve a steady state form of vector control.

3.3 Transient Model and Vector Control

The transient conditions are also discussed thoroughly in [14] (and to a lesser extent in [13]). The results of the analysis in

[14] show that changes in the load or commanded torque produce a transient rotor current (the so called d axis current from generalized machine theory) which in turn yields a sluggish torque response due to the disturbed rotor flux vector. It is also shown that if the flux is kept constant, torque commands follow instantaneously. The conclusion in [14] is that the difference between transient and steady state is that a transient rotor current (with a time constant L_r'/R_r') exists immediately after changes to the rotor flux vector.

Thus, if the rotor flux is kept constant in phase and magnitude (by keeping $I_{s\phi}$ equal to the full load value) the control system would not have to contend with these transient rotor currents. This is the basis for the indirect field orientation scheme as shown in Figure 3.4 and as applied in this thesis. The torque control now becomes a matter of controlling magnitude of I_{ST}^*, the torque command component, and phase compensating the reference stator current, I_S, during these transients. The change in phase angle avoids any alterations in $I_{s\phi}$ that would disturb the rotor flux vector by creating a current transient in the rotor with long time constants [14]. This phase compensation is accomplished by a one-time-only adjustment in the current source inverter frequency (a phase shift of $d\phi$ radians).

The speed control strategy in Figure 3.4 is a simple proportional (P) controller. Thus a steady state speed error will

always exist. This appears in the function block called Torque Control (since torque is the variable being manipulated by this controller) in Figure 3.4. Many other types of speed controllers, such as Phase Locked Loop (PLL) or Sliding Mode Control [26], could be placed in this position of the overall drive control strategy. The output of this control law is the desired motor torque.

Since $I_{S\phi}$ is held constant (constant rotor flux) it is necessary to adjust the slip frequency, ω_r, as the torque component, I_{ST}, is adjusted to comply to the changing requirements in torque. The output of the torque control law is the desired slip frequency. The slip frequency is related to the torque current via the constant expression given by Equation 3.11. As can be seen in Figure 3.4, the torque current, I_{ST}, is fed into two function generators (implemented as look up tables in software). The first one is the vector adder which simply specifies the magnitude of stator current based on the requested torque current. Since I_{ST} flows through a purely resistive component (in Figure 3.3) and $I_{S\phi}$ circulates through an inductive element they have a 90 degree phase shift between them. As a result, they can be resolved into the following instantaneous magnitude and phase representations for stator current:

$$i_s = \sqrt{i_{ST}^2 + i_{S\phi}^2} \qquad (3.12)$$

$$\phi = \arctan\frac{I_{S\phi}}{I_{ST}} \qquad (3.13)$$

Thus the vector adder, in Figure 3.4, calculates Equation 3.12, where as the function generator dϕ, calculates the change in the phase angle, expressed in equation 3.13. Both of these functions are implemented using look up tables in software.

As was the case with constant flux control, the inverter frequency is simply the sum of the rotor speed and desired slip frequency.

The speed/torque control strategy presented in Figure 3.4 is known as indirect field oriented control. In this case the instantaneous rotor flux vector position and magnitude is indirectly controlled by maintaining I_{ST} and $I_{S\phi}$ in a feed forward manner. It should be noted that since this motor controller was intended for traction applications, such as crane drives which do not require field weakening (reducing $I_{S\phi}$ below its maximum value to obtain a weaker field and thus achieve speeds higher than the base while the output torque is reduced), $I_{S\phi}$ is always constant. Thus ω_r and I_{ST} define the motor torque, which is the output of the speed controller.

It should be noted that vector control, as implemented here, is very similar to the Field Acceleration Method (FAM) control

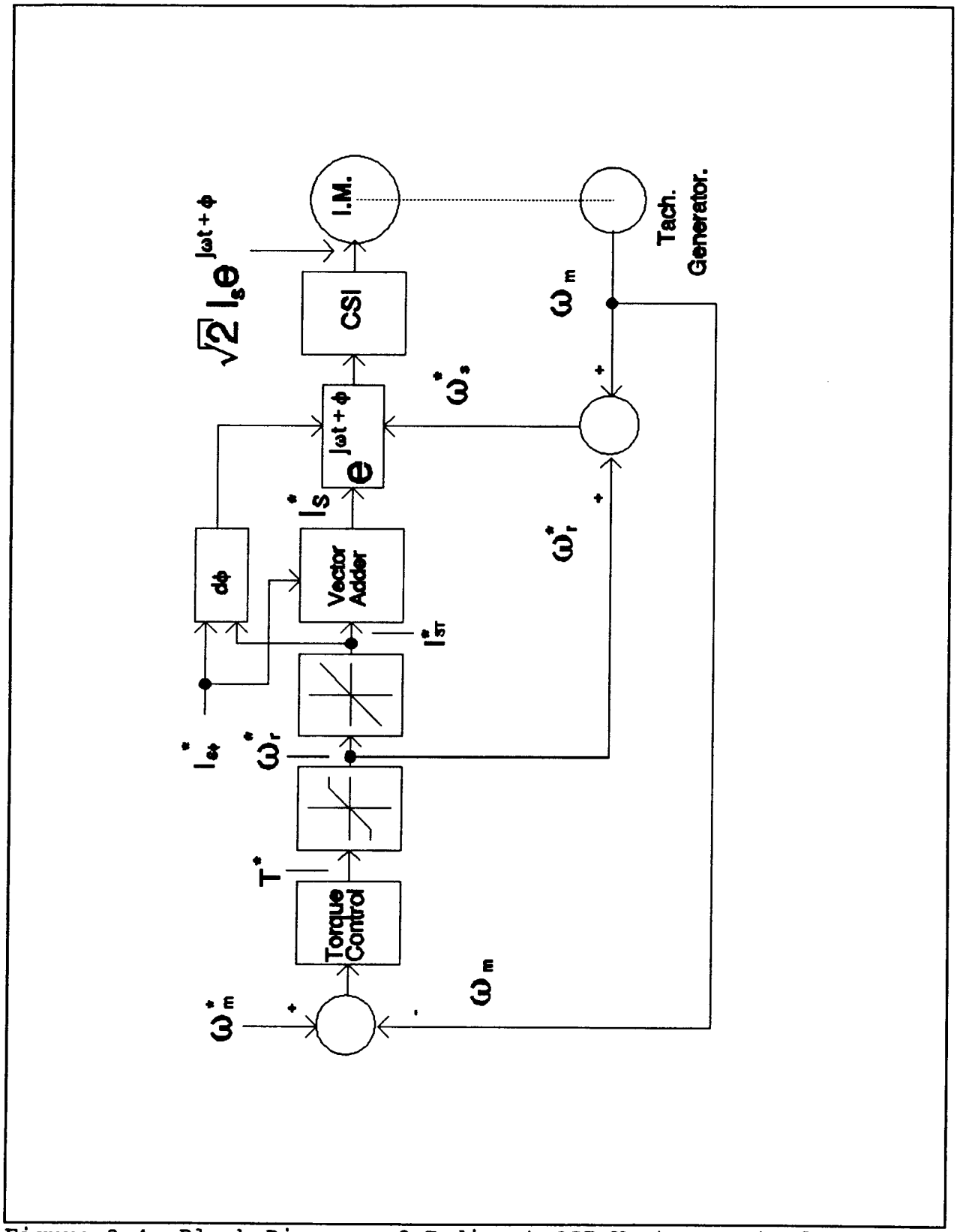

Figure 3.4: Block Diagram of Indirect CSI Vector Control.

scheme as outlined in [18]. Although this method will not be discussed in detail here, the basic philosophy is similar. An effort is made to keep the rotor flux constant and the fundamental stator current continuous (a detailed discussion appears in [18]). This is done by adjusting the phase angle of the stator current when a change in the torque component is requested by the control software in the same manner as FOC.

FOC, as used here, is an indirect field orientation scheme. That is, instantaneous flux angle is not directly measured, or even calculated in real time (based on the terminal conditions of stator current and voltage). Instead the slip relationship from Equation 3.11 is used in a feed forward manner to maintain field orientation. This has the limitations of being machine parameter dependent [13,14,20,21]. It can be seen from Equation 3.11 that if R_r' or L_r change (as they are very prone to do) the relationship between slip frequency and torque current changes. This degrades the performance of the vector controller since the software look up tables, as implemented here, do not compensate for the changes. There are many papers written on the topic of parameter sensitivity ([13,14,20,21] to mention a few) and the adaptive control methods used in combating the problem.

3.4 Summary

This chapter was an explanation of the indirect vector control methodology that could be used in a microcontroller based CSI-IM drive. As can be seen from the analysis in this chapter, decoupling the stator current of the induction machine into flux-producing and torque-producing components makes it possible to have the highly desirable D.C. machine like control. This is advantageous since the induction machine is one of the simplest and most robust rotating electric machines. Combining this ruggedness with excellent dynamic control makes the induction machine ideal for many high performance industrial applications.

CHAPTER 4

DESIGN OF THE CURRENT SOURCE

4.1 Introduction

For a CSI-IM drive to have good dynamic performance, the front end current source must be responsive to quick changes in reference signals and load conditions. To this end one needs to properly size the link inductance and to choose a link current controller that is responsive and stable. As was the case with the torque controller, there are many options for the link current control scheme. Two methods are chosen here in order to demonstrate the flexibility of the microcontroller. These schemes are the simple Proportional-Integral (PI) control and a relatively more complex procedure involving Direct Model Reference Adaptive Control (DMRAC) with back emf compensation. Using two different methods not only demonstrates the microcontroller's adaptability, but also provides two options (a simple, inexpensive, low performance solution and a more complex control law for high performance applications). Thus, the primary objective of this chapter is to describe the design of the front end current source, which feeds regulated current into the inverter of the microcontroller based CSI-IM drive.

There have been several different models of the d.c link used in link-current controller design [8,13,17]. One version is shown in Figure 4.1. This model is the starting point for the control law derivation and link inductance sizing in this thesis.

A simplified equation describing the relationship between the converter voltage, v_r, and link current is:

$$v_r=(L_l + 2L_{ls}) * \frac{di}{dt} + (R_l + 2R_s) * i + Dis(t) \qquad (4.1)$$

Where Dis(t) is a disturbance term (an unpredictable term which changes depending on the current operating point of the motor) used to represent the unknown impedance within the motor. Here the effects of two series combinations of the parallel magnetizing inductance and rotor impedance can be treated as an unknown since the slip varies greatly over the normal operating range [16,17]. This relationship can be used as a basis for the following sections.

4.2 Sizing the d.c. link inductor

To take advantage of the motor-terminal short-circuit ride through capability that a CSI drive could have, one should size the link inductance accordingly. Consider the following simple model shown in Figure 4.2.

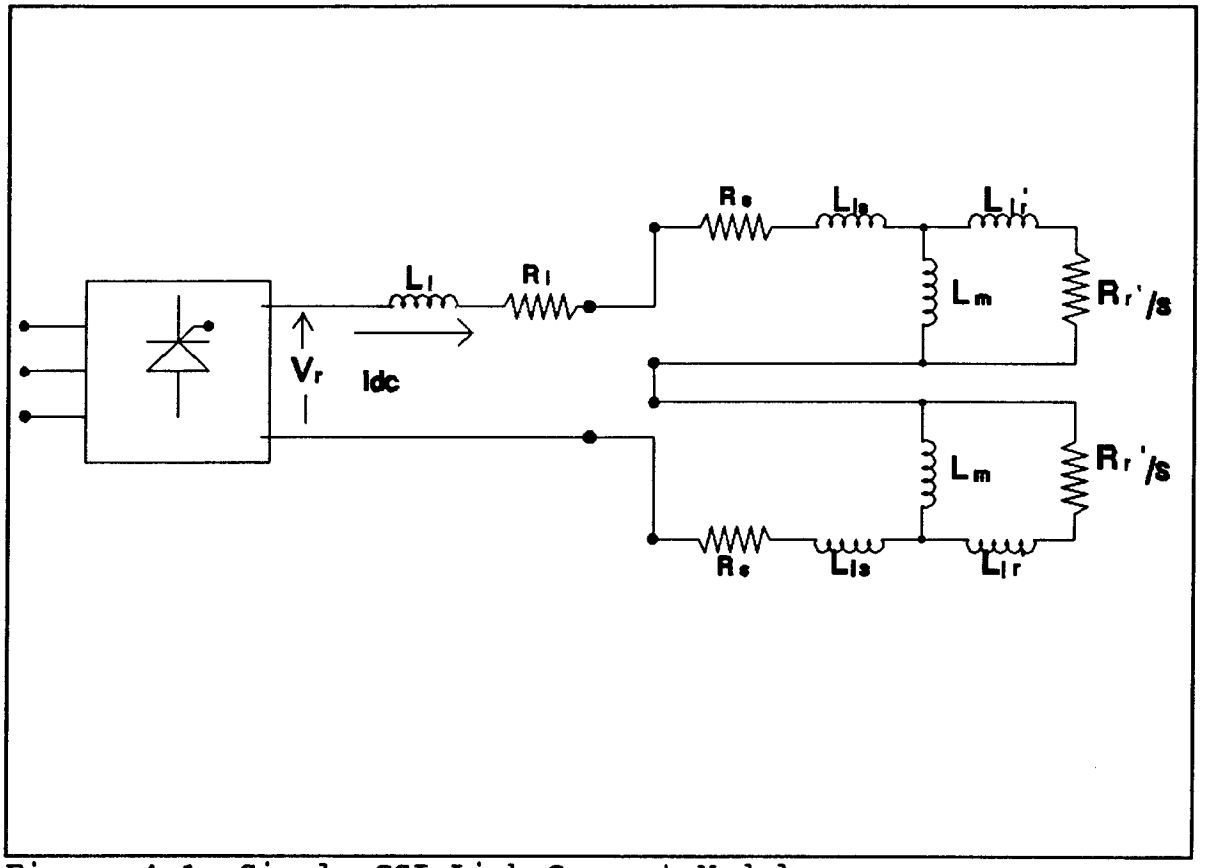

Figure 4.1: Simple CSI Link Current Model

If the following assumptions are made it is easier to analyze the short circuit:

- Resistance is small and can be neglected with negligible repercussions.
- E changes from approximately V_{ab} in magnitude at $t = 0^-$ to zero (short circuited rotor terminals) at $t = 0^+$.
- The system must wait T_s seconds (the sampling period) before the

control can sense the short circuit and take appropriate action.

- The response time of the phase controlled bridge is short when compared to that of the inductive link circuit.

Rearranging the differential equation 4.1 (considering the motor terminal short circuit removes the motor impedance parameters) the following is obtained:

$$v_{ab}=L_1*\frac{di}{dt} \qquad (4.2)$$

If i(t) is solved for with a sinusoidal voltage applied the result is:

$$i(t)=-\frac{V}{\omega_s*L_1}*\cos(\omega_s*t)+i(0^+) \qquad (4.3)$$

From this equation the maximum value of current that is realized after the short circuit can be calculated. This occurs at:

$$\cos(\omega_s*t)=-1 \quad ie \quad \omega_s*t=180^\circ$$

and has a value of:

Equation 4.4 can be solved to give a suitable minimum value for the

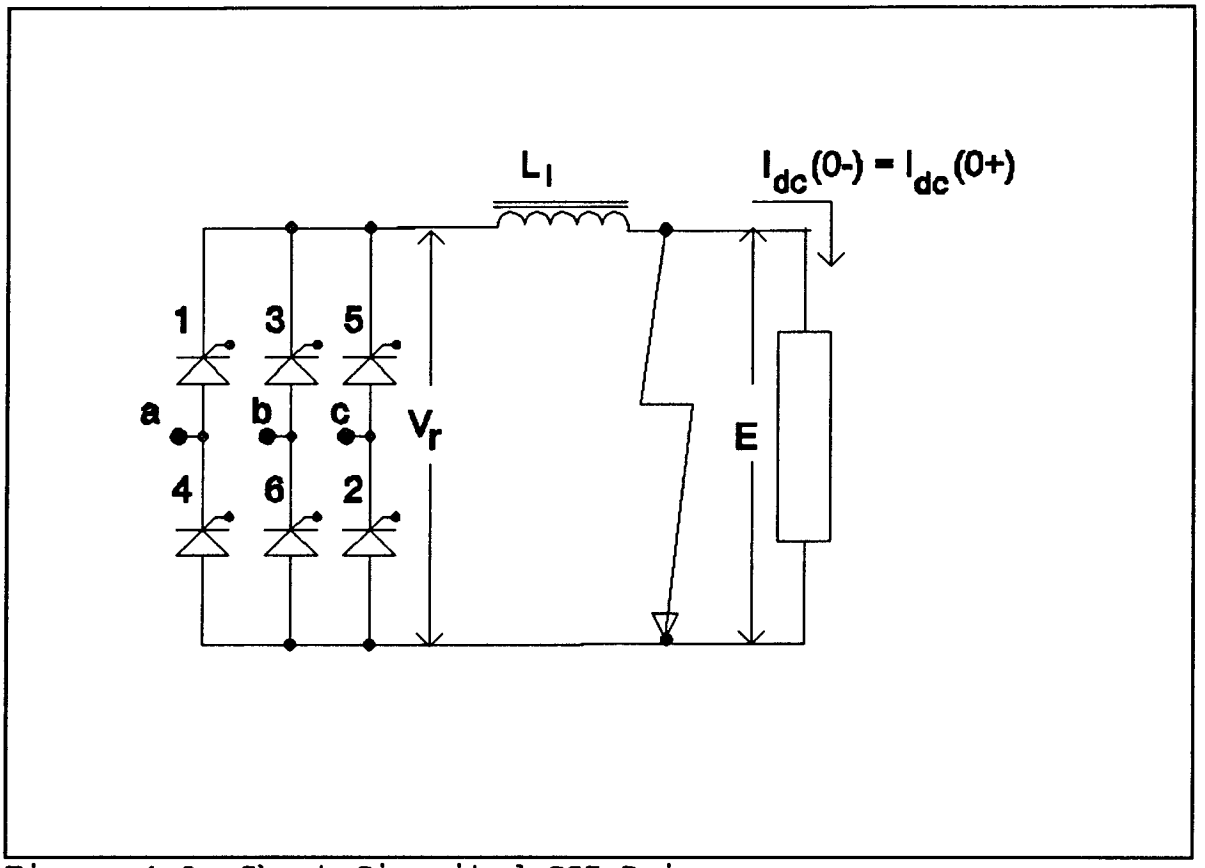

Figure 4.2: Short-Circuited CSI Drive.

link inductance, L_l:

$$L_{min} = \frac{V}{\omega_s * [I_{max} - i(0^+)]} \qquad (4.5)$$

This gives a starting point to determine the inductance based on the aforementioned criteria. For the motor and drive system used in this thesis the following parameters will be used:

$V = \sqrt{[2]}*208$ Volts

ω_s = 377 rads/second

$i(0^+)$ = 15 Amps. (Worst Case)

$I_{max} = 3*i(0^+)$ = 45 amps. (maximum tolerable current for the converter thyristors)

Now based on equation 4.5 the following minimum inductance is obtained:

L_{min} = 26 mH

If the inductance was chosen below 26 mH, the short circuit current will be above the maximum allowed value (of 45 Amps. in this case).

To narrow the selection of link inductance even further, it is possible to specify a minimum value of link current response time and a maximum link current ripple (at, say, full load conditions). This was not attempted in this thesis and a value of 40 mH was chosen based on the minimum acceptable inductance and empirical measurements of the ripple current at full load. Now some different control methodologies will be investigated.

4.3 Simple PID control

Figure 4.3 shows the functional control block for the control system using this simple strategy.

The PID controller works on the link current error signal ($e(t) = I_{dc}^* - I_{dc}$) as follows:

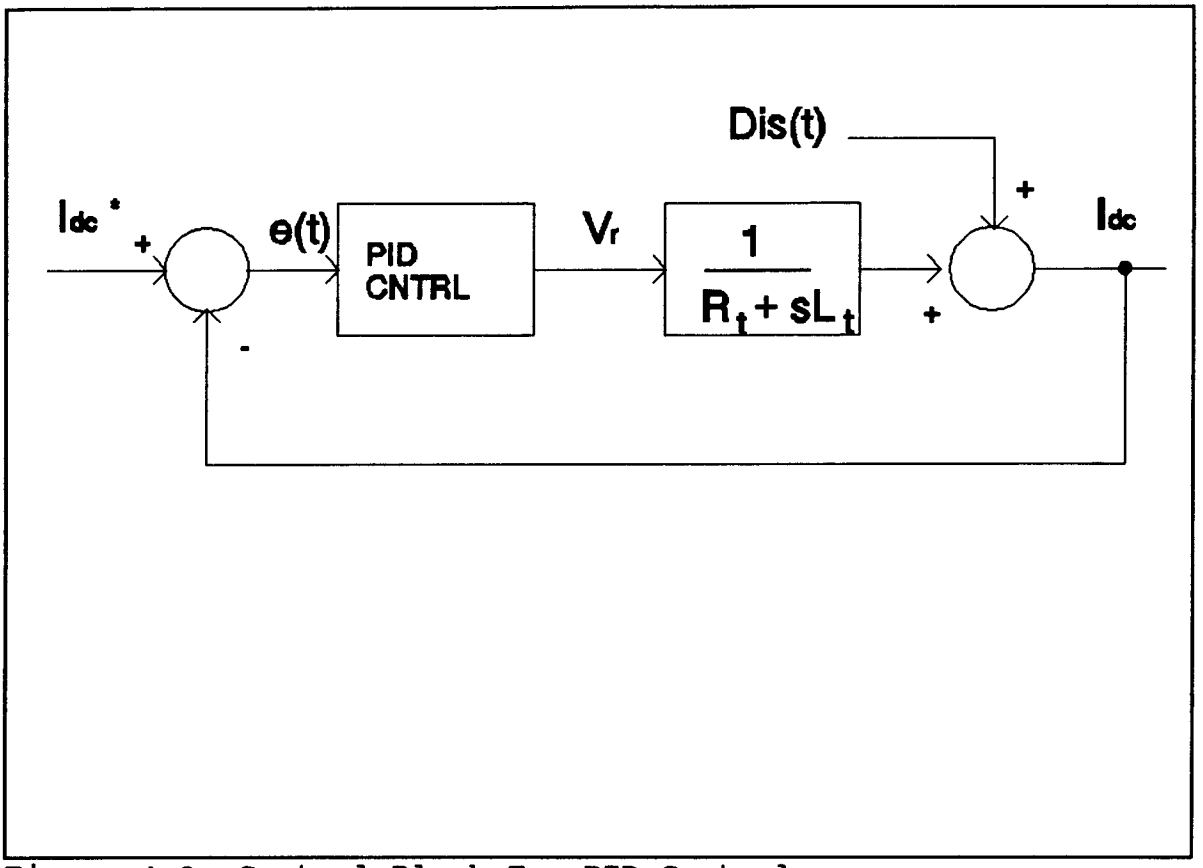

Figure 4.3: Control Block For PID Control

$$V_r = K_p * e(t) + K_i * \int e(t)\,dt + K_d * \frac{d}{dt} e(t) \qquad (4.6)$$

K_p, K_i, and K_d are the proportional, integral, and derivative gains respectively. The control law is used in its incremental digital form:

$$V_r(k) = V_r(k-1) + K_p[e(k) - e(k-1)] + T_s*K_i*e(k) + \frac{K_d}{T_s}[e(k) - 2e(k-1) + e(k+2)] \quad (4.7)$$

Since the disturbance term, Dis(t), is so large (ie the value of slip can change drastically over the normal operating range and thus large disturbances in link current would be part of the standard mode), good dynamic performance must be sacrificed (the system must be de-tuned by lowering the gains) in order to maintain system stability under all operating conditions. Now any changes in reference link current will have an even more pronounced lag effect on the accompanying actual link current. The controller response can be improved greatly if most of the disturbance term can be removed [16,17]. If the disturbance term is divided into two parts, those signals which can be quantified and those which are random, the following is obtained:

$$Dis(t) = emf(t) + Dis'(t) \quad (4.8)$$

The signal emf(t) is a back-emf term which can be quantified (as shown in [16,17]) and Dis'(t) represents the non-predictable disturbances). Non-predictable disturbances are influences on a controlled system which makes feedback adjustments necessary. These are forces which the control system has no way to measure or predict. In this case these are the ever changing machine parameters of the induction machine model used to derive the control laws. As shown in [17] the following d.c link equation (see

Appendix B for derivation) exists:

$$v_r(t) = R_T * i_{dc} + L_T \frac{di_{dc}}{dt} + emf(t) \quad ; Dis'(t) = 0.0 \quad (4.9)$$

Therefore, if back emf term is included as a feedforward term in the control law, faster dynamic response can be achieved. This will occur since changes in the back-emf can be compensated for immediately, thus avoiding the lag in compensation which is inevitable with a feedback control system (the error must exist for some period of time before it is reacted to). This was demonstrated in [16,17]. The terms R_t and L_t represent total circuit resistance and inductance, respectively, and are strongly influenced by the operating conditions of the drive system (rotor resistance as well as the other circuit parameters are known to vary widely as a function of temperature) [20,21]. Thus, an adaptive control strategy could be employed to compensate for these relatively slow variations in circuit parameters.

4.4 Direct Model Reference Adaptive Control

This proposed control scheme does not use a complicated dynamic model (the back emf term is removed independently of this control signal). Instead a PID feedback and PD^2 feedforward controller, both with directly adjustable gains, is used. All control laws are developed to make them computationally very fast.

Performance-based controllers (ie adaptive controllers), unlike standard model-based control systems, do not require precise knowledge of the plant dynamic model and parameters [24,25]. Thus, the control system performance is not affected by the validity of the plant model (parameters and order of the model [19]). This is particularly advantageous for an induction machine where the parameters R_s, L_{ls}, L_m, L_{lr}', R_r, and indeed the load itself (the slip term, s, reflects the load condition) are known to change widely with time.

The control laws used here were first developed for position control of a robot manipulator. They were adapted for use here by substituting the non-linear (recall back-emf term) time-varying link current model for the highly non-linear and time-varying robot plant model. In [19] the manipulator arm position is the controlled variable, where as here it is link current. In an attempt to remove the effects of the back emf, a feedforward type control is used digitally, in a manner similar to the analog version seen in [17]. This has the desirable effect of reducing the model to a simple R-L load whose parameters vary slowly with time (relative to the faster microcontroller). Thus the objective here will be to adjust the link-current control-law gains in real time such that the response of the total controlled system is acceptable (ie faster than PID control). The link current and voltage can then be said to have the following continuous relationship:

$$v_r(t) = f(t) + [K_0(t) + K_1(t)\frac{d}{dt}]e(t) \\ [q_0(t) + q_1(t)\frac{d}{dt} + q_2(t)\frac{d^2}{dt^2}]I_r^*(t) \qquad (4.10)$$

It should be noted that $V_r(t)$ is the applied d.c. voltage signal. Where as e(t), the link-current error, is the difference between reference current, $I_r^*(t)$, and measured current, $I_{dc}(t)$. The term $I_r^*(t)$ is a reference current that the system should follow. $I_r^*(t)$ was chosen to be an exponentially filtered version of the reference current as specified by the outer control law (either flux or vector control). An exponential reference was chosen since it is close to the expected response from the first order R-L link circuit. If step changes in $I_r^*(t)$ were allowed directly into the control law, the gains would be continually increased by the adaption laws in an attempt to have the system match the reference. This is physically impossible for a first order R-L circuit, with limited input voltage. The final result would be an over-responsive and unstable system. This would occur since the large gains would have the plant oscillating back and forth between full positive and full negative voltage. Thus, the choice of $I_r^*(t)$ must be something that is reasonable and physically obtainable for the actual circuit.

The auxiliary signal, f(t), includes an integrator term to improve tracking performance.

The term:

$$[K_0(t) + K_1(t)\frac{d}{dt}]e(t)$$

is a PD feedback controller with adjustable gains, $K_o(t)$ and $K_1(t)$ that operate on the link current error, e(t), and its derivative (d/dt{e(t)}) term.

The third term:

$$[q_0(t) + q_1(t)\frac{d}{dt} + q_2(t)\frac{d^2}{dt^2}]I_r^*(t)$$

has adjustable feedforward proportional ($q_o(t)$), derivative ($q_1(t)$), and second derivative ($q_2(t)$) gains. They operate on the reference signal, $I_r^*(t)$, and its first and second derivatives.

The controller adaptation laws should ensure asymptotic tracking of the reference signals [19] are based on the weighted error signal:

$$r(t) = [W_p + W_v\frac{d}{dt}]e(t) \qquad (4.11)$$

and are as follows:

Auxiliary Signal:

$$f(t) = f(0) + \delta\int_0^t r(t)\,dt + \rho r(t) \qquad (4.12)$$

Feedback gains:

$$K_j(t) = K_j(0) + \alpha\int_0^t r(t)e^j(t)dt + \beta_j r(t)e^j(t) \quad (4.13)$$
$$j = 0,1$$

Feed forward gains:

$$q_j(t) = q_j(0) + \gamma_j\int_0^t r(t)I_r^j(t)dt + \lambda_j r(t)I_r^j(t) \quad (4.14)$$
$$j = 0,1,2$$

With j representing the jth derivative. The constants δ, α, γ are positive scalar integral adaptation gains where as ρ, β, λ are zero or any positive proportional adaptation gain.

The terms W_v and W_p are positive scalar weighing factors which reflect the relative significance of the position and velocity errors e(t) and d/dt{e(t)} in producing the weighted error signal r(t).

The proof of stability is via Lyapunov-Based Model Reference Adaptive Control (MRAC) techniques. Please see [19] for the details of the derivation and stability analysis.

From an implementation point of view the auxiliary signal, f(t), is a constant gain PID feedback controller driven by the link-current error, e(t). The above relationships can be rearranged into another form which will make it easier to use in our controller:

$$f(t) = f(0) + \rho\left[W_p + W_v\frac{d}{dt}\right]e(t) + \delta\int\left[\left(W_p + W_v\frac{d}{dt}\right)e(t)\right]dt \tag{4.15}$$

or

$$f(t) = f(0) + [\rho W_p + \delta W_v]\,e(t) + \rho W_v\frac{de(t)}{dt} + \rho W_p\int e(t)\,dt$$

Thus, the result is a PID feedback controller and a PD^2 feed forward controller:

$$V(t) = V(0) + \left[\overline{K_p} + \overline{K_i}\int dt + \overline{K_v}\frac{d}{dt}\right]e(t) \left[q_0 + q_1\frac{d}{dt} + q_2\frac{d^2}{dt^2}\right]I_r^*(t) \tag{4.16}$$

with

$$\begin{aligned} \overline{K_p} &= K_0 + \rho W_p + \delta W_v \\ \overline{K_i} &= \delta W_p \quad ;a\ constant \\ \overline{K_v} &= K_1 + \rho W_v \end{aligned} \tag{4.17}$$

From a digital implementation point of view, an approximate version of the above control law (including the back-emf term) is as follows:

$$
\begin{aligned}
V_r(k) \quad = \quad & V_r(k-1) + K_{pp}(k)\,[e(k) - e(k-1)] + K_{ii}(k)\,e(k) \\
& + K_{vv}(k)\,[e(k) - 2e(k-1) + e(k-2)] \\
& + q_{00}(k)\,[I_r(k) - I_r(k-\,)] + q_{11}(k)\,[I_r(k) - I_r(k-1) + I_r(k-2)] \\
& + q_{22}(k)\,[I_r(k) - 3I_r(k-1) + 3I_r(k-2) - I_r(k-3)] \\
& + emf(k)
\end{aligned}
\tag{4.18}
$$

The term emf(k) was developed for an analog system in [17] and is used in the following digital approximation form:

$$
emf(k) = [K_a\omega_m(k) + K_b f_r(k)]\,K_c\frac{f_r(k)}{I_{dc}(k)} \tag{4.19}
$$

The derivation of the law and the gains K_a, K_b, K_c can be found in [17] and is repeated in Appendix B in the interest of completeness.

The adaptation laws were also implemented digitally using the following approximations of the continuous relationships [19]:

$$
\begin{aligned}
K_{pp}(k) &= K_{pp}(k-1) + \alpha_{00}[e(k)r(k) + e(k-1)r(k-1)] \\
&\quad + \beta_{00}[e(k)r(k) - e(k-\,)r(k-1)] \\
K_{vv}(k) &= K_{vv}(k-1) + \alpha_{11}[\frac{de(k)}{dt}r(k) + \frac{de(k-1)}{dt}r(k-1)] \\
&\quad + \beta_{11}[\frac{de(k)}{dt}r(k) - \frac{de(k-1)}{dt}rZ(k-1)]
\end{aligned}
\tag{4.20}
$$

$$q_{jj}(k) = qjj(k-1) + \gamma_{jj}\left[\frac{d^j I_r(k)}{dt^j} r(k) + \frac{dt^j I_r(k-1)}{dt^j} r(k-1)\right] T_s^j$$

$$\beta_{jj}\left[\frac{d^j I_r(k)}{dt^j} r(k) - \frac{d^j I_r(k-1)}{dt^j} r(k-1)\right] T_s^j$$

$$j = 0, 1, 2$$

The adaptation gains α_{xx}, β_{xx}, γ_{jj}, λ_{jj}, W_{pp}, W_{vv} were all determined empirically. Thus, not only did the control laws have to be given some reasonable value of gain to start from, the adaptation gains can only be determined experimentally. This is one of the major criticisms with this type of adaptive control. The other problem is the long term drift the gains have as a result of some small finite error signal. This error signal could be a result of plant saturation or quantization effects realized through integer mathematics. One way to try and control long term drift is to use a small dead band for the weighted error. This of course has some negative repercussions, namely, decreased response times for the adaptation of controller gains. It should also be noted that since this thesis was not an attempt to defend the ideas of DMRAC, just to employ them in an integrated drive system, no theoretical basis for the adaptive control method will be put forward.

4.5 Summary

In the interest of having the current source, which feeds the CSI, respond quickly to changes in load conditions and reference current levels, the sizing of the link inductor and control law strategies were discussed. It was noted that a minimum value of inductance would allow the CSI-IM control system to handle a short-circuit, without allowing the current to reach destructive levels. Two different link current control laws (PI and DMRAC with back emf compensation) were discussed in the interest of showing the agility of the microcontroller in accepting different control strategies. The details of the software and hardware implementation of the link current controller appear in Chapter 5. The experimental results of using these control laws to run the CSI-IM drive system appear in Chapter 6.

CHAPTER 5

MICROCONTROLLER DESIGN CONSIDERATIONS: HARDWARE/SOFTWARE

5.1 Introduction

One of the main advantages of using a powerful microcontroller, such as Intel's 80196KC (a detailed description can be found in [22]), is the substantial saving in peripheral interface devices. This particular controller is well suited for A.C. motor control since it has features such as ten built in sample-and-hold analog-to-digital converters, high speed outputs and inputs, 28 interrupt sources, two built in 16 bit timers, and a fast multiply and divide ability. Thus, if one can fully utilize all of these functions, hardware can be minimized, with the advantage being increased robustness. Increased ruggedness is realized through reducing the number of electrical hardware components (therefore reducing the probability of complete system failure) and vulnerability to electrical noise (the communication between control systems is within a single chip and not along less shielded circuitry).

This chapter has two objectives. The first one is to explain

the lay out of the hardware components that form the controller portion of this microcontroller based CSI-IM drive. The other goal is to explain the modular software lay out and how the different subroutines communicate with one another.

5.2 Hardware

A block diagram showing the basic lay out of the controller and the interface circuits (connection to the power components) is shown in Figure 5-1. From the diagram it is possible to see that, 80196KC aside, there are five different interface functional blocks: speed, d.c link current, zero crossing detection (ZCD), converter, and inverter signals.

The speed signals are the result of two quadrature pulse trains that come directly from a 1000 pulse per revolution generator (which is mounted on the drive shaft). This signal is processed in two ways. First, the two quadrature signals are fed into a type "d" flip-flop (one into the data terminal the other into the clock) and subsequently relayed into a high-speed input to determine the motor direction. The second processing function is to XOR the two signals together to give 4000 rising and falling edges per motor revolution. This higher frequency signal is fed directly into a counter of the Intel 80196KC. The counter is read and reset at each sampling instant of the speed control algorithm (1/8 of a second in this case). Thus, knowing the number of pulses

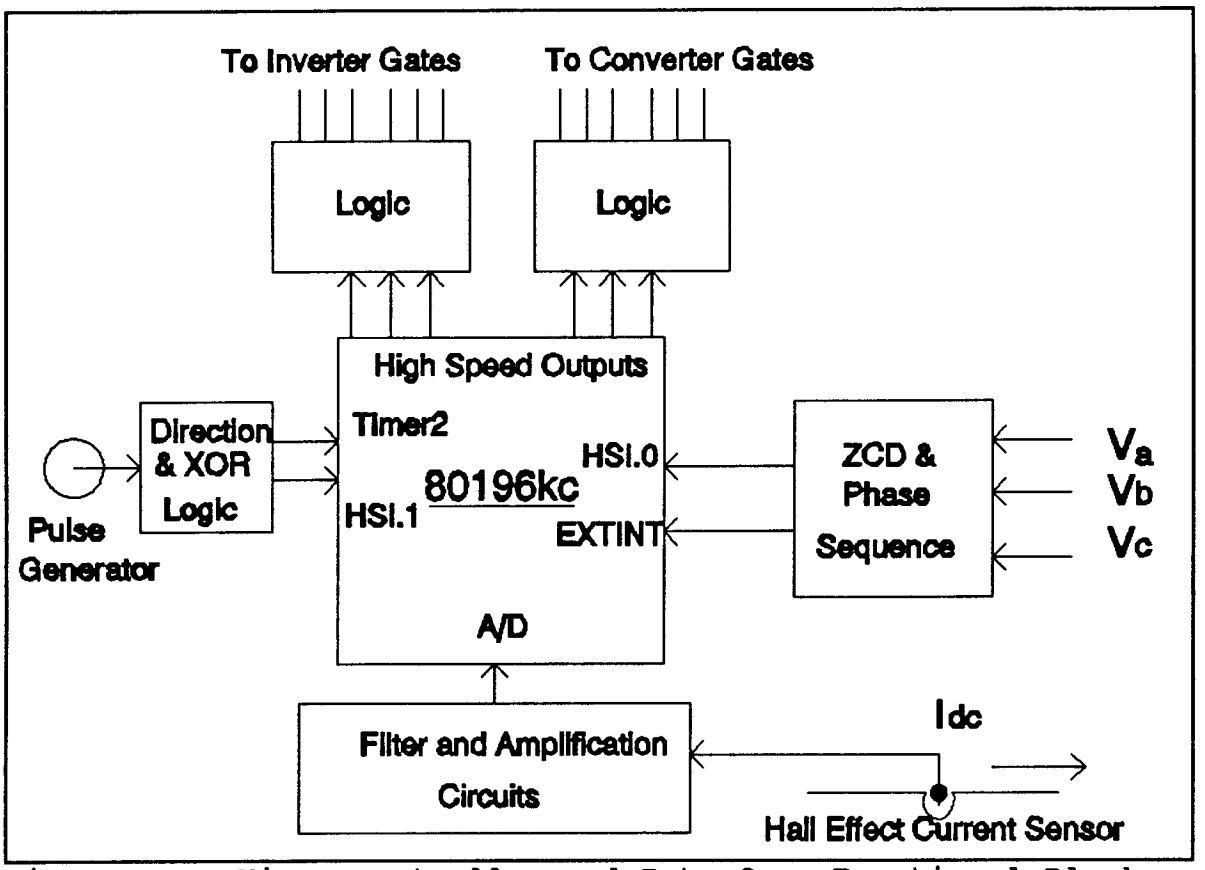

Figure 5.1: Micro-controller and Interface Functional Blocks.

per sampling period, the sampling rate and the number of pulses per revolution, the mechanical speed of the rotor can be calculated in software (by the microcontroller). Also, since this pulse generator has an index pulse, rotor position can be determined fairly accurately.

The d.c. current sensing circuit consists of a Hall effect transducer, a filter and an amplifier. The signal from the Hall effect sensor is filtered and amplified in such a way that a zero

to 50 Ampere current signal becomes a zero to 5 Volt potential for the A/D converter. The filter time constant is kept small enough to avoid affecting current source performance.

The zero crossing detector (ZCD) functional block accomplishes two tasks. First, the "squared" representation of the voltages V_{ab} and V_{ac} are compared to determine the rotation of the three phase converter supply. The information, which only needs to be sampled once when the CSI is first switched on, is used to determine the gating sequence of the six converter thyristors. This enables the drive to be phase rotation insensitive. The second function of this circuit is to ensure proper timing of the firing delay angle, α, with respect to the positive zero crossing of the supply voltage V_{ab}. Thus, this circuit helps the controller avoid the inevitable timing drift that occurs as a result of timing with microcontrollers.

The converter and the inverter circuit blocks have the same function. These circuits de-multiplex the six signals from the microcontroller's high-speed output cam into the required gating patterns. Thus, these decoded signals become the twelve individual gating signals for both of the controlled thyristor bridges. With a 16 Mhz. microcontroller these signals can be timed down to the one micro-second level. This gives excellent resolution with the firing angle and frequency of the converter and inverter respectively.

5.3 Software

The software is written in a modular fashion and can be represented as shown in the block diagram of Figure 5-2. The important input and output variables of each functional block are also shown.

The initialization and main program blocks have simple tasks to perform. The initialization routine sets up the control registers (this defines the functions of various I/O points), the interrupt masks (enable the interrupts that are to be used in the program and disable the rest) and sets all the data registers to their respective beginning values. This initialization is machine dependent. Since the program is modular and interrupt driven, the main program is only a simple loop. This loop is interrupted when one of the subroutines that belongs to either the current source, speed control or inverter function blocks, requires attention (hardware or software interrupt).

As can be seen from Figure 5-2, the current source functional block has four inputs (reference and measured d.c link current, voltage V_{ab} zero crossing interrupt, and a back emf signal used for DMRAC) and one coded three bit output signal (used to indicate which converter thyristors should be triggered). The current and the back emf (if DMRAC is used) signals are put through one of the

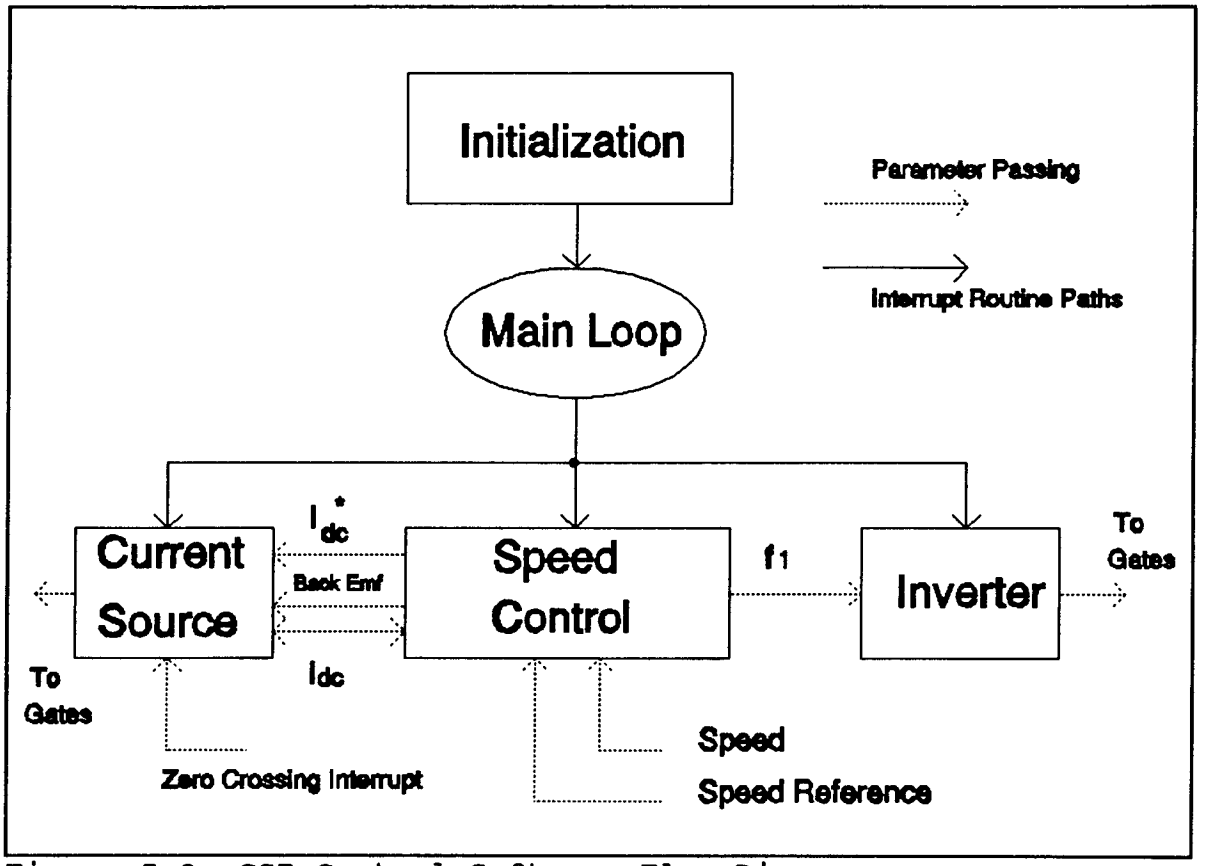

Figure 5.2: CSI Control Software Flow Diagram.

control laws, as outlined in chapter four, at each sampling instant. The output of the control law is the desired converter d.c. link voltage. This potential is related to the firing angle, α, via the expression:

$$V_{dc} = \frac{3}{\pi}\sqrt{2}V_{ab\ rms}COS(\alpha) \qquad (5.1)$$

The firing angle must be solved for in real time. This is

accomplished with an inverse cosine look up table which has an input of V_{dc} and an output of the delay angle, α, represented in microseconds (ie ωt = angle ω = 377 rad/sec at 60 Hz). This linearizes the control process and removes the errors and degraded performance that would be the result of a linear approximation to equation 5.1 . The control law is used once per sampling instant and takes between 50 and 200 microseconds to execute depending on which of the strategies outlined in Chapter 4 is employed. The sampling period, T_s, was chosen to be 2777 microseconds. This was done since there are six different converter states per fundamental cycle to the 60 Hz supply. Thus:

$$\frac{1}{60} Seconds * \frac{1}{6} cycle^{-1} = 2777 \frac{\mu\ seconds}{cycle}$$

$$\therefore \quad T_s = 2777 \ \mu\ seconds$$

Execution of the control law is initiated every T_s seconds through one of the software timers in the 80196KC.

The output of this sub-section is the firing angle, α, which is used by another section of the current source functional block. This other software uses this latest reference firing angle to determine when to output the next converter gating sequence code to the high speed output cam of the 80196KC. These electrical signals

are subsequently relayed via external circuiting to the converter thyristor gates.

The final portion of the current source functional block is the supply voltage, V_{ab}, zero crossing interrupt. This is simply used to correct any errors realized in predicting this timing point. These errors are a result of the round off quantization effect one has to deal with when using integer mathematics in microcontrollers.

The inverter software functional block is a very simple piece of software. It takes the desired reference stator frequency, f_s, from the speed control functional block and inverts it to a reference period. This reference period determines when the next inverter switching state is to be entered into (there are six states per fundamental cycle). The signal to change an inverter state is relayed to the inverter-thyristor gates via the 80196KC's high speed outputs and the external de-multiplexing circuits in much the same way as it was for the converter bridge.

The speed control functional block not only has several input and output variables, but also has a control law based on one of the two strategies outlined in Chapter two and three. The sampling time for this control law has to be slower than that for the other two functional blocks since it provides their reference values and a response time must be allowed for. Since the CSI system is made

up of several highly non-linear and strongly-coupled subsystems, it is difficult, if not impossible, to find an adequate sample time analytically. Thus, the sampling time was determined experimentally. It was found that 0.125 seconds was suitable for fast stable speed response. Similar to the current source functional block, the speed control laws are invoked once per sampling instant when a software timer forces an interrupt. When this occurs a chain of events is triggered. It starts with calculation of the motor speed and determination of the motor speed error. From this point on, the rest of the steps in speed control sequence are different for the two methods (flux and vector control) and are outlined in Chapters two and three.

5.4 Summary

A description of the CSI-IM drive controller hardware and software was presented in this chapter. An attempt was made to minimize hardware by taking advantage of some of the features the I80196KC microcontroller has to offer. The motor speed was obtained using an on board counter and a pulse generator. The reference value of speed and measured value of link current were communicated to the microcontroller through its built-in A/D converters. High speed inputs were used to time the converter gating signals (which in turn are relayed to the thyristors via the HSO cam) to the three phase input supply.

The minimized hardware design was done so that all the control systems could be placed in software in the microcontroller. Although this made the software fairly complex, generous use of small software modules and interrupts breaks the larger task into a series of small independent control systems problems. Each of these smaller systems (converter timing control, thyristor gate firing signals, control laws, sampling instant timing etc.) was then easier to manage.

CHAPTER 6

CONTROL SYSTEMS RESPONSE TESTS

6.1 Introduction

To test the merits of the different control systems previously discussed, the CSI drive was put through a series of transient tests. The goals of this chapter are to demonstrate the experimental microcontroller based CSI-IM drive system and try and draw some conclusions regarding the merits of the control schemes developed in Chapters two through four. Thus the tests are split into two major categories that were designed to focus on the outer (speed/torque) control loop and the inner (link current) control loop:

1) Tests to compare the response characteristics of flux control to vector control.

2) Tests to compare the advantages and disadvantages of proportional integral (PI) control to those of direct model reference adaptive control (DMRAC).

The two outer loop control strategies (flux and vector

control) were put through the following tests that highlight their advantages and disadvantages:

1) Start-up test 0 to 900 RPM.

2) Step change from 750 RPM to 1500 RPM.

3) Regeneration test, -900 to 0 to 900 FOC, and 1200 to 900 for flux control (the inferior flux control is not capable of a complete speed reversal in one step, it requires a series of negative speed step changes, each followed by a stabilization period).

The microcontroller was used as part of the data acquisition system (DAS). The response data presented here were sampled (as will be specified later) at different rates and stored in the 8K byte ram located on the I80196KC development system. They were then transferred to a DOS file through the host computer (used to communicate with the I80196KC development board). The data was scaled and plotted using the program "MATLAB". The scaling was necessary since the integer numbers used in the control laws software are not in standard engineering units. Standard engineering units (Amps, Volts, Radians/Second etc.) are not convenient to use since they must fall in the range: -32768 and 32767 (for a 16 bit number). A good example of this is the link current. The expected range is between zero and fifteen amps. If a

conversion to milli-Amps is done, the new range is between zero and 15,000 milli-Amps. This gives us superior resolution and is better usage of the 16 bit word length available with the microcontroller.

It should be noted that some of the data presented here is affected by electrical noise (caused by the harmonically rich CSI currents) and aliasing (sample frequency is too low to reproduce the original signal properly). The result of this is an output signal that does not appear to be very smooth. In particular, this is noticeable with the link current measurements. Although it was not done in this CSI-IM project, a separate low pass filter could be constructed to facilitate data acquisition of the link current signal.

6.2 Outer Control Loop

6.2.1 Start-up test

The experimental results for the start-up test under FOC are shown in Figure 6.1 to 6.4, whereas those for flux control are shown in Figures 6.5 to 6.7. Each figure has two captions. The upper caption displays the names of the parameters in the figure, whereas the lower one mentions which types of control methodologies were being employed. This data was sampled at a rate of 120 Hz. A faster sampling rate was not possible since the I80196KC

development board has finite space (approximately 7.5K bytes) for the data acquisition results. Although this sampling rate is fast enough for the speed response, it can be seen that the aliasing effect is quit prominent with measured link current. Thus the average value between successive spikes in the current signal should be considered the value of that current at a given sampling instant. This method gives a reasonable approximation to the D.C. level of the link current.

The FOC scheme has a 30% faster rise time for start up response than does flux control. However, it should be noted that both systems use acceleration limiting when the speed error is too large (ie speed error > 300 RPM for FOC, and speed error > 120 RPM for flux control per sampling instant). These additions to the speed control laws were necessary to avoid excessive de-tuning of the simple outer loop P speed control scheme. De-tuning is the reduction in magnitude of a gain, in order to avoid drive system instability, that is actually a result of nonlinearities in the controlled system (which was assumed to be linear). A good example of a nonlinear effect is the finite magnitude of torque current, I_{ST} (which is the output of speed feedback control law) available. The torque current has a maximum value of approximately seven Amps (for the motor used here) and therefore must be clamped at that value. One method of clamping is to limit the maximum speed error in such a way as to avoid having I_{ST} going above seven Amps (this was the method chosen here). The point were the P controller for the FOC

system takes over from the acceleration limiting control can be seen at the 1.5 sec mark on Figures 6.1 through 6.4 (notice the pulse in torque current I_{ST} at the 1.5 second mark in Figure 6.3). This point is not noticeable for the flux control scheme. From the plots of the currents (Fig 6-2 for FOC and Fig. 6-6 for flux control) we can see a fairly good response. The heavy oscillations around the 0.5 to 1.5 sec points are a result of the transient condition that exists in the motor during the step speed change (ie changing instantaneous slip frequency etc.). Fig. 6.3 shows the proportional relationship that exists between torque current and slip frequency, for FOC, which was the result of the adaption to the decoupled equivalent circuit for an induction machine (recall from Chapter 4). Figures 6.4 and 6.7 illustrate the change in inverter frequency for the FOC and flux control methods respectively. Both of these results show similar transient responses. The change in angle phi, seen in Figure 6.4 and explained in Chapter 4, is to avoid changing the rotor flux vector by phase compensating the stator current during inverter frequency changes. This avoids exciting any of the so called "d" axis currents, from generalized machine theory, that retard dynamic performance. This also keeps the flux fields oriented as required (stator and rotor fluxes at 90°) and avoids having to make other, more difficult, real time compensations.

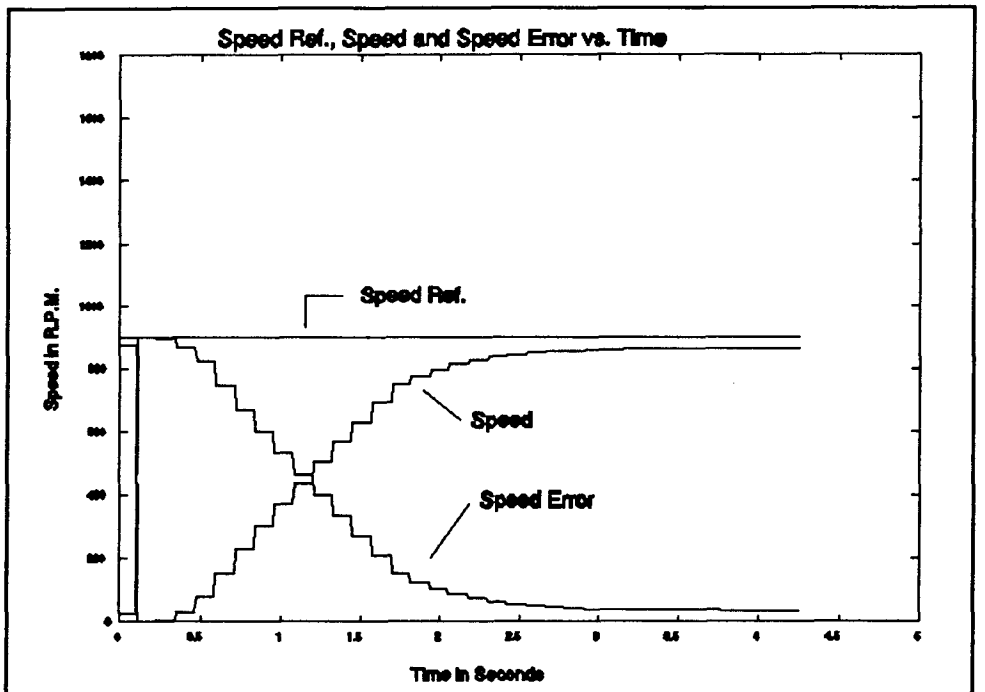

Figure 6.1: Start Up Speed Response of CSI-IM Drive Under FOC & DMRAC.

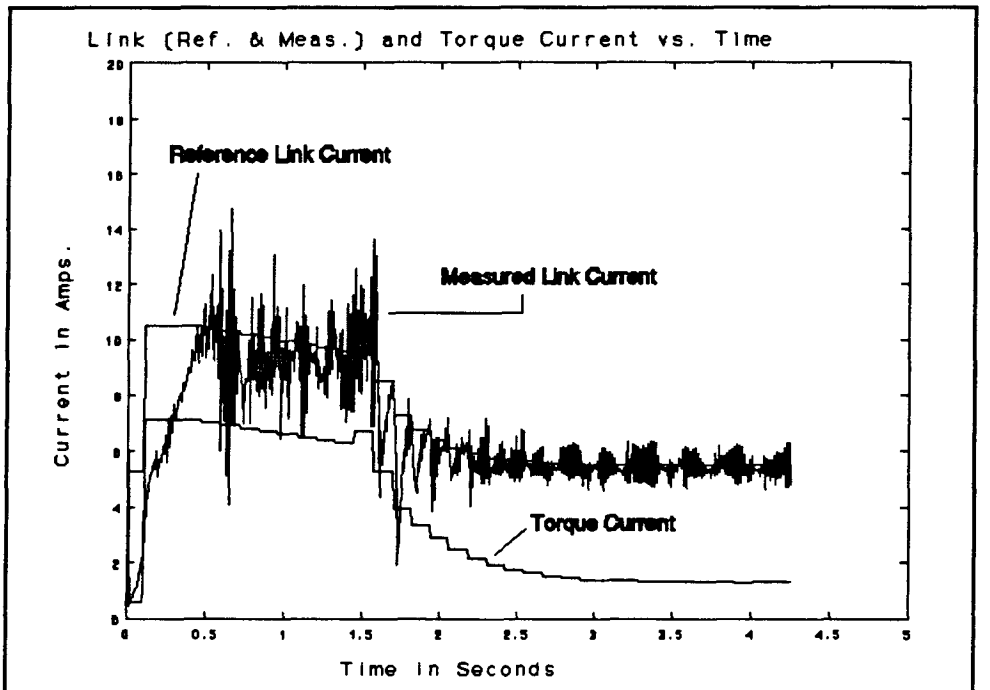

Figure 6.2: CSI-IM Drive Currents From Start up Test under FOC & DMRAC.

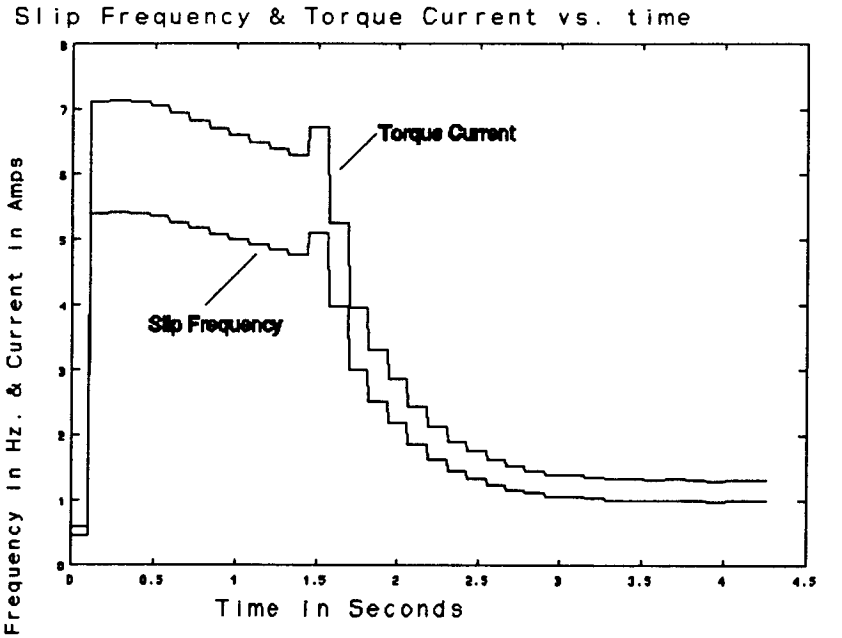

Figure 6.3: Slip Frequency and Torque Currents vs. Time for the Start up test under FOC & DMRAC.

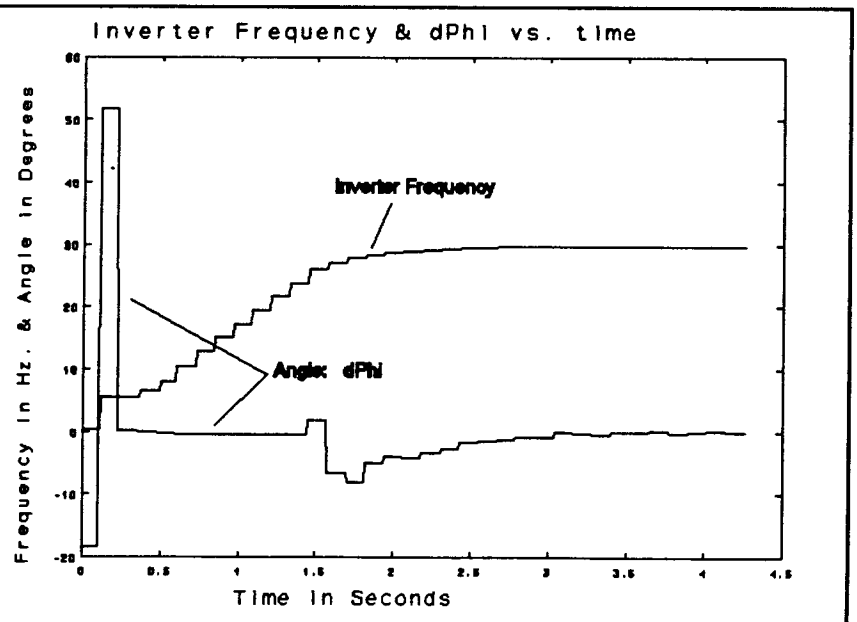

Figure 6.4: Inverter Frequency and Change in Inverter Current Phase Angle, dphi, vs. Time for the Start up Test under FOC & DMRAC.

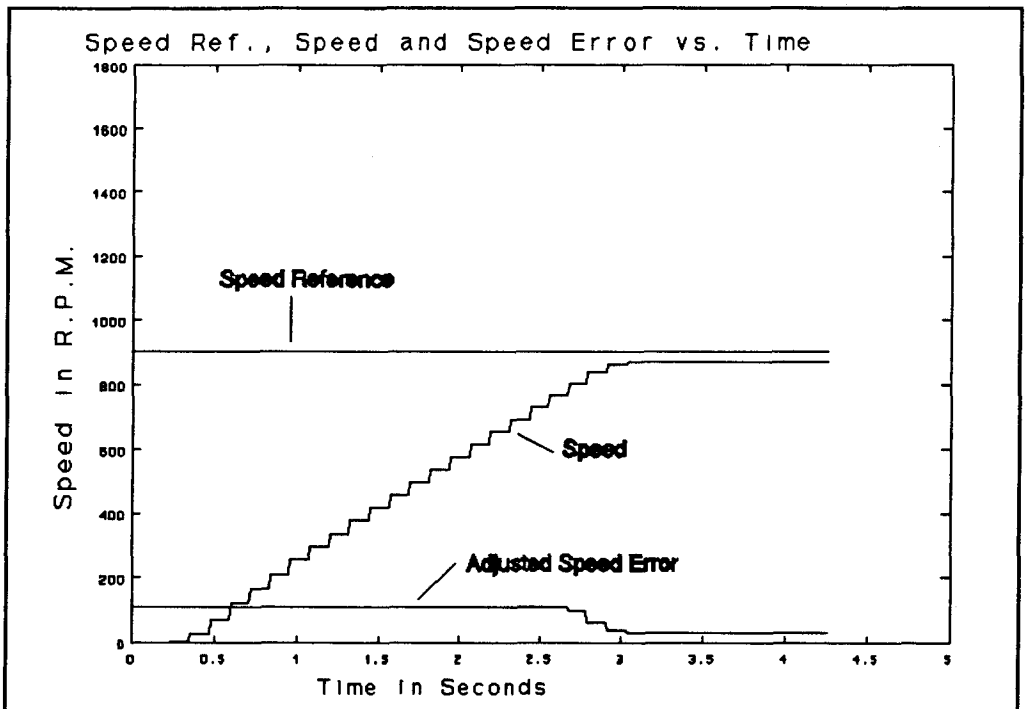

Figure 6.5: Flux Control & DMRAC Start up Response.

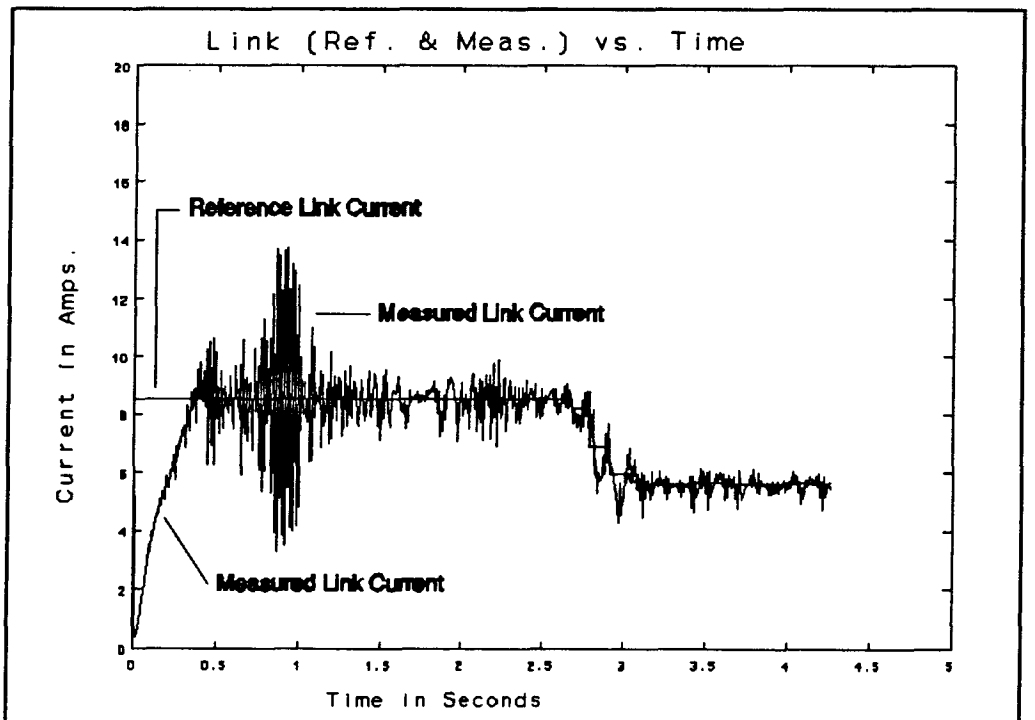

Figure 6.6: Flux Control & DMRAC Start up Response.

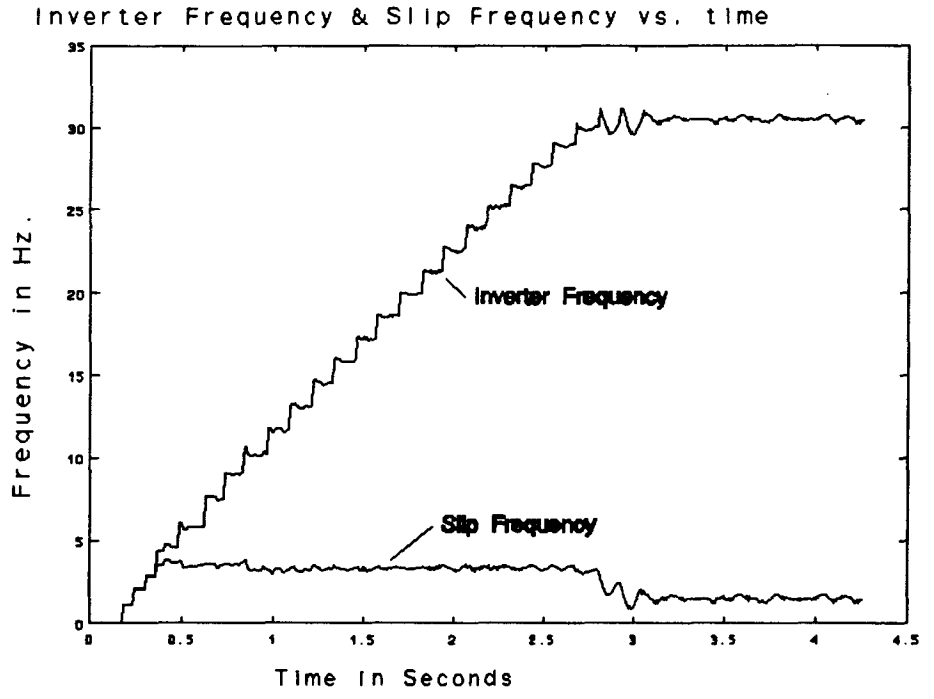

Figure 6.7: Flux Control & DMRAC Start up Response.

6.2.2 Step Change

This test was performed over the range 750 to 1500 RPM for FOC (see Figure 6.8), and 750 to 1200 RPM for flux control (see Figure 6.12). This difference in step sizes necessary, illustrates the much inferior performance of the flux control. Any step changes larger than this can cause large destructive currents, that the relatively slow thyristor converter cannot compensate for. These large currents can be seen in Figure 6.13, the flux-control link current response. There is a large current fluctuation at the start

of the step change in speed. The large drop in current at the beginning of the transient stage is due to the increase in slip frequency, which was required to accelerate the motor. Although the link current does dip at the start of the acceleration period for the FOC case (see Figure 6.9), it is much smaller than for flux control. This superior performance is mainly due to the feed forward compensation to inverter angle Phi that takes place during torque current transients. Since the current dip results in a retarded torque and hence speed response it is necessary to try and control it (as FOC does). Again, with the FOC method there are large changes in the angle phi at the start of the transient period. Here the control system is trying to force the rotor flux vector to be constant, thus, allowing a smoother acceleration period. Again, the overall conclusion is that FOC has demonstrated superior performance.

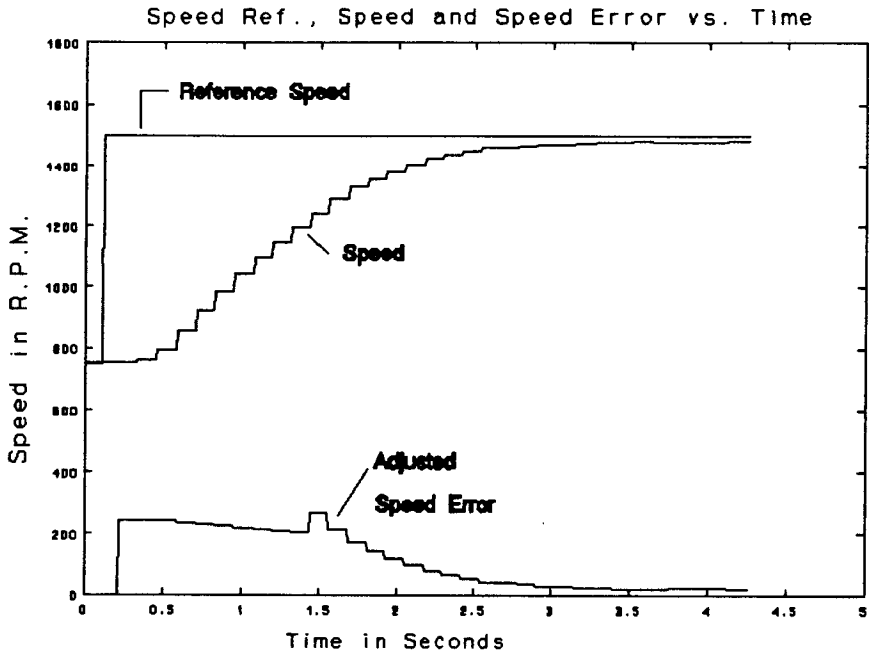

Figure 6.8: Speed Step Change Response under FOC & DMRAC.

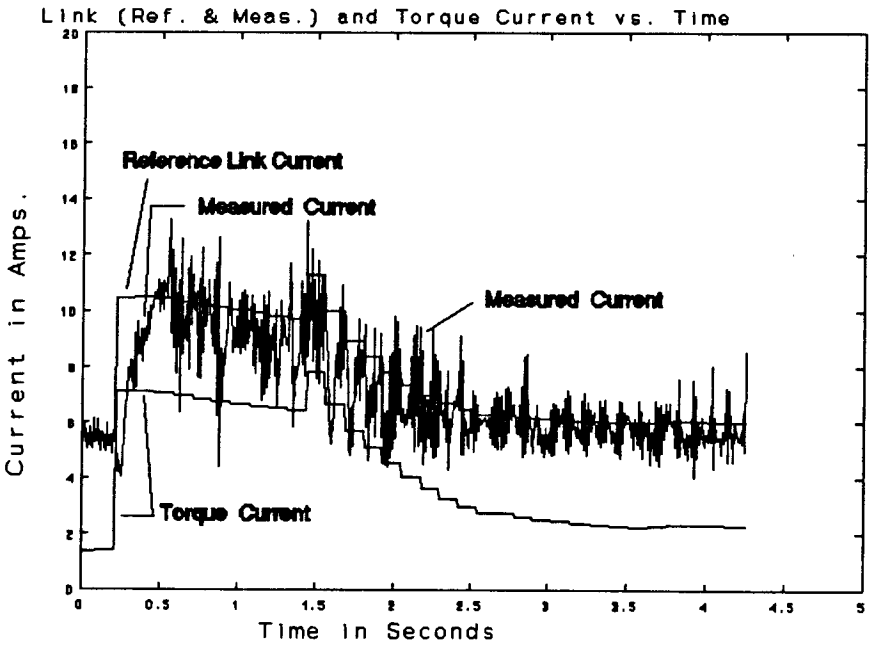

Figure 6.9: Speed Step Change Response under FOC & DMRAC.

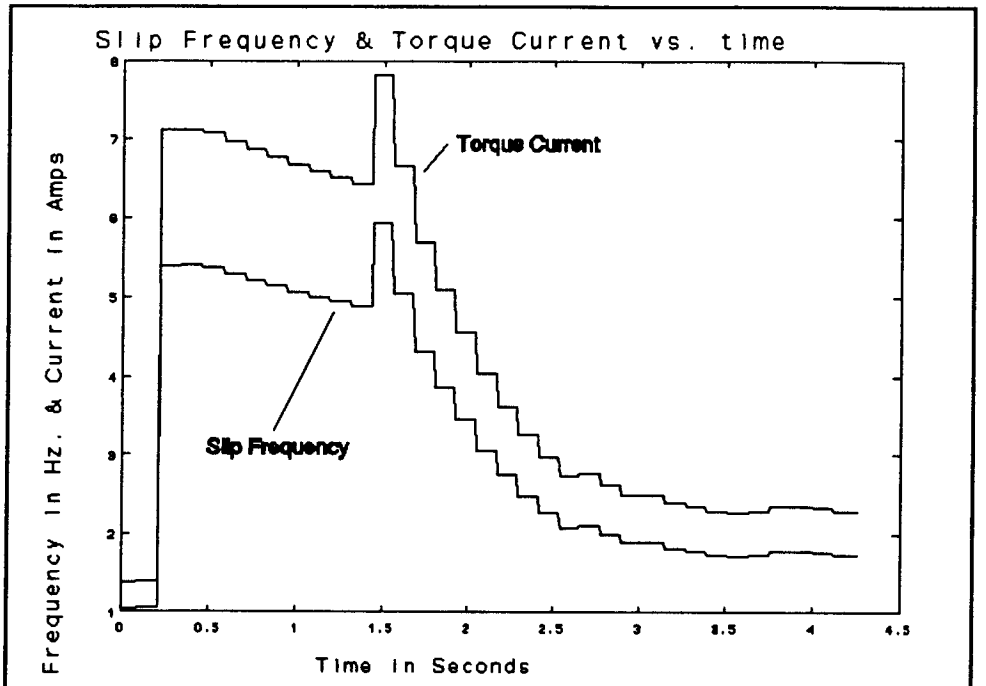

Figure 6.10: Speed Step Change Response Under FOC & DMRAC.

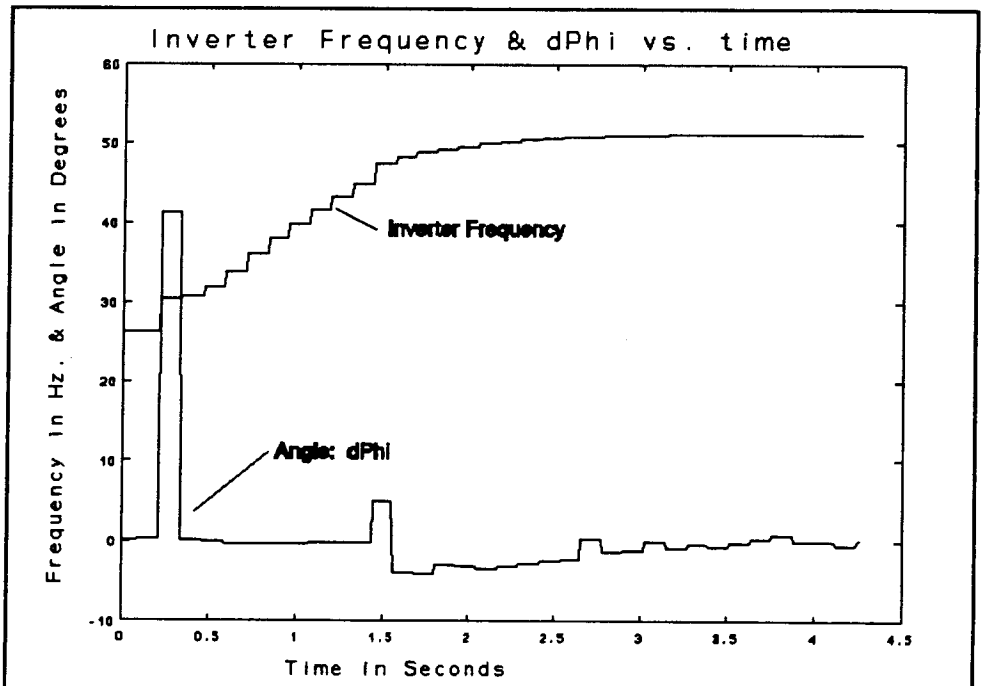

Figure 6.11: Speed Step Change Response Under FOC & DMRAC.

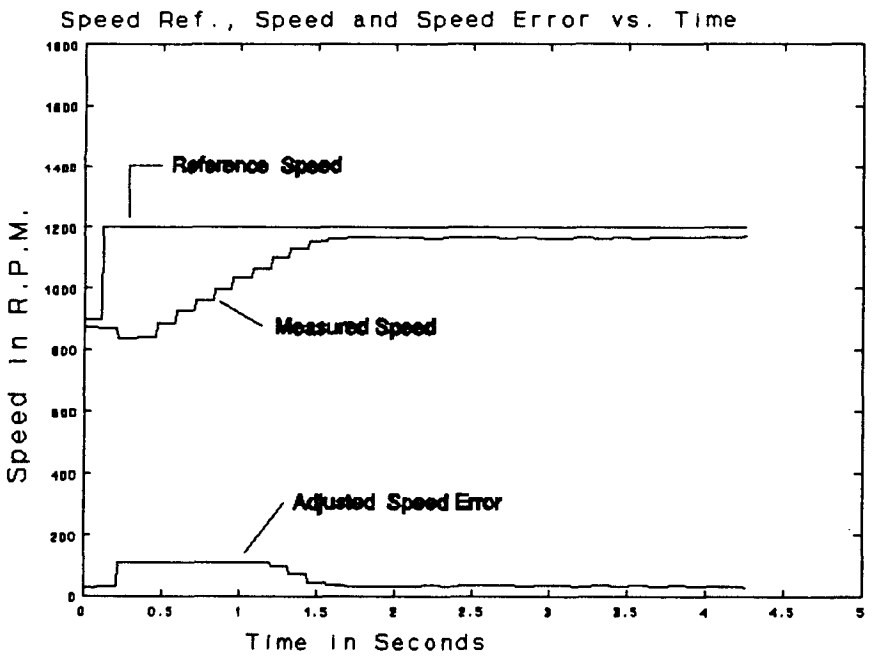

Figure 6.12: Step Speed Change Response Under Flux Control & DMRAC.

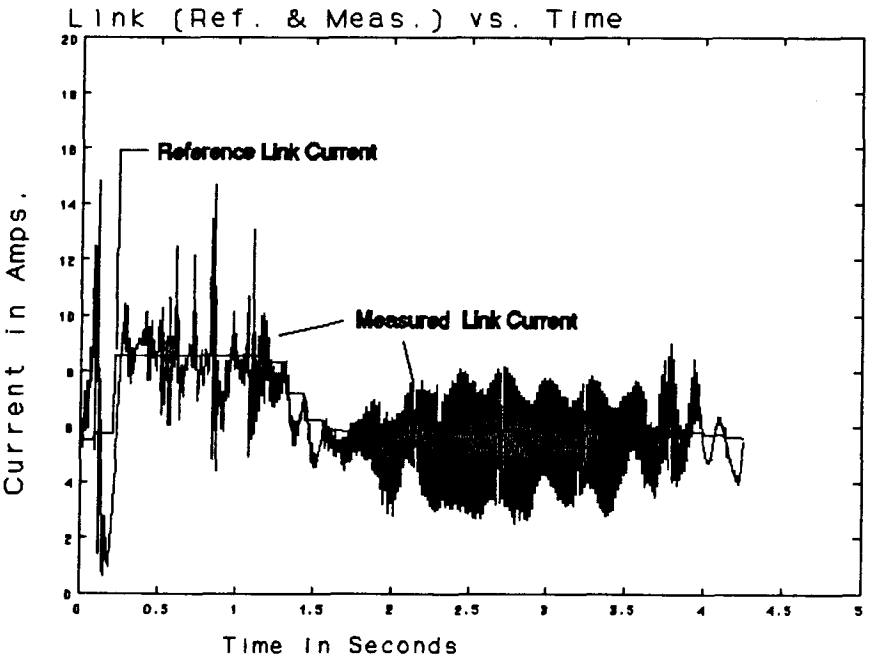

Figure 6.13: Step Speed Change Under Flux Control & DMRAC.

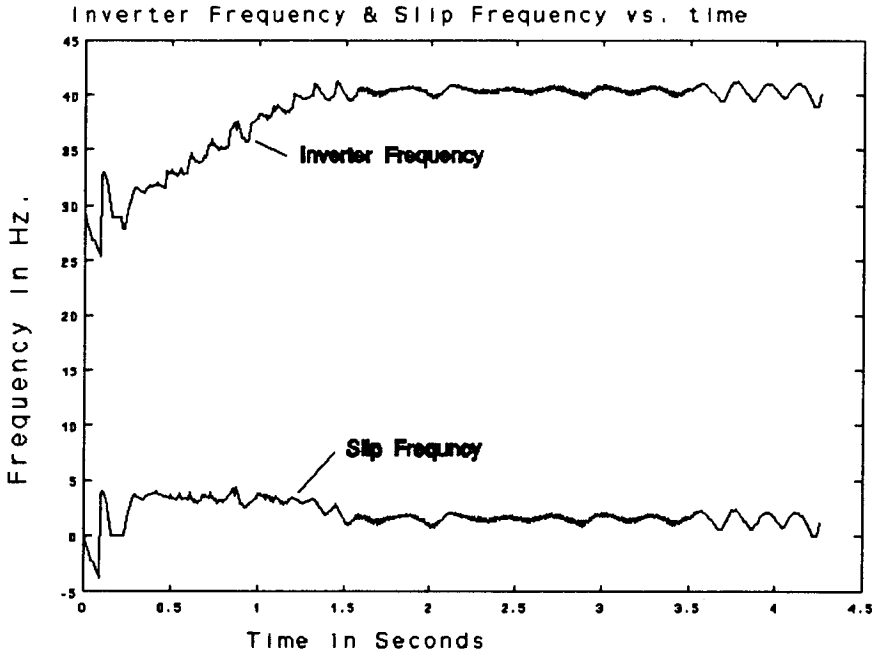

Figure 6.14: Step Speed Change Response Under Flux Control & DMRAC.

6.2.3 Regeneration Test

This test points out the inferiority of flux control more so than the others. The small negative step change in speed (from 1200 R.P.M. to 900 R.P.M.) causes large oscillations in the link current, (see Figure 6.20) while the CSI-IM drive is under the flux control scheme. These are the result of the poor performance that flux control has under transient conditions (recall flux control is based on a steady state equivalent circuit). These large di/dt's cause significant voltage spikes in the CSI power network. High

voltage spikes are potentially very damaging to power semiconductors in both the inverter and converter circuits. In fact, it was necessary to put a metal oxide varistor (MOV's) across each semiconductor to avoid the catastrophic results these spikes have. As a result of this, any large negative speed change with flux control would have to be a series of small changes. Each small negative change has to be followed by a period of time which allows the CSI-IM drive system to stabilize.

The FOC controller performs quite well in its regeneration test (900 R.P.M. to -900 R.P.M.). The results of this test are shown in Figure 6.15 to 6.18. The different stages of the complete speed reversal can be seen in Figure 6.15. At around the 0.1 second mark, the negative step change is realized by the control system (see the large negative change in speed error). The drive then regenerates down to approximately 200 R.P.M. at which time plugging takes place (ie. applying negative inverter phase rotation). The point at which plugging takes place is marked by the large positive swing in speed error (at roughly the 1.9 second point). The drive system then accelerates through 0 R.P.M. at the 2.4 second point. There appears to be a positive speed pulse at 2.4 seconds. This does not take place in the motor, but instead shows the point in time when the control system recognizes the change in motor direction (the negative going edge of that pulse). The direction and speed sensing software subroutines work independently from one another. Just prior to the negative going edge at 2.4

seconds the speed sensing software is picking up the increase in speed but does not perceive the direction change. At the negative going edge the independent direction sensing module notes the change in direction a few milli-seconds after it actually happened. This pulse does not affect motor performance. The rest of the acceleration takes approximately 1.2 seconds to reach nearly -900 R.P.M. The total reversal takes approximately 3.6 seconds.

This last test (the regeneration test) really shows the superiority of FOC. The flux control has great difficulty trying to control the motor under regeneration. Since this is probably the greatest of all the CSI's inherent advantages over a voltage source inverter (VSI), the flux control seems to be inadequate for high performance applications. Thus to use the CSI-IM drive to full potential seems to require the use of a superior torque/speed control methodology, such as FOC. This inadequacy to handle severe load transients with flux control is due to the fact that it is derived from the steady state equivalent induction motor model and makes no attempt to address the transient conditions. Since this model is not valid for the induction machine under transient cases, flux control cannot cope and the result is degraded performance.

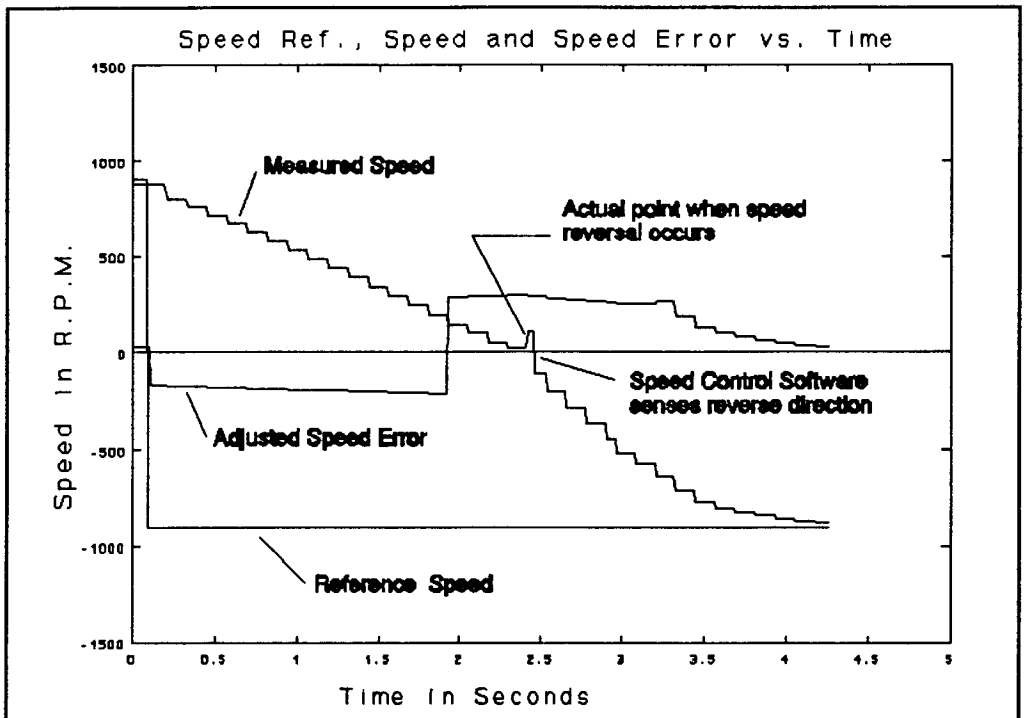

Figure 6.15: Regeneration Response under FOC & DMRAC.

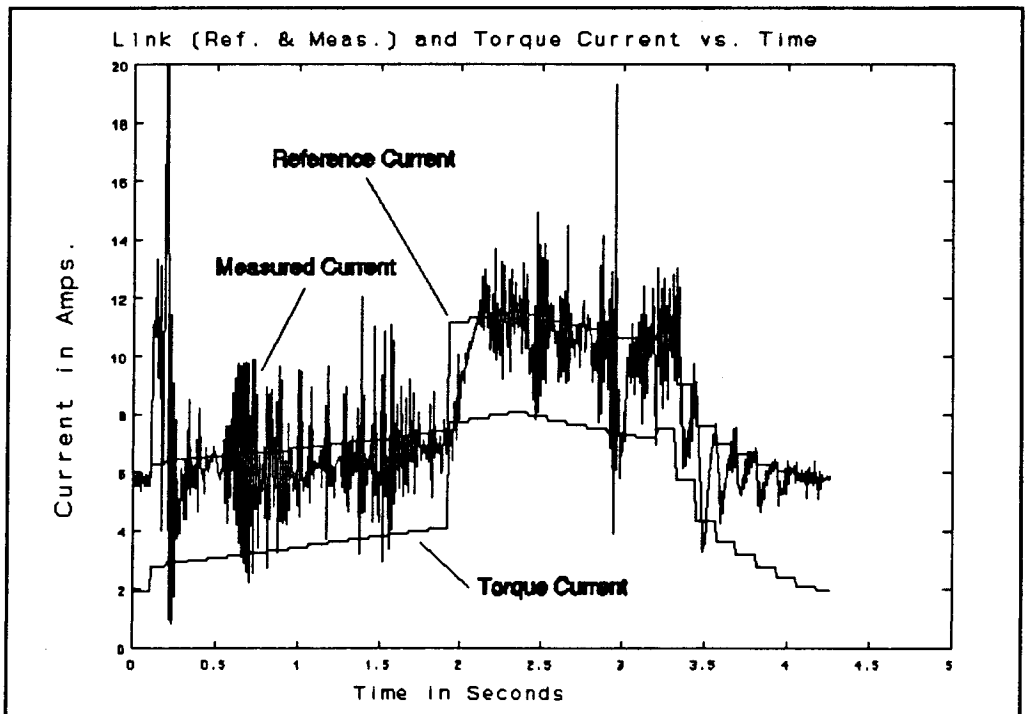

Figure 6.16: Regeneration Response Under FOC & DMRAC.

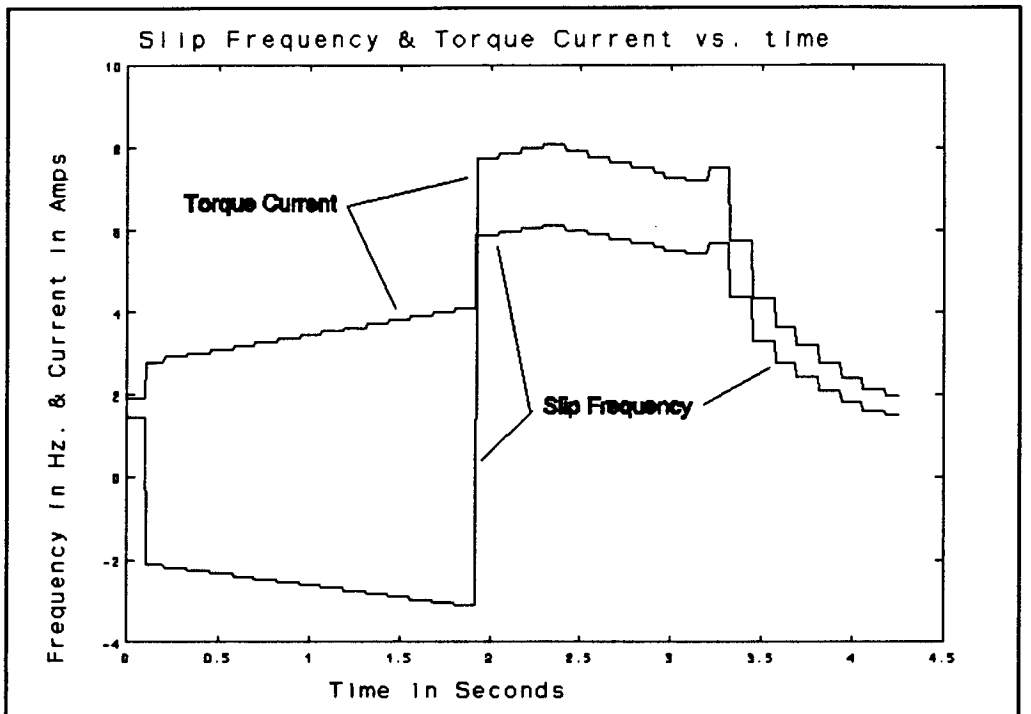

Figure 6.17: Regeneration Response Under FOC & DMRAC.

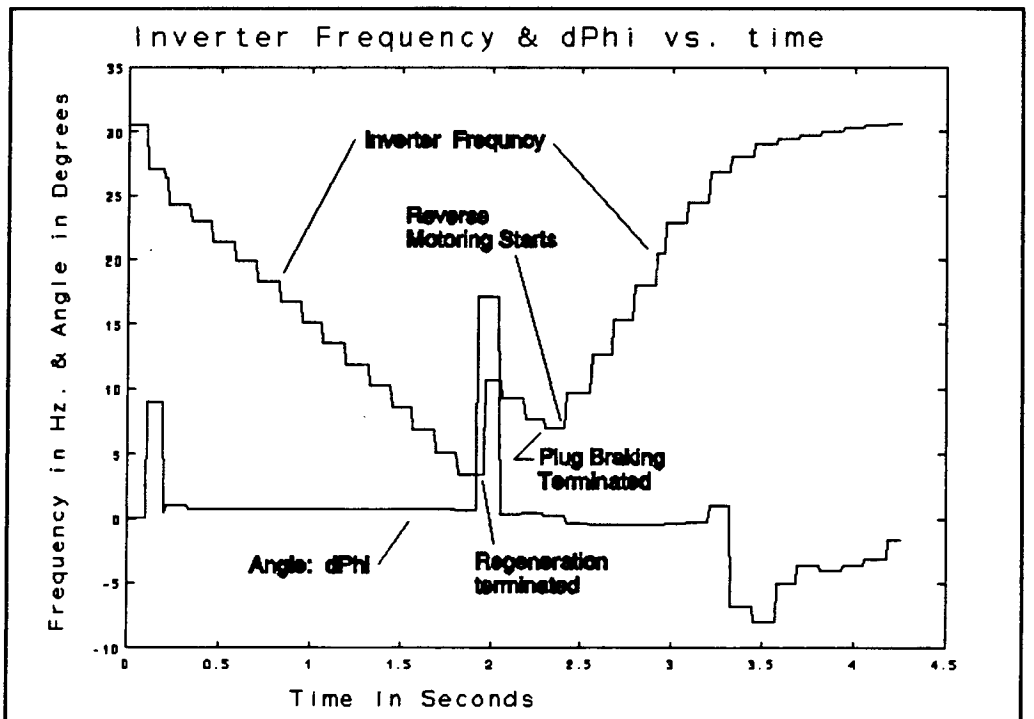

Figure 6.18: Regeneration Response Under FOC & DMRAC.

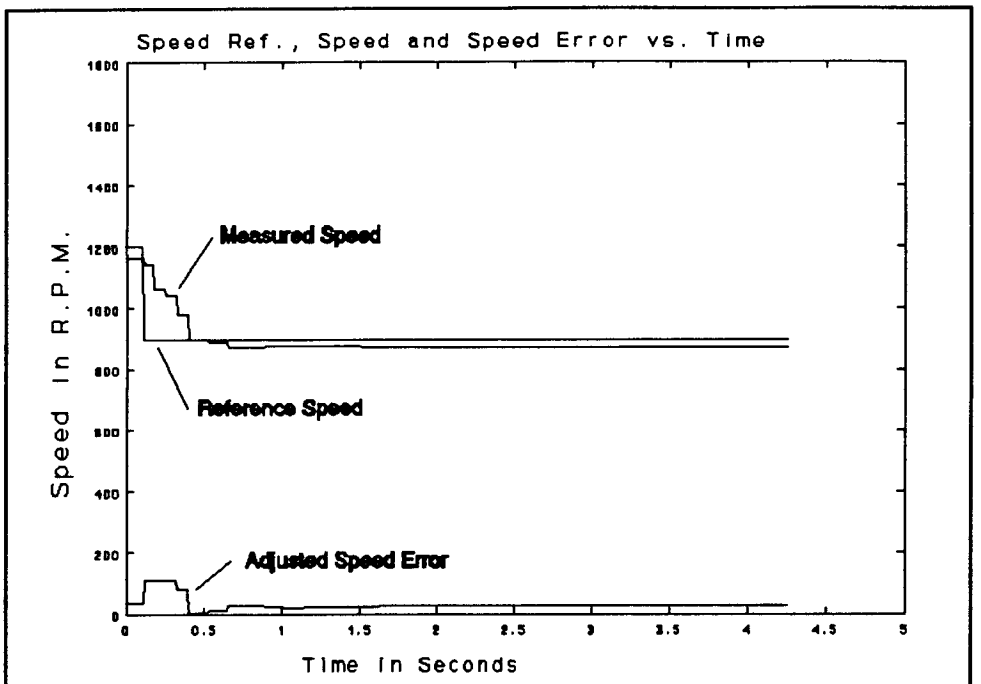

Figure 6.19: Regeneration Response Under Flux Control & DMRAC.

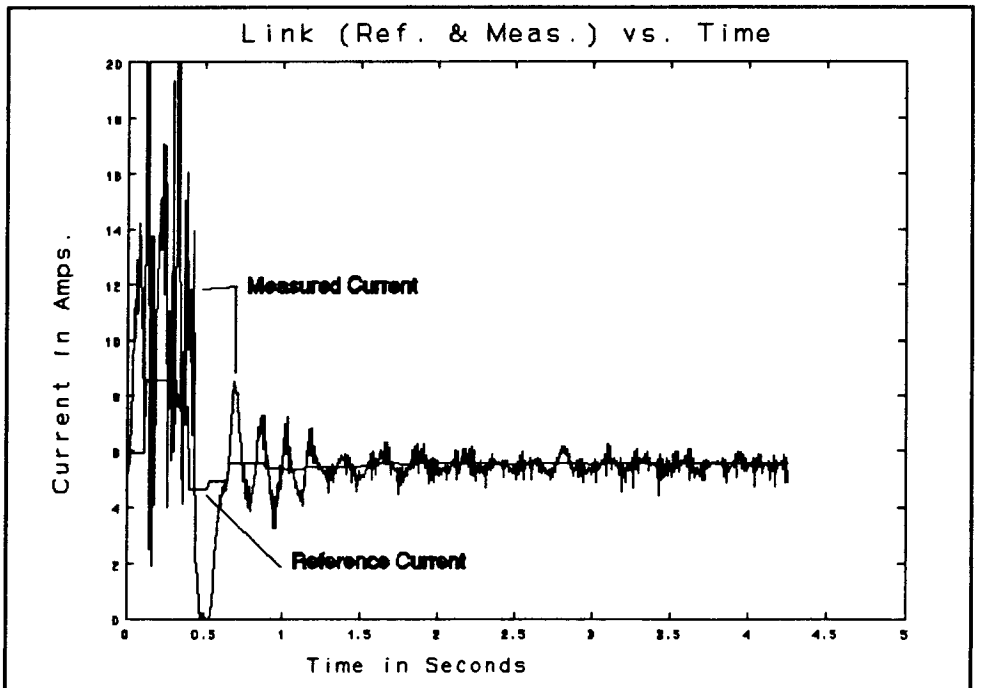

Figure 6.20: Regeneration Response Under Flux Control & DMRAC.

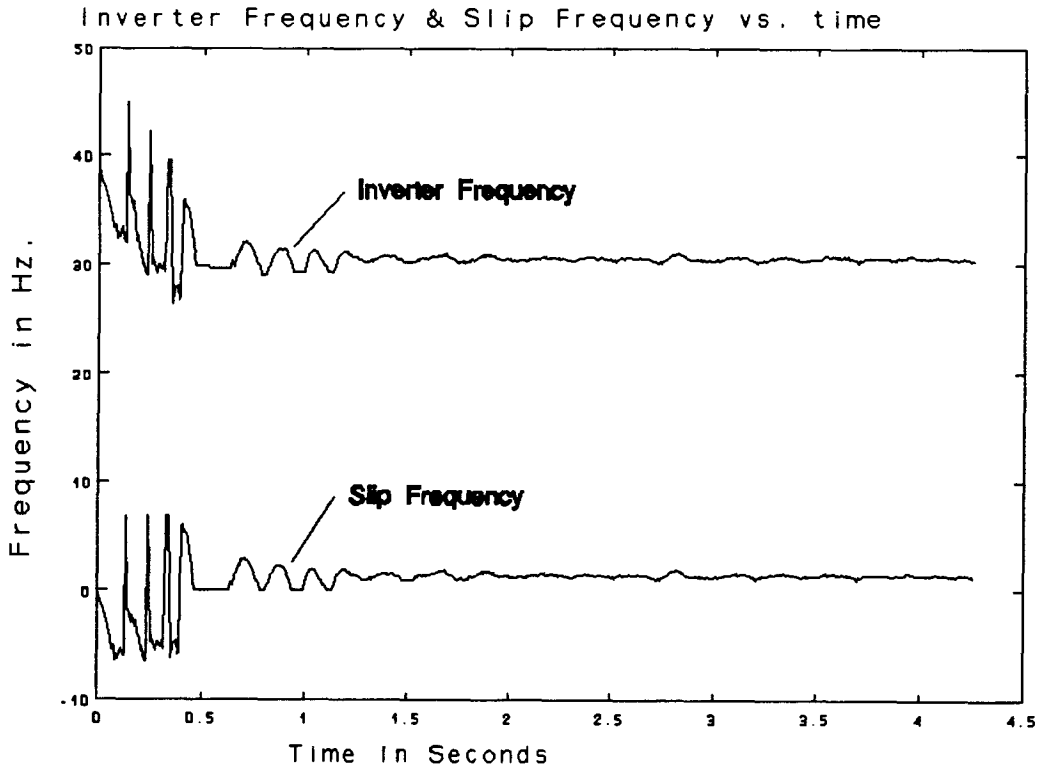

Figure 6.21: Regeneration Response Under Flux Control & DMRAC.

6.3 Current Control Loop

One test was performed to show the merits of the two different current loop control strategies (PI and DMRAC). A positive step change in speed, from 900 to 1500 R.P.M., was commanded to the drive system and the relevant results were recorded. These results are shown in Figure 6.22 to 6.24 for DMRAC, and in Figures 6.25 to 6.27 for PI control. The results seem to indicate that DMRAC gives superior performance as implemented here. This is evident when Figure 6.23 and Figure 6.26 are compared. DMRAC seems to have tighter control of the link current. However, since it was not one of the goals of this thesis to exhaustively compare these control methodologies, but instead to demonstrate that a CSI-IM drive could be satisfactorily controlled by a single microcontroller using control laws with differing degrees of complexity, it would be premature to make a judgment regarding the superiority of DMRAC.

Figure 6.24 shows the d.c. converter reference link voltage under DMRAC over this transient period. This signal is basically a step change in voltage (ignoring the spikes) and reflects the increase in power necessary to accommodate the higher speed of the load. Included in the graph is the back emf term that should remove some of the non-linearity of the induction machine as seen from the terminals of the CSI. It is unclear how well this feed forward control signal is functioning. This again is another area that

requires extensive study to determine its worth and is beyond the scope of this thesis.

It would seem that DMRAC, as implemented here, has some advantages over standard PI control. The tighter link current control (as implemented here) helps the overall CSI-IM drive performance. This is most noticeable for regeneration, when fast and accurate current control would help alleviate some of the large L-di/dt voltage spikes and torque fluctuations. This in turn would give a more robust drive system that would not have to face the large destructive spikes and degraded torque response. Appendix C shows the real time tuning of the DMRAC under two transient loading conditions: Start up and speed step changes.

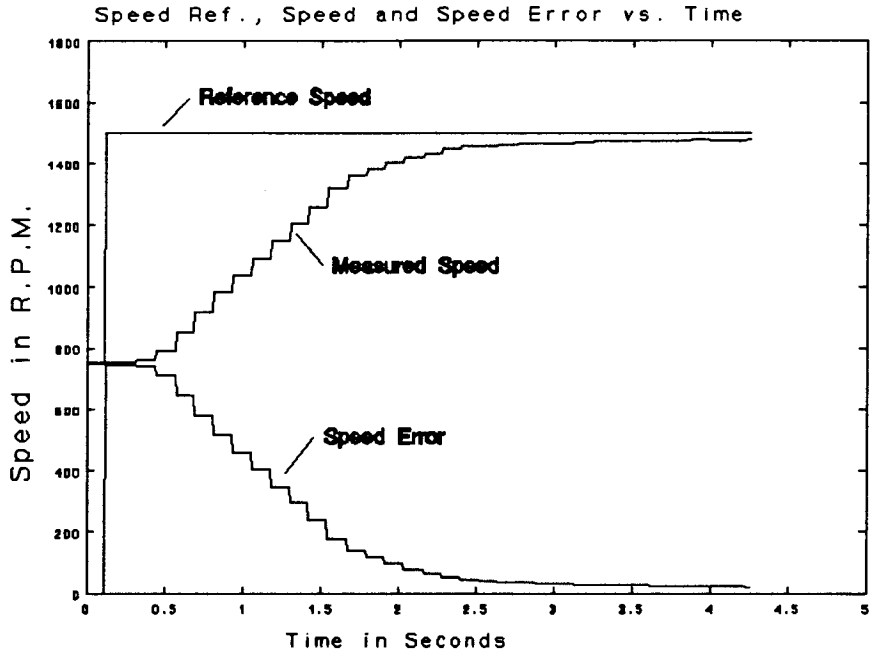

Figure 6.22: Speed Step Change Response Under FOC and DMRAC Current Control.

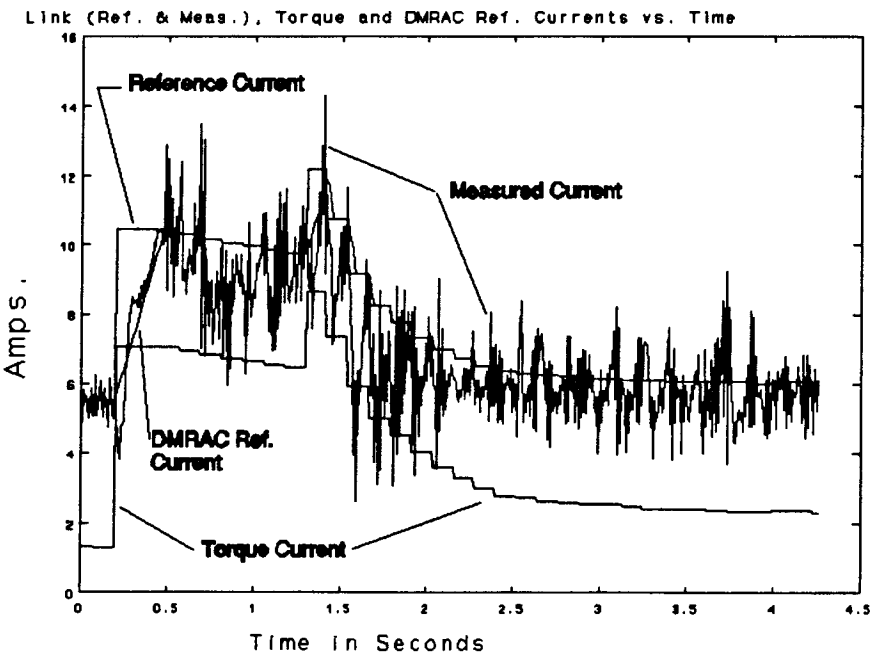

Figure 6.23: Speed Step Change Response Under FOC and DMRAC Current Control.

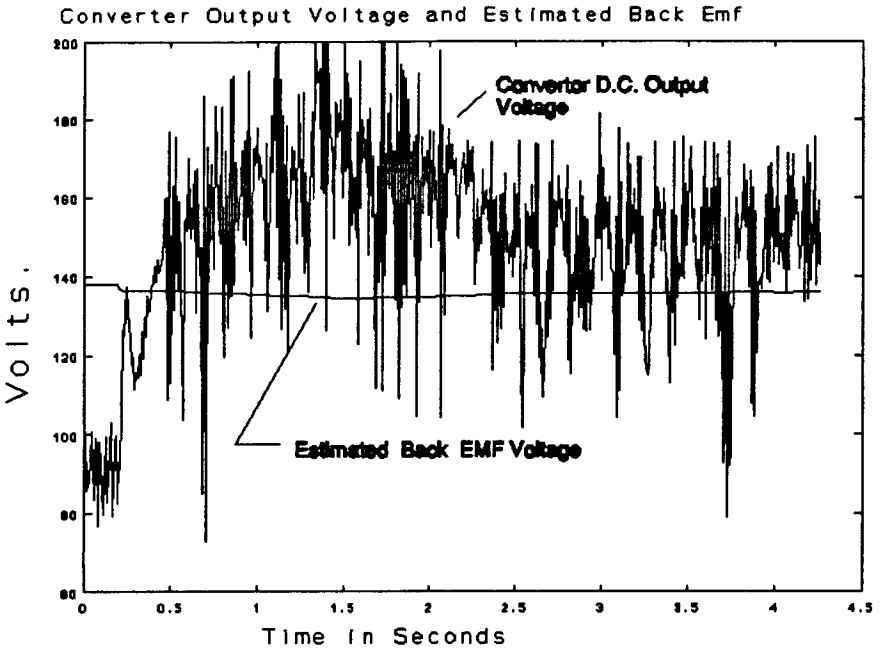

Figure 6.24: Speed Step Change Response Under FOC and DMRAC Current Control.

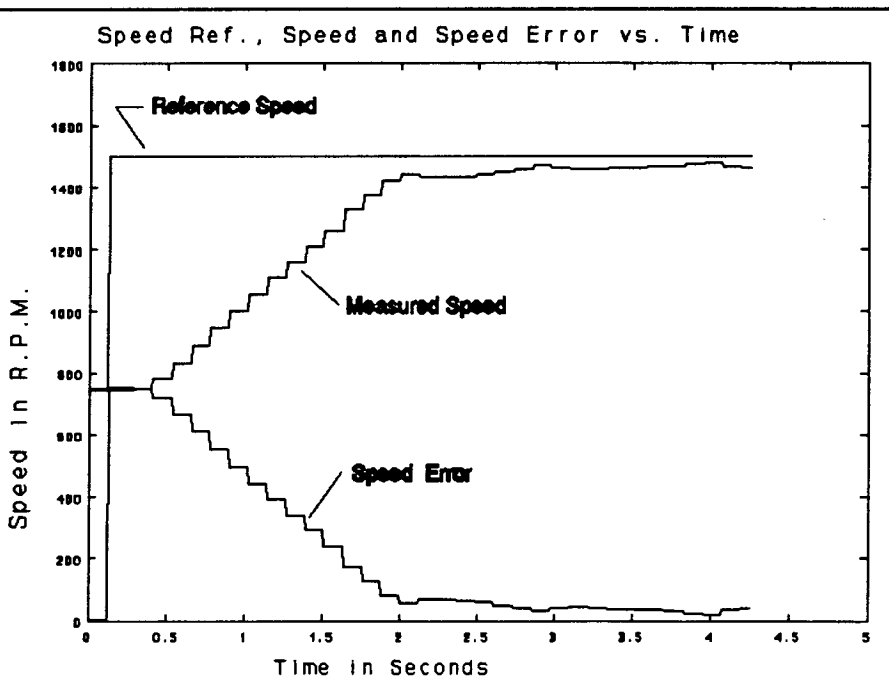

Figure 6.25: Speed Step Change Response Under FOC and PI Current Control.

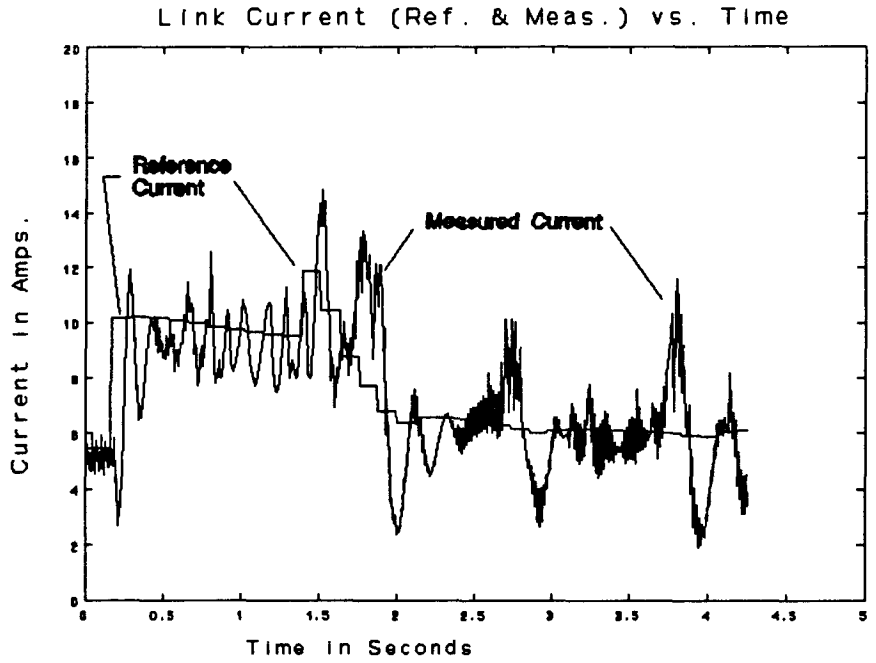

Figure 6.26: Step Speed Change Response Under FOC and PI Current Control.

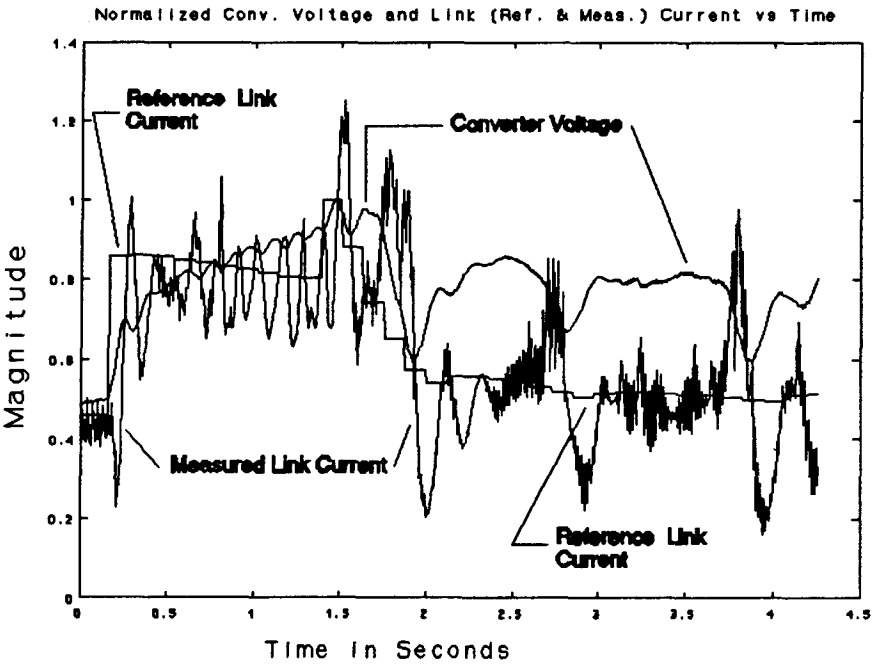

Figure 6.27: Speed Step Change Response Under FOC and PI Current Control.

6.4 Summary

The general findings here, on outer control loop methodology, agree well with previously published [7,13,14] conclusions which showed that vector control gives superior dynamic performance compared to that obtained with flux control.

It was also noticed that the link current performance could be enhanced with a more sophisticated control strategy, such as DMRAC with back emf compensation.

It is evident, from the data presented in this chapter, that the single microcontroller based CSI-IM drive system is capable of the excellent dynamic response characteristics it needs to compete with the D.C. motor. It is also possible to run advanced control schemes, such as FOC for torque/speed control and DMRAC for link current control, in real time. This not only gives the CSI-IM drive enhanced performance, but also there is still enough computing power left to perform simple data acquisition.

CHAPTER 7

CONCLUSION

7.1 Introduction

The objective of this thesis was to design and analyze a flexible single chip microcontroller based CSI-IM drive system. To this end the induction motor was analyzed using the simplified steady state circuit as a base for flux control and a more complex model for vector control. From these two different points of view came the constant flux and vector control laws. This analysis also formed the basis for the D.C. link current control laws. Two different means of controlling this link current were presented, simple proportion-integral and direct model reference adaptive control. The analysis presented here is groundwork for further research into the behaviour of the induction motor under the developed control laws.

7.2 Results

It was found that this microcontroller was fast enough to perform all the control laws necessary to control the motor, supply gating signals, and act as a simple data acquisition system (all in

real time). Thus this single chip microcontroller based system is very well suited for induction machine control. This allows for a large reduction in chip count for the complete drive control system. This reduced hardware further allows the drive to be more robust (lower chip count means a lower potential of complete drive system failure) and less influenced by its environment (lower probability of radiated electrical interference affecting the control system when it all resides inside one chip).

It was also determined that vector or field oriented control was superior to simple flux control. Although FOC is highly parameter dependent it still out performs flux control. There are also several methods to reduce this parameter sensitivity which could be added to the control laws to enhance their performance [7,13,20,21].

It was also found that the DMRAC with back emf compensation improves link current control. As was demonstrated in Chapter 6, being able to control the link current quickly is extremely beneficial for a high performance CSI drive.

The primary goal of this thesis was to design and analyze a flexible single chip microcontroller based CSI-IM drive. This goal was achieved. The secondary objectives of designing and implementing torque controllers, derived from both constant airgap flux and vector control theories, and link current controllers,

based on simple PI and the more complex DMRAC with back emf compensation, were also achieved.

7.3 Future Research Topics

Future research with this drive system may include adding an adaptive controller to the outer speed/torque loop in order to compensate for the parameter dependency problem. It would also be worthwhile to investigate speed control laws that could be added to the complete drive package (PLL, SMC etc.). Examining suitable tuning techniques for the DMRAC would also prove beneficial. Since these laws were tuned manually it is difficult to tell whether they will perform under all circumstances. Thus further research with them would be useful.

7.4 Summary

Thus, with these potential improvements, the CSI driven induction motor will be able to replace the high maintenance and therefore less desirable D.C. motor for large, high-performance applications which require extensive regeneration (traction and crane drives). A simple and more robust drive package would be the end result.

REFERENCES

[1] **Maag, R.B.,:** Characteristics and Application of Current Source/Slip Regulated A.C. Induction Motor Drives, Conf. Rec. IEEE Ind. Gen. Appl. Group Annual Meeting, 1971

[2] **Slemon, G.R., Dewan, S.B.:** Induction Motor Drive with Current Source Inverter, Conf. Rec. IEEE Ind. Appl. Soc. Annual Meeting, 1974

[3] **Lipo, T.A., & Cornell, E.P.:** State-Variable Steady_State Analysis of a Controlled Current Induction Motor, IEEE Trans. Ind. Appl., Nov./Dec. 1975.

[4] **Abbondanti, A., & Brennen, M.B.:** Variable Speed Induction Motor Drives use Electronic Slip Calculator Based on Motor Voltages and Currents, IEEE Trans. Ind. Appl., Sept./Oct. 1975.

[5] **Kim, H.G., Sul, S.K., & Park, M.H.:** Optimal Efficiency Drive of a Current Source Inverter Fed Induction Motor by Flux Control, IEEE Trans. Ind., Appl., Nov./Dec. 1984.

[6] **Walker, L.H. & Espelage, P.M.:** A High-Performance Controlled-Current Inverter Drive, IEEE Trans. Ind. Appl., Mar./Apr. 1980

[7] **Gabriel, R., Leonhard, W., & Norby, C.:** Field-Oriented Control of a Standard A.C. Motor using Microprocessors, IEEE Trans. Ind. Appl., Mar./Apr. 1980.

[8] **Phillips, K.P.:** Current-Source Convertor for AC Motor Drives, IEEE Trans. Ind. Appl., Nov./Dec., 1972.

[9] **Cornell, E.P., & Lipo, T.A.:** Modelling and Design of Controlled Current Induction Motor Drives Systems, IEEE Trans. Ind. Appl., Jul./Aug., 1977.

[10] **Krishnan, R., & Lindsay, J.F.:** Stefanovic, V.R., Control Principles in Current Source Induction Motor Drives, IEEE Ind. Appl. Soc. Annual General Meeting, 1980.

[11] **Krishnan, R., & Lindsay, J.F.:** Stefanovic, V.R., Design of an Angle Controlled Current Source Inverter-Fed Induction Motor Drive, IEEE Trans. Ind. App., May/June 1983.

[12] **Lander, C.W.:** Power Electronics, McCraw-Hill Book Company (1987)

[13] **Murphy, J.M.D., & Turnbull, F.G.:** Power Electronic Control of A.C. Motors, Pergamon Press (1988)

[14] **Novotny, D.W., & Lorenz, R.D.:** Introduction to Field Orientation and High Performance A.C. Drives, IEEE IAS Annual General Meeting (1985)

[15] **Dewan, S.B., & Slemon, G.R.:** Straughen, A., Power Semiconductor Drives, John Wiley and Sons (1984)

[16] **Lorenz, R.D., & Lawson, D.B.:** Performance of FeedForward Current Regulators for Field-Orientated Induction Machine Controllers, IEEE Trans. on IAS, Jul./Aug. 1987

[17] **Bolognani, S., & Buja, G.S.:** DC Link Current for High-Performance CSIM Drives, IEEE Trans. on IAS Nov./Dec. 1987

[18] **Yamamura, S.:** AC Motors for High-Performance Applications: Analysis and Control, Marcel Dekkon Inc. (1986)

[19] **Homayoun, S.:** Decentralized Adaptive Control of Manipulators: Theory, Simulation, and Experimentation, IEEE Trans on Robotics & Automation, April 1989.

[20] **Krishnan, R., & Doran, F.C.:** Study of Parameter Sensitivity in High-Performance Inverter Fed Induction Motor Drive Systems,

[21] **Nordin, K.B., Novotny, D.W., & Zinger, D.S.:** The Influence of Motor Parameter Deviations in FeedForward Field Orientation Drive Systems, Conf.,Rec. IEEE Ind. Appl. Soc. Annual General Meeting, 1984.

[22] Intel 16-Bit Embedded Controllers Handbook 1990, Intel Corporation Literature Sales.

[23] **Kelly, D.O., Simmons, S.:** Introduction to Generalized Electric Machine Theory, McGraw Hill Publishing Co. Ltd., 1968.

[24] **Soltine, J.J.E., Li,.W.:** Applied Nonlinear Control, Prentice-Hall Inc., 1991.

[25] **Astrom, K.J., Wittenmark, B.:** Computer Controlled Systems Theory and Design, Prentice-Hall Inc., 1990.

[26] **Nandam, P.K.,:** Variable Structure Speed Control of a Self Controlled Synchronous Motor Drive, Ph.D Dissertation, Queen's University, Kingston, Canada, 1990.

APPENDIX A

Derivation of the relationships for constant flux Control

As was seen in chapter 2, one must start with the basic steady state equivalent circuit of the induction machine (see Figure A.1 repeated from chapter 2).

Using current division the magnetizing current can be found and is as follows:

$$I_m = \left[\frac{R_r'/s + j\omega_s L_{lr}'}{R_r'/s + j\omega_s (L_{lr}' + L_m)}\right] I_s \qquad (A.1)$$

or

$$I_m = \left[\frac{R_r' + js\omega_s L_{lr}'}{R_r' + js\omega_s (L_{lr}' + L_m)}\right] I_s$$

and since:

$$s^*\omega_s = \omega_r \qquad (A.2)$$

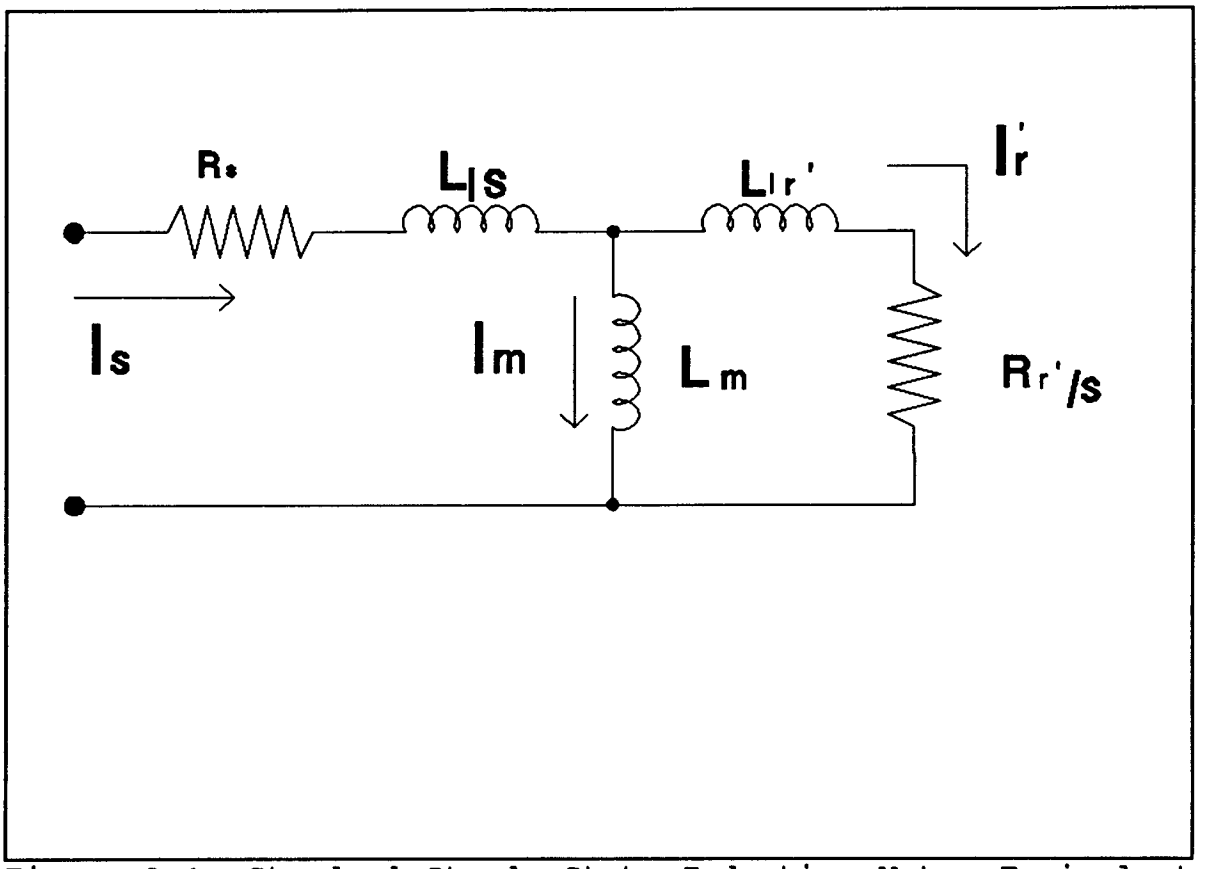

Figure A.1: Standard Steady State Induction Motor Equivalent Circuit.

it can be said that:

$$I_m = \left[\frac{R_r' + j\omega_r L_{lr}'}{R_r' + j\omega_r (L_{lr}' + L_m)}\right] I_s$$

or in absolute terms:

$$I_m = \left[\frac{(R_r')^2 + (\omega_r L_{lr}')^2}{(R_r')^2 + (\omega_r (L_{lr}' + L_m))^2}\right]^{\frac{1}{2}} I_s \qquad \text{(A.3.)}$$

Thus, this is equation 2.1. Likewise one can derive equation 2.2 through current division:

$$I_r' = \left[\frac{j\omega_s L_m}{R_r'/s + j\omega_s(L_{lr}' + L_m)}\right] I_s$$

$$= \left[\frac{js\omega_s L_m}{R_r' + js\omega_s(L_{lr}' + L_m)}\right] I_s \qquad \text{(A.4.)}$$

and using equation A.2. the end result is:

$$I_r' = \left[\frac{j\omega_r L_m}{R_r' + j\omega_r(L_{lr}' + L_m)}\right] I_s$$

Therefore once again looking for the absolute value, the expression quoted in chapter 2 (equation 2.2 this time) is obtained:

$$I_r' = \left[\frac{\omega_r L_m}{[(R_r')^2 + (\omega_r(L_{lr}' + L_m))^2]^{\frac{1}{2}}}\right] I_s \qquad \text{(A.6.)}$$

Derivation of the torque equation used in chapter 2 also comes from analyzing the equivalent circuit shown in figure A.1. The term R_r'/s represents rotor I^2R losses as well as mechanical power (output and mechanical-loss power). Thus the mechanical power is:

$$P_{mech\ 1p} = (I_r')^2 R_r'/s - (I_r')^2 R_r' \quad \textit{per phase}$$

$$\textit{or} \qquad \text{(A.6.)}$$

$$P_{mech\ 3p} = 3(I_r')^2 R_r'\left[\frac{1 - s}{s}\right] \quad \textit{three phase}$$

Since torque is defined as:

$$T = \frac{P_{mech\ 3p}}{\omega_m} \qquad \text{(A.6.)}$$

With ω_m being the mechanical rotor speed. This leads to the torque expression:

$$T = 3\frac{(I_r')^2 R_r'}{\omega_m}\left(\frac{1 - s}{s}\right) \qquad \text{(A.7.)}$$

Knowing that mechanical speed can be related to stator frequency as follows:

$$\omega_s = np*\frac{\omega_m}{1 - s} \qquad ;\ np = number\ of\ pole\ pairs \qquad \text{(A.8.)}$$

and re-arranging while substituting in equation A.2. leads to:

$$\omega_m = \frac{\omega_r}{np}\left(\frac{1 - s}{s}\right) \qquad \text{(A.9.)}$$

This can now be substituted into equation A.7. to get:

$$T = \frac{3*np*(I_r')^2*R_r'}{\omega_r} \qquad \text{(A.10.)}$$

and since:

$$(I_r')^2 = \frac{[\omega_r L_m I_s]^2}{(R_r')^2 + (\omega_r (L_{lr}' + L_m))^2}$$

the final result is:

$$T = \frac{3 * np * I_s^2 (\omega_r L_m)^2 R_r' / \omega_r}{(R_r')^2 + (\omega_r (L_{lr}' + L_m))^2} \qquad \text{(A.11.)}$$

This is equation 2.3. Thus, torque is a function of stator current and slip frequency (and of course the machine parameters) only, and is independent of the supply frequency ω_s.

APPENDIX B

Derivation of the Back EMF Voltage Term

The following derivation can be found in [17] and is included here for completeness. Some assumptions are necessary to simplify the analysis: Lossless inverter, no motor saturation, eddy currents, hysteresis, or spatial flux harmonics. The D.C. link voltage can be expressed as follows:

$$v_r = R_l i_{dc} + L_l p i_{dc} + v_i \qquad \text{where } p = \frac{d}{dt} \tag{B.1}$$

whereas the stator voltage can be represented using spatial vectors (d-q axis reference frame synchronous with the rotor flux spatial vector from generalized machine theory):

$$\overline{v_s} = R_s \overline{i_s} + p\overline{\lambda_s} + j\omega_r \overline{\lambda_s} \tag{B.2}$$

This expression is made up of the resistance, transformer and generated voltage terms respectively.

The two spatial flux vectors are defined as:

$$\overline{\lambda_s} = L_s\overline{i_s} + L_m\overline{i_r} \tag{B.3}$$

and

$$\overline{\lambda_r} = L_r\overline{i_r} + L_m\overline{i_s} \tag{B.4}$$

If B.3 is inserted into B.2 the following is obtained:

$$v_s = R_s\overline{i_s} + p(L_s\overline{i_s} + L_m\overline{i_r}) + j\omega_r(L_s\overline{i_s} + L_m\overline{i_r}) \tag{B.5}$$

Now by adding and subtracting the terms as shown below:

$$\begin{aligned} v_s = {} & R_s\overline{i_s} + p(L_s\overline{i_s} + L_m\overline{i_r}) + j\omega_r(L_s\overline{i_s} + L_m\overline{i_r}) \\ & + \frac{L_m^2}{L_r}p\overline{i_s} - \frac{L_m^2}{L_r}p\overline{i_s} + j\omega_r\frac{L_m^2}{L_r}\overline{i_s} - j\omega_r\frac{L_m^2}{L_r}\overline{i_s} \end{aligned} \tag{B.6}$$

this equation can be regrouped into:

$$\begin{aligned} v_s = {} & R_s\overline{i_s} + p(L_s - \frac{L_m^2}{L_r})\overline{i_s} + j\omega_r(L_s - \frac{L_m^2}{L_r})\overline{i_s} + \\ & j\omega_r(\frac{L_m^2}{L_r}\overline{i_s} + L_m\overline{i_r}) + p(\frac{L_m^2}{L_r}\overline{i_s} + L_m\overline{i_r}) \end{aligned} \tag{B.6}$$

and by defining a total leakage inductance term as:

$$L_\sigma = L_s - \frac{L_m^2}{L_r} \tag{B.7}$$

equation B.6 can be further simplified to:

$$\begin{aligned} v_s = {} & R_s\overline{i_s} + pL_\sigma\overline{i_s} + j\omega_r L_\sigma\overline{i_s} + p\frac{L_m}{L_r}(L_m\overline{i_s} + L_r\overline{i_r}) \\ & + j\omega_r\frac{L_m}{L_r}(L_m\overline{i_s} + L_r\overline{i_r}) \end{aligned} \tag{B.8}$$

By using the rotor flux expression B.4, equation B.9 is obtained:

$$\overline{v_s} = R_s\overline{i_s} + L_o p\overline{i_s} + j\omega_r L_o\overline{i_s} + \frac{L_m}{L_r}(p\overline{\lambda_r} + j\omega_r\overline{\lambda_r}) \quad \text{(B.9)}$$

The last two terms can be defined as the motor back EMF term since they are made up of the transformer and rotational voltages. This leads to the definition B.10.

$$EMF = \frac{L_m}{L_r}(p\overline{\lambda_r} + j\omega_r\overline{\lambda_r}) \quad \text{(B.10)}$$

Now using the notion of power invariance the following can be stated:

$$v_{dc} \cdot i_{dc} = RE(\overline{v_s} \cdot \overline{i_s^*}) \quad \text{(B.11)}$$

Equations B.9 - B.11 can be manipulated into the following:

$$v_i = k_i^2(R_s i_i + L_o p i_i) + emf_i$$
$$k_i = \frac{i_s}{i_i} \approx 3\frac{\sqrt{2}}{\pi} \quad \text{(B.12)}$$

Where

$$emf_i = \frac{RE(\overline{emf}\cdot\overline{i_s^*})}{i_i} \quad \text{(B.13)}$$

If the d axis of the d-q reference frame is aligned with the rotor flux spatial vector, λ_r, then the following scalar expression drops out:

$$emf_i = \frac{L_m}{L_r}\left(\frac{i_{ds}}{i_i}p\lambda_r + \omega_r\frac{i_{qs}}{i_i}\lambda_r\right) \tag{B.14}$$

The D.C. link voltage now becomes:

$$v_r = R_t i_i + L_t p i_i + emf_i \tag{B.15}$$

The vector control analysis from [13,14] 3 led to the torque expression:

$$T_{elec} = np\frac{L_m}{L_r}\lambda_r i_{qs} \tag{B.16}$$

and if q-axis rotor voltage and flux expressions are used:

$$\begin{aligned} 0 &= R_r i_{qr} + \omega_{slip,rotor}\lambda_r \\ 0 &= L_r I_{qr} + L_m i_{qs} \end{aligned} \tag{B.17}$$

the following variation of the back EMF is obtained:

$$emf_i = \left(\omega_m + \frac{R_r T_{elec}}{np\lambda_r^2}\right) * \frac{T_{elec}}{npi_i} \tag{B.18}$$

Now the back EMF term can be expressed in a digital control law. The law, B.19, is in terms of motor speed, torque reference (since

this is a good approximation to T_{elec}) and link current.

$$emf(k) = (K_a\omega_m(k) + K_bT^*_{elec}(k))K_c\frac{T^*_{elec}(k)}{I_{dc}(k)} \qquad \text{(B.19)}$$

The constants (K_a, K_b, and K_c) which appear in the above equation (B.19) not only contain motor parameters, but also scaling factors used to adjust the input analog to digital integer values.

APPENDIX C

Real Time Tuning of DMRAC

C.1 Introduction

Two tests were performed to demonstrate the self tuning of the DMRAC gains. Both tests have a 65 second duration. The first test is the start-up test and shows the tuning process from the initial settings. The initial value of the control law gains were determined through a manual tuning process (as were the adaption gains). These values were found to give a fast response while maintaining stability. The other test is a series of step changes (between 750 and 1500 R.P.M.) and is included to show how DMRAC adjusts itself to the differing load conditions over the same period of time (65 seconds). This differing load condition represents different equivalent circuits for the induction machine, and thus DMRAC should adjust itself accordingly.

C.2 Start-up test

The results of this test are shown in Figures C.1 to C.3. Figure C.1 shows the reference and measured link current over the 65 second test period. The link tracks the reference closely. The

slight offset is due to the quantization effect realized by using integer mathematics and only a 10 bit A/D converter. The feedback gains (which are normalised against their maximum values to allow relative comparisons to be made) K_{pp} and K_{vv} undergo constant adjustments while K_{ii} stays constant (as explained in Chapter 4 K_{ii} turns out to be a constant).

A small steady state error with link current exists over the duration of the test. This error is caused by the quantization error and by the relatively small number of accurate bits that we do have when using a 10 bit A/D converter. With this type of a converter, eight accurate bits [22] can be expected. Thus having the following resolution:

$$\frac{50 \ Amps.}{2^8} = \frac{200 \ milli\text{-}Amps}{increment}$$

This error tends to continually increase the control law gains, via the adaptation laws. This is not a desirable situation and must be compensated for. The proper method to deal with this problem would be to go to a 16 bit (or even higher) A/D converter and have a small dead band for the error signal that drives the adaption laws. This would help ignore the quantization effect that drives these gains to values that are too high. If a 16 bit A/D converter was used, 14 accurate bits would be available. Thus the following resolution would be available to the control laws:

$$\frac{50\ Amps}{2^{14}\ Increments} = \frac{3\ milli\text{-}Amps}{Increment} \qquad (C.1)$$

A dead band of, say, 5 milli-Amps could then be used. Then the adaption law gains could be higher, giving faster adaptation to the changing load conditions.

The adaptation of the feed forward gains are shown in Figure C.3. All of these gains undergo constant tuning in response to the error link current.

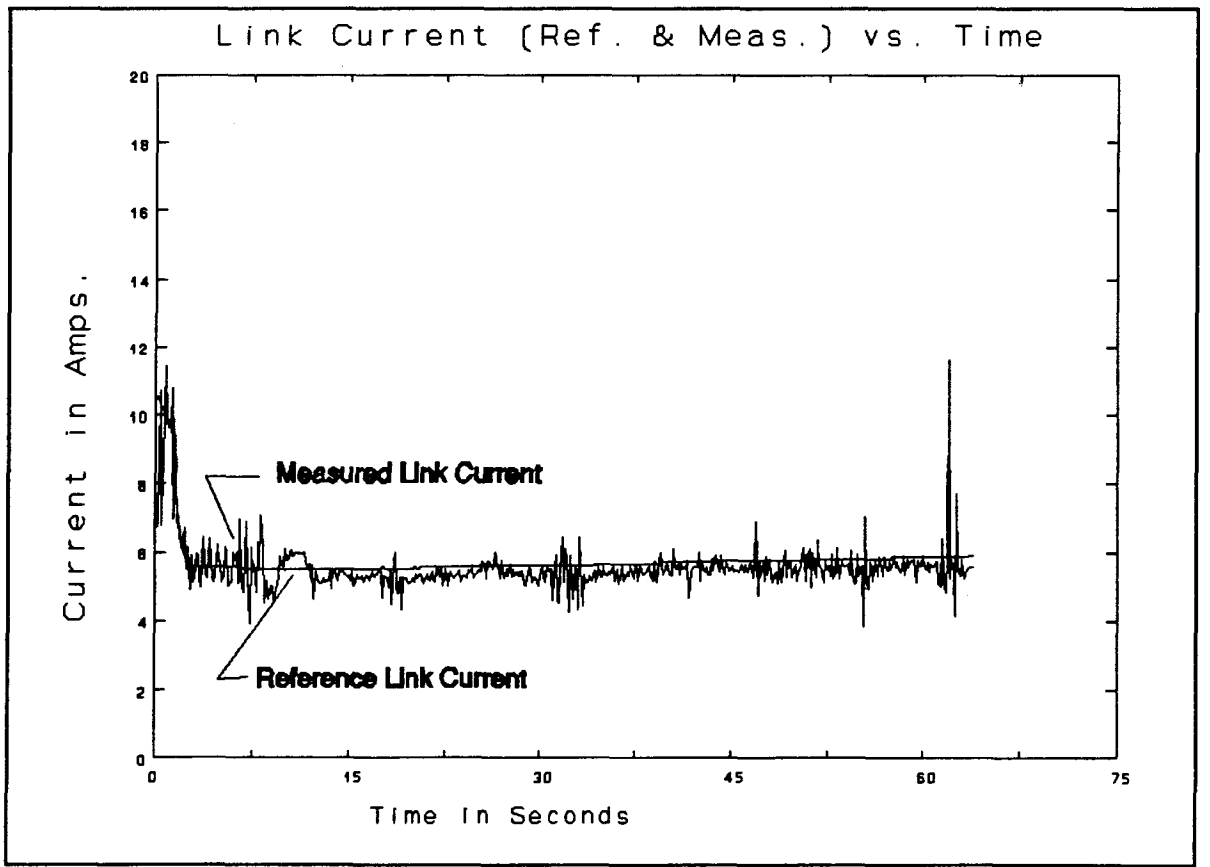

Figure C.1: Start up Response Under FOC and DMRAC Current Control.

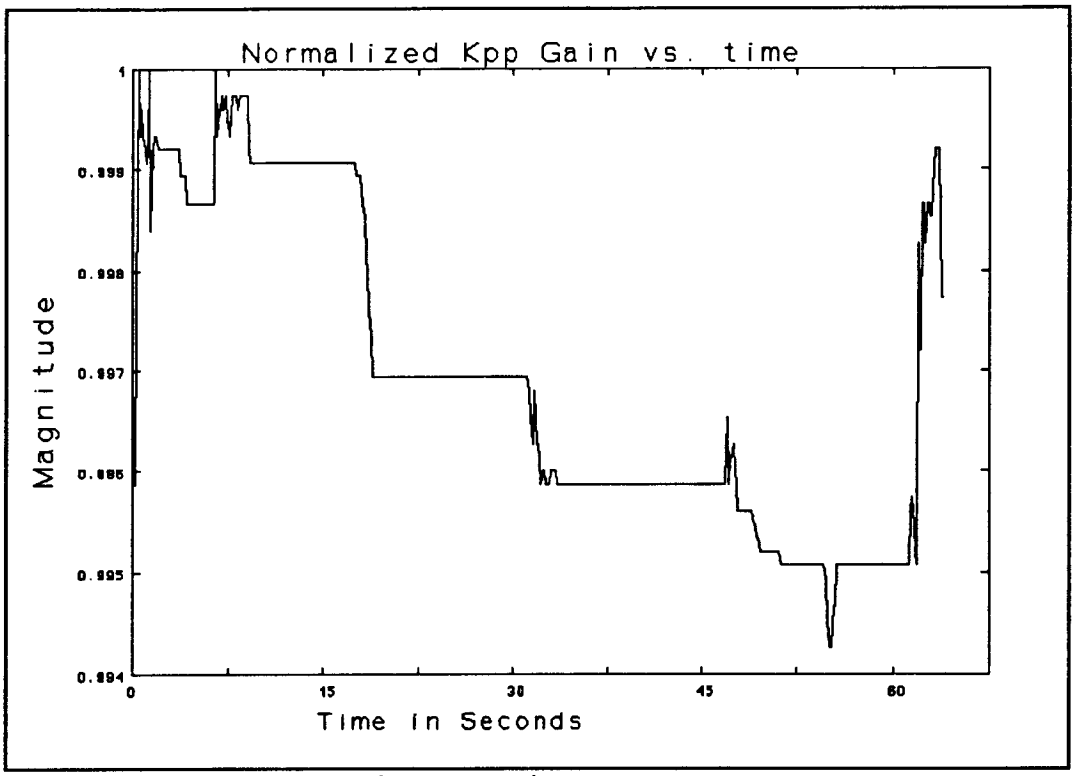

Figure C.2a: Kpp Gain Immediately after Start up.

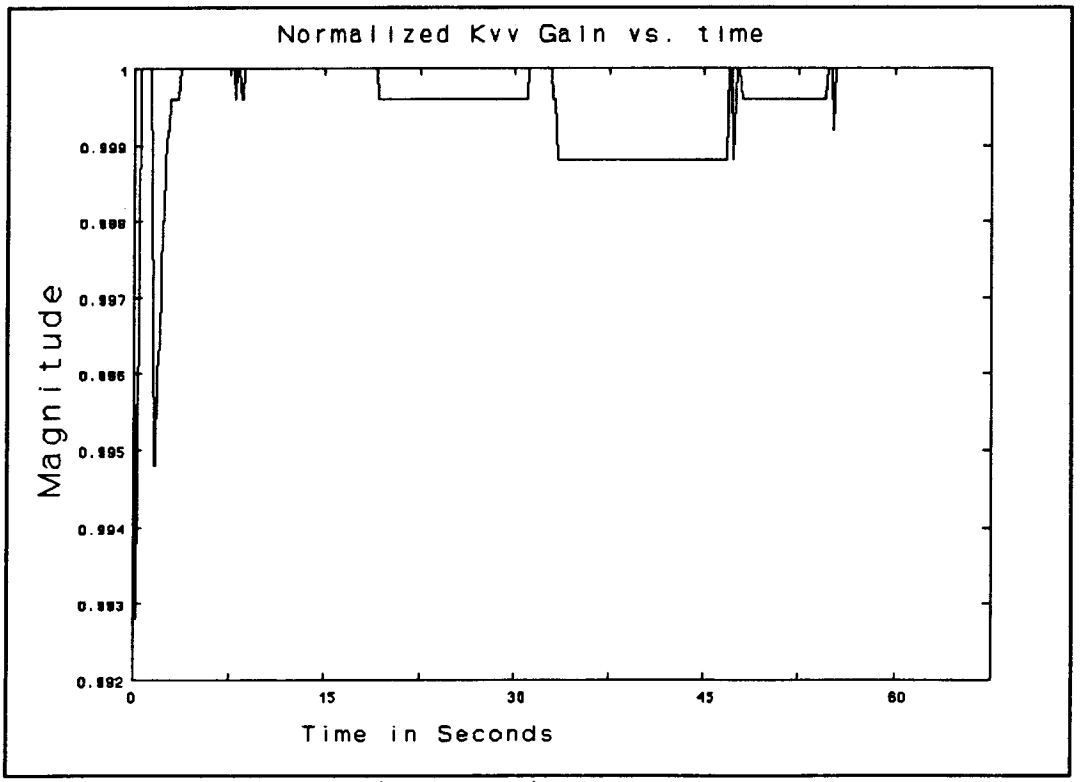

Figure C.2b: Kvv Gain Immediately after Start up.

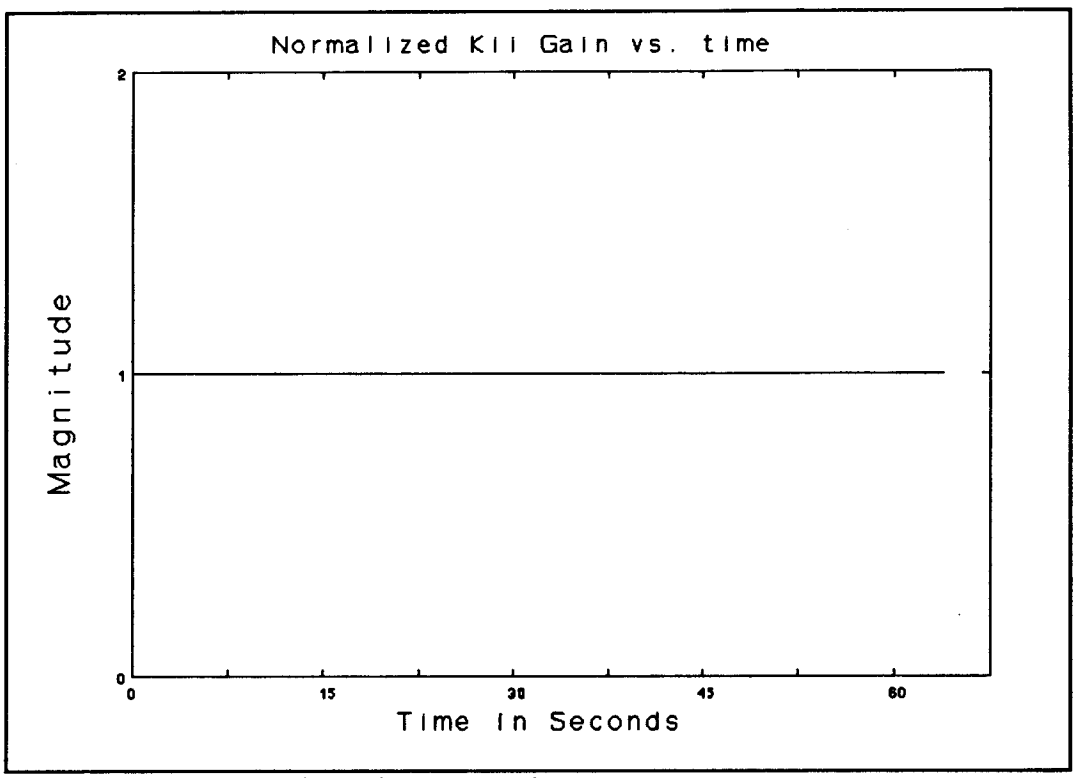

Figure C.2c: Kii Gain Immediately after Start up.

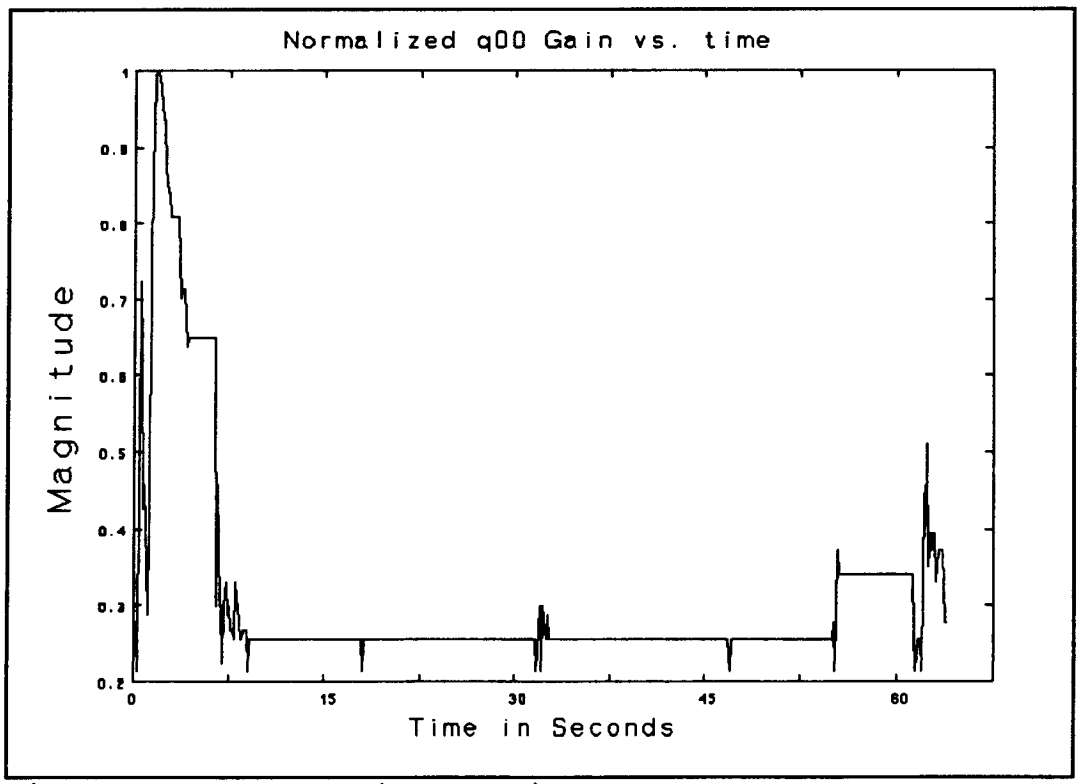

Figure C.3a: q00 Gain Immediately after Start up.

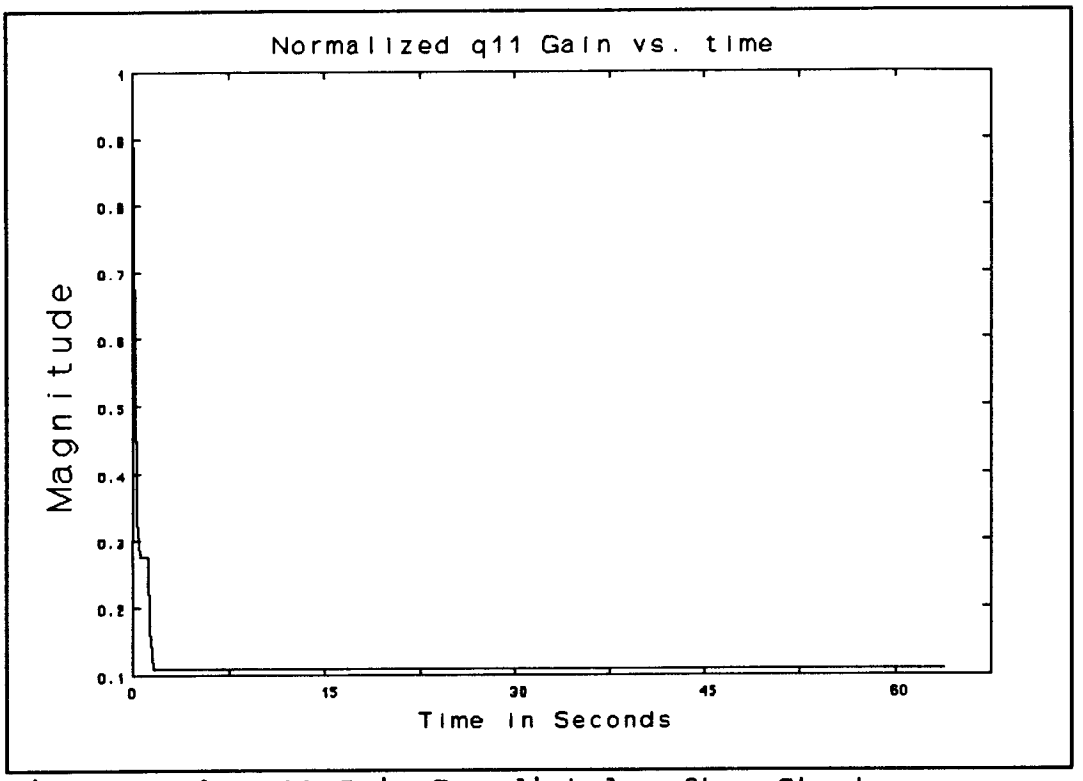

Figure C.3b: q11 Gain Immediately after Start up.

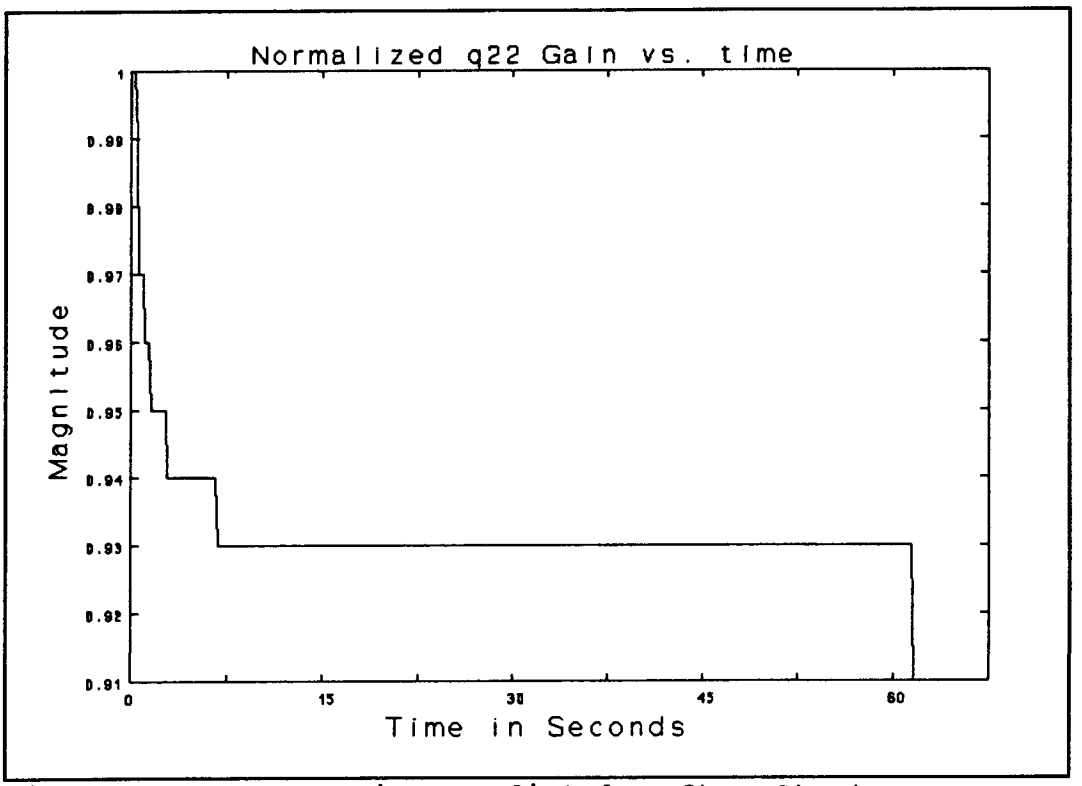

Figure C.3c: q22 Gain Immediately after Start up.

C.3 Series of Step Changes

The results of this test are shown in Figure C.4 to C.7. The speed changes are illustrated in Figure C.4. The resulting reference and measured-link currents appear in Figure C.5. Again the measured link currents track the reference value closely. As with the start-up case continual adjustment of the proportional, K_{pp}, and derivative ,K_{vv}, gains are observed. This adjustment does represent a significant change in the gain magnitude. The feed forward gains q_{11} and q_{22} have stabilized. This indicates that the reference and measure link current values correspond closely to one another. The feed forward gain q_{00} undergoes the most change. This is mainly due to the choice of adaption gain that allows it to be responsive. This larger adaptation gain was chosen after some experimentation, and found to have an acceptable affect on the link current response.

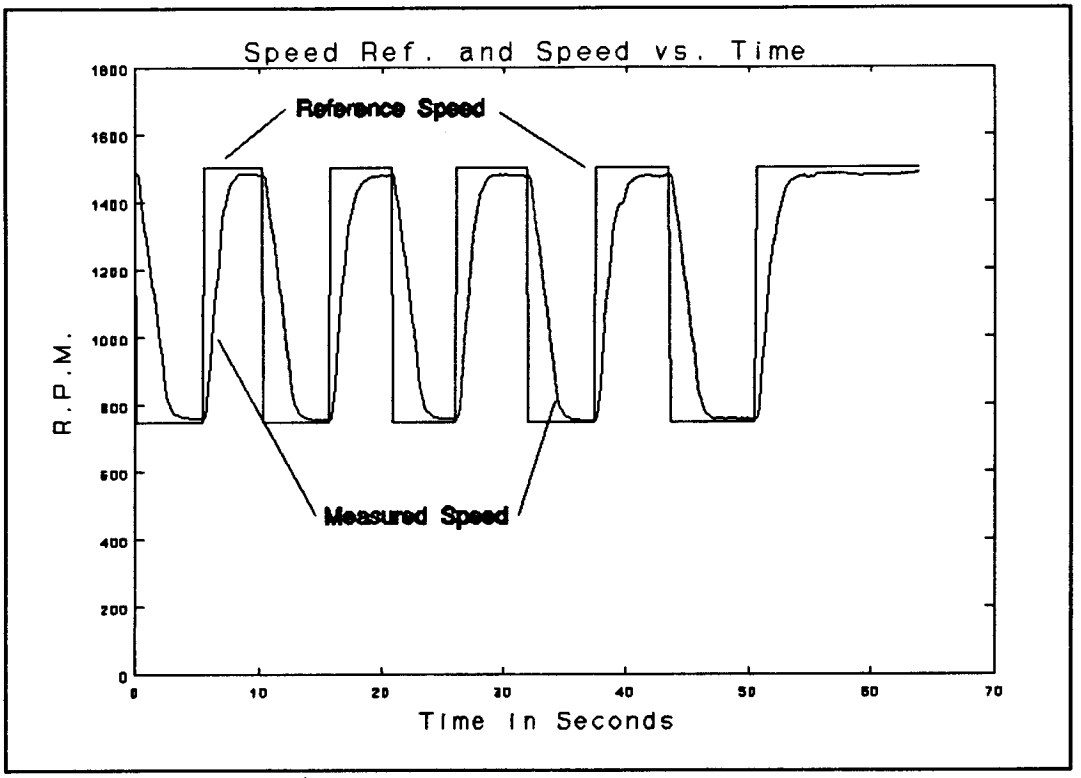

Figure C.4: Series of Speed Step Changes.

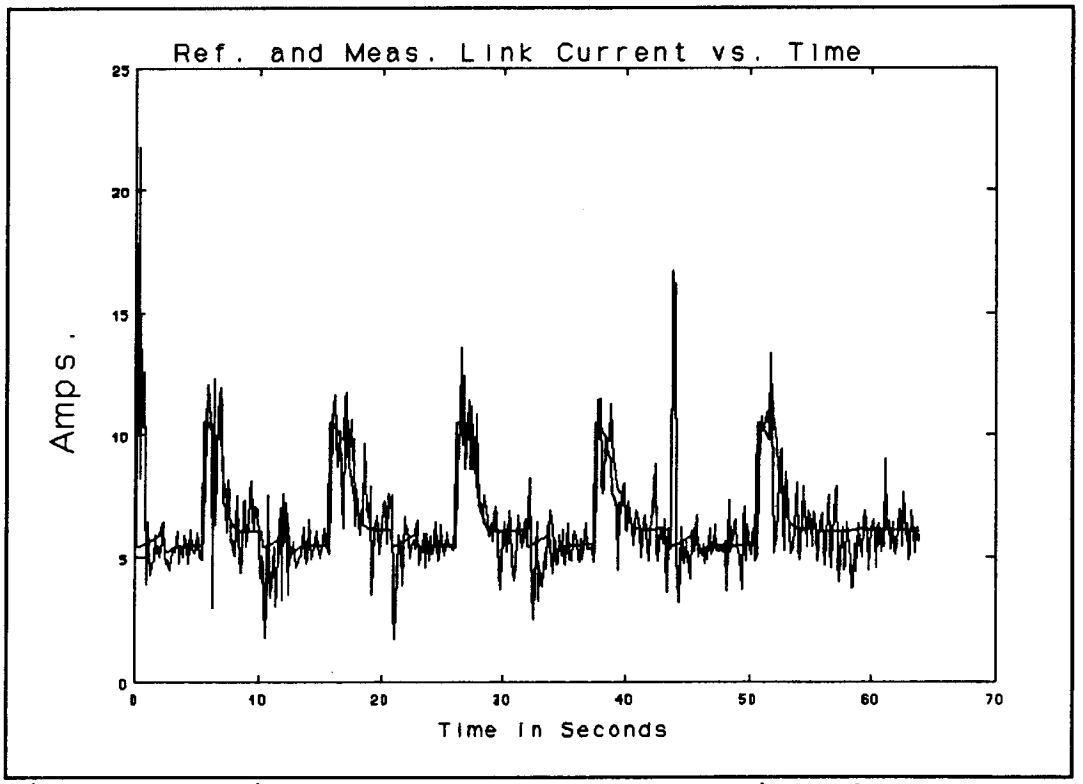

Figure C.5: Link Current Response to Series of Step Speed Changes under FOC and DMRAC.

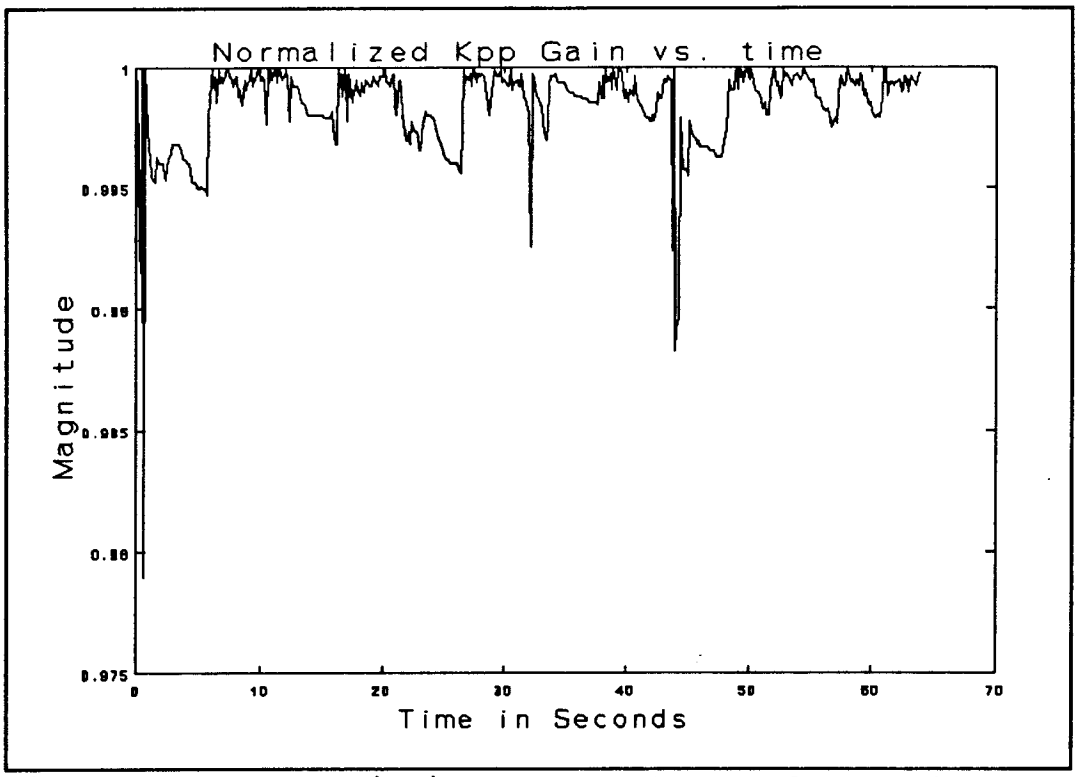

Figure C.6a: Kpp Gain in Response to Speed Step Changes.

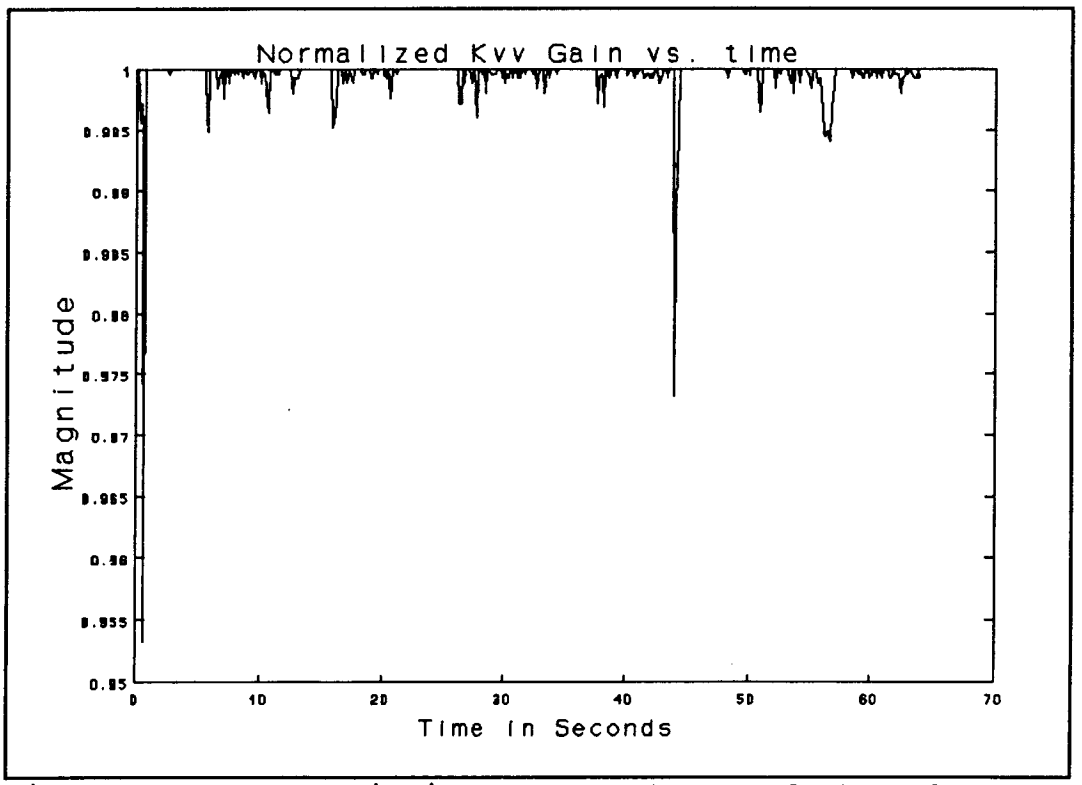

Figure C.6b: Kvv Gain in Response to Speed Step Changes.

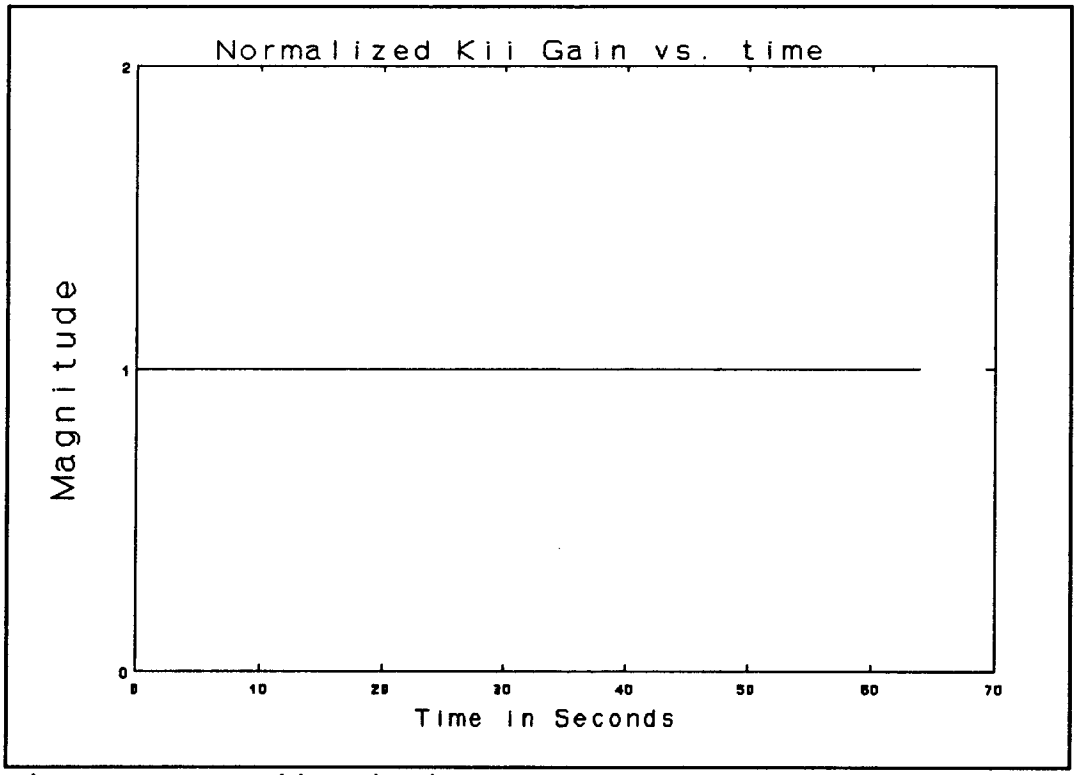

Figure C.6c: Kii Gain in Response to Speed Step Changes.

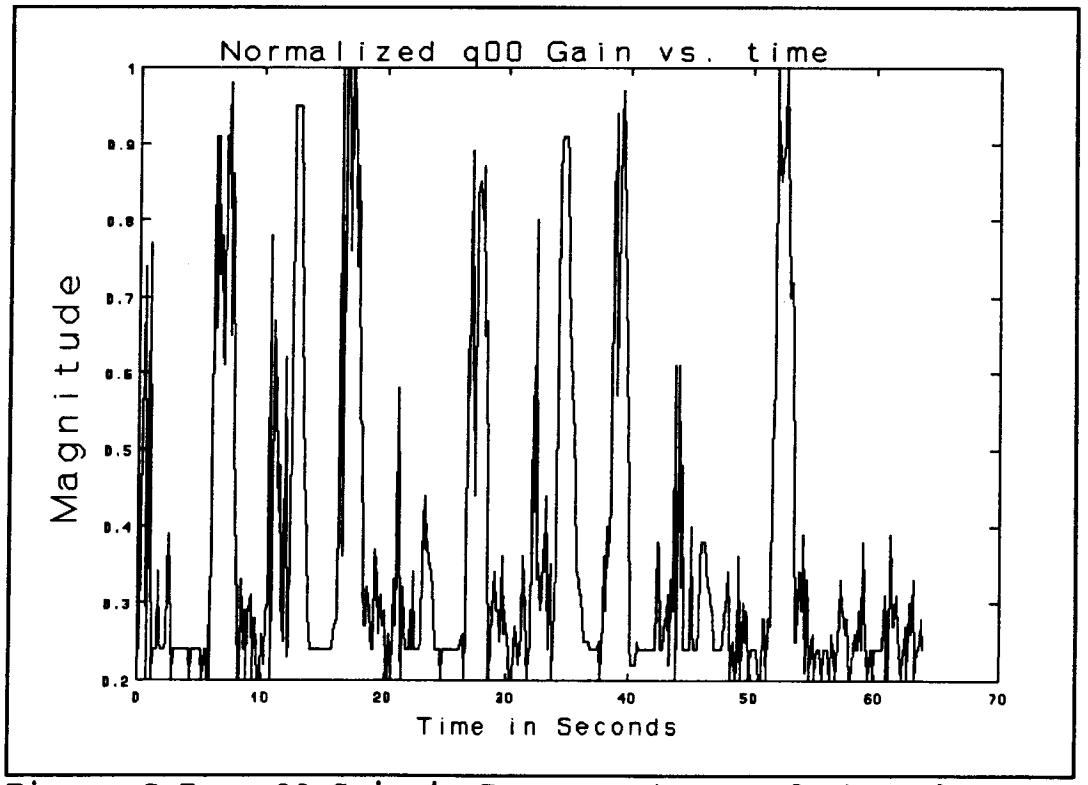

Figure C.7a: q00 Gain in Response to Speed Step Changes.

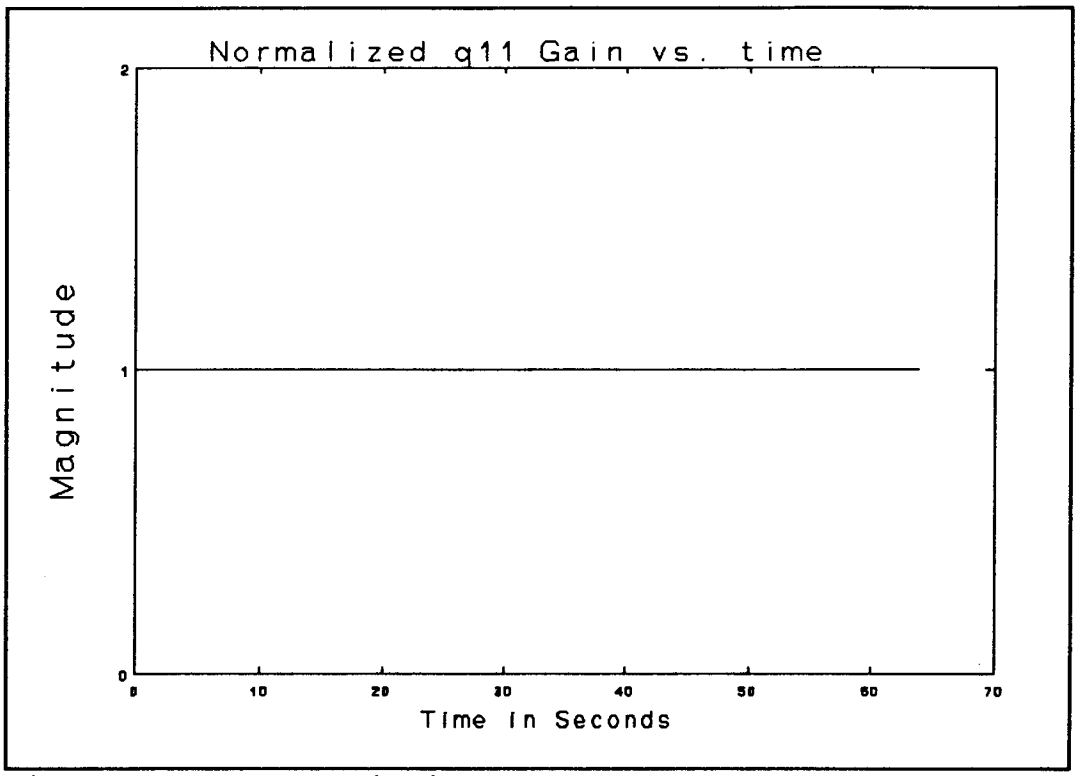

Figure C.7b: q11 Gain in Response to Speed Step Changes.

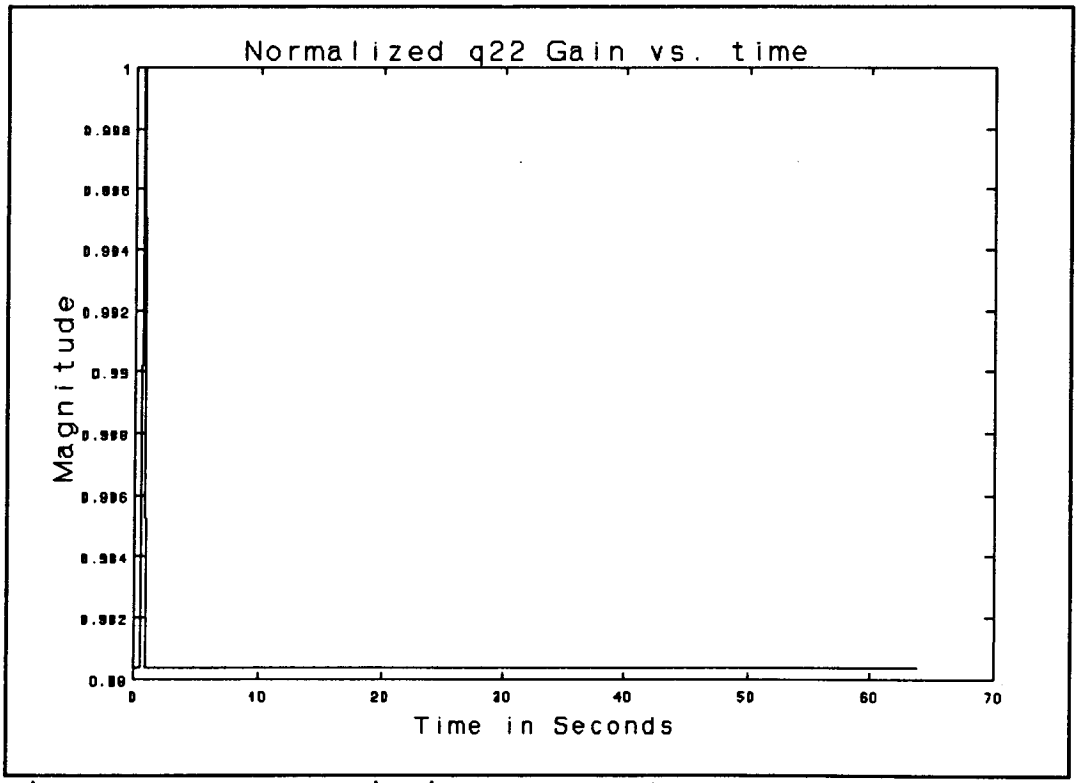

Figure C.7c: q22 Gain in Response to Speed Step Changes.

C.4 Summary

The DMRAC tuning process was demonstrated for two different loading conditions. The start up sequence and a series of step changes in speed. This controller is a challenging topic for further research and may be found to be very useful since it has the ability to adapt to changing load conditions. This feature lends itself nicely to induction machine control where circuit elements, like R_r', are known to vary widely over the normal operating range [20,21].